Supporting Information

Dialkyl Ether Formation at High Valent Nickel

Franck Le Vaillant, Edward J. Reijerse, Markus Leutzsch, and Josep Cornella*

Max-Planck-Institut für Kohlenforschung, Kaiser-Wilhelm-Platz 1,

Max-Planck-Institut für Chemische Energiekonversion, Stiftstrasse 34–36,

Mülheim an der Ruhr, 45470, Germany

E-mail: cornella@kofo.mpg.de

Table of Contents

1. General Methods

Unless otherwise stated, all manipulations were performed using Schlenk techniques under dry argon in heatgun-dried glassware. Anhydrous solvents were distilled from appropriate drying agents and were transferred under Argon: THF, Et_2O (Mg/anthracene), CH_2Cl_2 (CaH_2), CH_3CN (CaH_2), hexane, toluene (Na/K), benzene-d (MS) CD_2Cl_2 (MS), CD_3CN (MS). GC-MS (FID): GC-MS-QP2010 equipped (Shimadzu Europe Analytical Instruments). ESI-MS: ESQ 3000 (Bruker). Accurate mass determinations: Bruker APEX III FT-MS (7 T magnet) or MAT 95 (Finnigan). NMR spectra were recorded using a Bruker AVIIIHD 300 MHz, Bruker AVIIIHD 400 MHZ, Bruker AVIII 500 MHz or Bruker AVneo 600 MHz NMR spectrometer. The chemical shifts (δ) are given in ppm and were measured relative to solvent residual peak as an internal standard. For ^{1}H NMR: $CDCl_3$, δ 7.26; CD_3CN, δ 1.94; CD_2Cl_2, δ 5.32; C_6D_6, δ 7.16. For ^{13}C NMR: $CDCl_3$, δ 77.16; CD_3CN, δ 1.32; CD_2Cl_2, δ 53.84; C_6D_6, δ 128.06. The data is being reported as (s = singlet, d = doublet, t = triplet, q = quartet, quint = quintet, m = multiplet or unresolved bs = broad signal, coupling constant(s) in Hz, integration, interpretation). X-Band EPR spectra were recorded on a Bruker Elexsys E-500 CW X-band spectrometer. The sample tubes of 5 mm outer diameter were placed in a standard TE102 resonator. Low temperature measurements (10-30K) were obtained using an Oxford ESR 900 helium flow cryostat and a Mercury series temperature controller. Baseline corrections were performed by subtracting a background spectrum, obtained under the same experimental conditions from an empty tube. Unless otherwise noted, all reagents were obtained from commercial suppliers and used without further purification. N_2O is provided by Air Liquid (Distickstoffmonoxid UHP 5.0). Avicel is received from Merck (PH-101 mikrokristallin Ph Eur, Merck). $Ni(COD)_2$ is prepared according to literature procedure.[1] 4CzIPN was synthesized according to literature procedure.[2] A LED Kessil® A160WE was used as the light source for the photoredox experiment.

2. Preparation of nickel complexes

BipyNi($CH_2CH_2CH_2CH_2$) (4a)

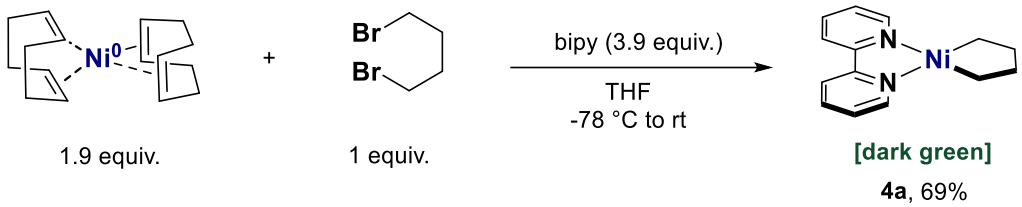

Following a reported procedure,[3] a solution of 1.97 g (12.6 mmol, 3.9 equiv.) of 2,2'-bipyridine in 10.0 mL of THF was added dropwise to a solution of $Ni(COD)_2$ (1.69 g, 6.14 mmol, 1.9 equiv.) in 30 mL of THF, at –78 °C under argon. The resulting yellow solution was allowed to warm up to 25 °C, at which point the solution started to turn violet. After 45 min of stirring at 25 °C, the deep violet solution was cooled down to –78 °C and 0.39 mL (3.23 mmol, 1 equiv.) of dry and degassed 1,4-dibromopentane was added dropwise via syringe. The solution was warmed up to 25 °C and some green color appeared. After 5 h30 of additional stirring, the deep blue/grey solution was filtered under argon using D4 fritte and the insoluble material was washed with 4×15 mL of THF (until the filtrate is colorless). At this stage, the total volume of solution recovered in a Schlenk is around 100 mL. Then the filtrate is reduced to about 20 mL using the vacuum line and 50 mL of pentane is added to precipitate the Ni complex. The solids were then filtered off under argon, via canula, and washed with 3×15 mL of pentane, before being dried under high vacuum to give 608 mg (2.24 mmol, 69% yield) of microcrystalline deep green solid **4a**.

^{1}H NMR (400 MHz, C_6D_6, 25 °C) δ 9.09 (d, *J* = 5.0 Hz, 2H, Ar*H*), 6.96 (td, *J* = 7.7, 1.6 Hz, 2H, Ar*H*), 6.71 (d, *J* = 8.0 Hz, 2H, Ar*H*), 6.49 (ddd, *J* = 7.2, 5.5, 1.3 Hz, 2H, Ar*H*), 2.72 (t, *J* = 7.0 Hz, 4H, NiC*H*$_2$CH$_2$),), 2.19 (p, *J* = 3.6 Hz, 4H, NiCH$_2$C*H*$_2$).

^{13}C NMR (101 MHz, C_6D_6, 25 °C) δ 154.4 (s, bipy), 148.2 (s, bipy), 133.2 (s, bipy), 125.7 (s, bipy), 120.2 (s, bipy), 36.9 (s, CH_2), 29.7 (s, CH_2).

The values of the NMR spectra are in accordance with reported literature data.[3]

BipyNi(CHMeCH$_2$CH$_2$CH$_2$) (4b)

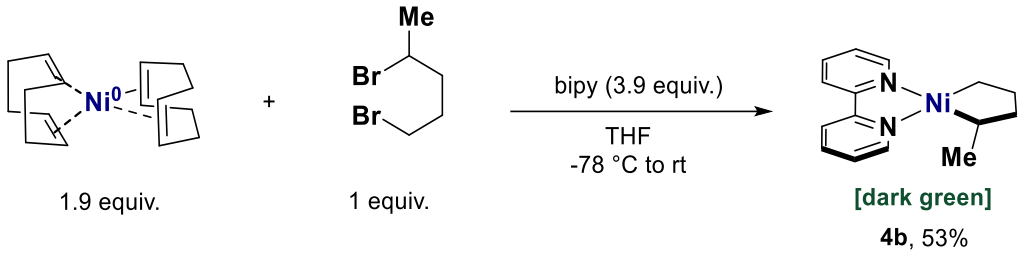

Following a reported procedure,[4] a solution of 1.57 g (10.1 mmol, 3.9 equiv.) of 2,2'-bipyridine in 7.0 mL of THF was added dropwise to a solution of Ni(COD)$_2$ (1.35 g, 4.91 mmol, 1.9 equiv.) in 25 mL of THF, at –78 °C. The resulting yellow solution was allowed to warm up to 25 °C, at which point the solution started to turn violet. After 45 min of stirring at 25 °C, the deep violet solution was cooled down to –78 °C and 330 µL (594 mg, 2.58 mmol, 1 equiv.) of degassed 1,4-dibromopentane was added dropwise via syringe. The solution was warmed up to 25 °C and some green color appeared. After 5 h30 of additional stirring, the deep blue solution was filtered under argon and the insoluble material was washed with 4×10 mL of THF (until the filtrate is colorless). At this stage, the total volume of solution recovered in a Schlenk is around 72 mL. Then the filtrate is reduced to about 15 mL using the vacuum line and 40 mL of pentane is added to precipitate the Ni complex. The solids were then filtered off under argon, via canula, and washed with 3×10 mL of pentane, before being dried under high-vacuum to give 394 mg (1.38 mmol, 53% yield) of microcrystalline deep green solid **4b**.

^{1}H NMR (500 MHz, C$_6$D$_6$, 25 °C) δ 9.17 (d, *J* = 5.6 Hz, 1H, Ar*H*), 9.07 (d, *J* = 5.5 Hz, 1H, Ar*H*), 7.03 (t, *J* = 7.7 Hz, 1H, Ar*H*), 6.97 (t, *J* = 7.6 Hz, 1H, Ar*H*), 6.74 (d, *J* = 8.0 Hz, 2H, Ar*H*), 6.58 (t, *J* = 6.6 Hz, 1H, Ar*H*), 6.49 (t, *J* = 6.6 Hz, 1H, Ar*H*), 2.97 (m, 1H, C*H*), 2.85 (m, 1H, C*H*$_2$), 2.55 – 2.42 (m, 2H, C*H*$_2$), 2.36 (m, 1H), 2.18 (m, 1H, C*H*$_2$), 1.88 (m, 1H, C*H*$_2$), 1.86 (d, *J* = 7.4 Hz, 3H, *Me*).

^{13}C NMR (101 MHz, C$_6$D$_6$, 25 °C) 154.6 (s, bipy), 154.4 (s, bipy), 148.4 (s, bipy), 148.3 (s, bipy), 133.4 (s, bipy), 133.0 (s, bipy), 126.1 (s, bipy), 125.5 (s, bipy), 120.4 (s, bipy), 120.2 (s, bipy), 45.2 (s, CH$_2$), 37.5 (s, CH), 32.3 (s, CH$_2$), 27.6 (s, CH$_2$), 22.3 (s, CH$_3$).

The values of the NMR spectra are in accordance with reported literature data.[4]

BipyNi(Et)$_2$ (11)

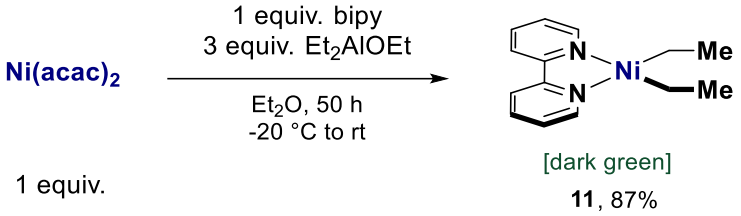

Following a slightly modified procedure,[5] in a flame dried Schlenk under argon, Ni(acac)$_2$ (2.56 g, 9.96 mmol, 1 equiv.) and bipy (1.56 g, 9.96 mmol, 1 equiv.) are mixed together at 25 °C in 40 mL of Et$_2$O. Then, this light green unsoluble mixture is cooled down to –20°C using an aliphatimine-ice bath. At this point, 4.5 mL of Et$_2$AlOEt (3.89 g, 29.9 mmol, 3 equiv.) is carefully added dropwise under argon, and the resulting mixture is stirred at –20 °C for 2 h. After 2 h, the bath is removed and the solution is allowed to warm up to 25 °C and is kept stirring for 50 h at 25 °C under positive argon flow. At this point, addition of 10 mL of pentane followed by filtration using D3 fritte and washing with Et$_2$O and pentane gave 2.36 g (8.65 mmol, 87%) of **11** as a dark green solid.

^{1}H NMR (400 MHz, C$_6$D$_6$, 25 °C) δ 9.19 (d, *J* = 5.6 Hz, 2H, Ar*H*), 7.02 (t, *J* = 7.1 Hz, 2H, Ar*H*), 6.75 (d, *J* = 7.9 Hz, 2H, Ar*H*), 6.60 (t, *J* = 6.3 Hz, 2H, Ar*H*), 1.76 (app t, *J* = 7.2 Hz, 6H, C*H*$_3$), 1.68 (app t, *J* = 7.4 Hz, 4H, C*H*$_2$).

^{13}C NMR (101 MHz, C$_6$D$_6$, 25 °C) δ 154.5, 147.7, 133.3, 125.9, 120.4, 16.4, 11.4.

The characterization data is in accordance with reported literature values.[5]

BipyNi($OCH_2CH_2CH_2CH_2$) (1a)

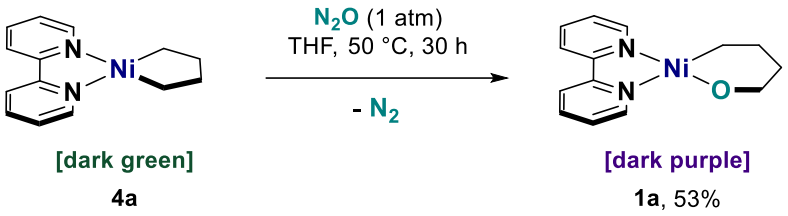

[dark green] **4a** [dark purple] **1a**, 53%

Following a reported procedure,[4] a solution of 194 mg (0.716 mmol) of Ni complex **4a** in 20 mL of THF was exposed to N_2O atmosphere (about 1atm) for 30 h at 50 °C. (47-53 °C due to heating regulation). The solution changed from deep green to deep blue after 12 h, and further turned dark purple upon time. The bluish-purple solution was filtered through D4 fritte, and the insoluble materials were washed with THF until the filtrate was colorless. The resulting solution was concentrated under high vacuum until about 1 mL or less. Pentane was then added (9 mL), allowing further precipitation. The solids were then filtered off under argon, through D3 fritte, washed 3 times with pentane (3×4 mL), and residual solvent was removed under high vacuum to afford 110 mg (0.383 mmol, 53% yield) of the complex **1a** as deep purple microcrystalline solid.

Note: The solution in C_6D_6 is deep blue.

^{1}H NMR (400 MHz, C_6D_6, 25 °C) δ 9.73 (d, *J* = 4.9 Hz, 1H, Ar*H*), 8.27 (d, *J* = 5.9 Hz, 1H, Ar*H*), 6.95 (t, *J* = 7.0 Hz, 1H, Ar*H*), 6.88 (t, *J* = 7.5 Hz, 1H, Ar*H*), 6.83 (d, *J* = 7.8 Hz, 1H, Ar*H*), 6.76 – 6.73 (m, 1H, Ar*H*), 6.70 (d, *J* = 7.8 Hz, 1H, Ar*H*), 6.28 (t, *J* = 6.3 Hz, 1H, Ar*H*), 4.09 (t, *J* = 5.2 Hz, 2H, OC*H*$_2$), 2.11 (p, *J* = 5.3 Hz, 2H OCH_2CH_2), 2.06 (t, *J* = 6.6 Hz, 2H, NiC*H*$_2$), 1.34 (p, *J* = 6.3 Hz, 2H, $NiCH_2CH_2$).

^{13}C NMR (151 MHz, C_6D_6, 25 °C) δ 155.9, 151.2, 148.1, 147.3, 135.9, 132.8, 124.7, 124.3, 120.8, 118.5, 65.4, 39.1, 26.7, 15.7.

The characterization data is in accordance with reported literature values.[4]

Note: It was noticed that remaining Ni particles were contaminating the samples of all oxanickelacycles. Therefore, to increase their purity, solution in minimal amount of THF were prepared in a Schlenk. Then, about the same weight of Avicel was introduced to trap the particles. Filtration under argon and through D4 fritte allowed the isolation of each complex in purities ranging from 83 to 95%.

BipyNi(OCHMeCH$_2$CH$_2$CH$_2$) (1b)

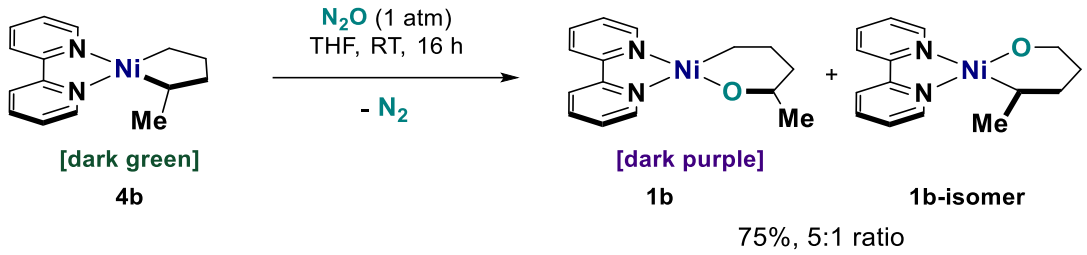

Following a reported procedure,[4] a solution of 450 mg (1.58 mmol, 1 equiv.) of Ni complex **4b** in 20 mL of THF was exposed to N_2O atmosphere (about 1atm) for 16 h at 25 °C. The solution changed from deep green to deep blue after 7 h, and further turned dark purple upon time. The purple solution was filtered, through D4 fritte, and the insoluble materials were washed with THF until the filtrate was colorless. The resulting solution was concentrated under high vacuum until about 5 mL. Pentane was then added (45 mL), allowing further precipitation. The solids were filtered off under argon, through D3 fritte, washed 3 times with pentane (3×10 mL), and residual solvent was removed under high vacuum to afford 355 mg (1.17 mmol, 75% yield) of the complex **1b** as deep purple microcrystalline solid. It was found that the regioisomer of O-insertion **1b-isomer** is also formed as a minor product in a 5:1 ratio major/minor.

Note: The solution in C_6D_6 is deep blue.

Major **1b**: **^{1}H NMR (600 MHz, C_6D_6, 25 °C)** δ 9.86 (d, *J* = 4.7 Hz, 1H, Ar*H*), 8.33 (d, *J* = 5.7 Hz, 1H, Ar*H*), 6.93 (td, *J* = 7.7, 1.6 Hz, 1H, Ar*H*), 6.83 (t, *J* = 7.6 Hz, 1H, Ar*H*), 6.80 – 6.75 (m, 1H, Ar*H*), 6.75 (d, *J* = 7.8 Hz, 1H, Ar*H*), 6.60 (d, *J* = 7.8 Hz, 1H, Ar*H*), 6.24 (ddd, 7.4, 5.7, 1.2, 1H, Ar*H*), 4.10 (dqd, *J* = 8.5, 5.9, 2.8 Hz, 1H, OC*H*), 2.34 (ddt, *J* = 11.9, 6.0, 2.8 Hz, 1H, OCHCH*H*), 2.15 (dd, *J* = 8.2, 5.1 Hz, 2H, NiC*H*$_2$), 1.76 (d, *J* = 5.9 Hz, 3H, *Me*), 1.61 – 1.52 (m, 1H OCHCH*H*), 1.51 – 1.41 (m, 1H, NiCH$_2$CH*H*), 1.34 – 1.25 (m, 1H NiCH$_2$CH*H*).

^{13}C NMR (151 MHz, C_6D_6, 25 °C) δ 155.9, 151.2, 148.1, 147.5, 135.8, 132.5, 124.7, 124.3, 120.6, 118.3, 68.0, 45.6, 27.7, 26.4, 17.2. The characterization data is in accordance with reported literature values.[4]

Minor **1b-isomer**: not all the peaks are fully resolved: **^{1}H NMR (600 MHz, C_6D_6, 25 °C)** δ 9.82 (d, *J* = 5.0 Hz, 1H, Ar*H*), 8.50 (d, *J* = 5.7 Hz, 1H, Ar*H*), 6.90 – 6.86 (m, 1H, Ar*H*), 6.34 (ddd, *J* = 7.5, 5.7, 1.3 Hz, 1H, Ar*H*), 4.16 (dt, *J* = 8.7, 4.2 Hz, 1H, OCH*H*), 2.28 – 2.20 (m, 1H, OCH$_2$CH*H*), 1.94 (dddd, *J* = 14.3, 11.5, 5.3, 2.9 Hz, 1H, NiCHCH*H*), 1.52 (d, *J* = 7.0 Hz, 3H, *Me*), 0.89 – 0.82 (m, 1H, NiCHCH*H*).

^{13}C NMR (151 MHz, C_6D_6, 25 °C) δ 155.9, 151.3, 148.6, 147.7, 135.7, 132.4, 125.3, 124.4, 120.8, 118.4, 65.9, 35.3, 34.0, 23.0, 22.2.

Table S1. Overview over NMR assignments after 1D and 2D NMR analysis:

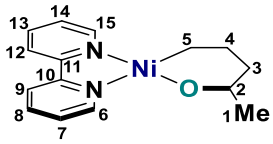

Atom		*δ (ppm)*	*J (hz)*	*COSY*	*HSQC*	*HMBC*	*ROESY*
1	C	27.72			1		
	H3	1.764	5.90(2)	2	1	2, 3	6
2	C	67.951			2	1, 3", 4', 4"	
	H	4.105	5.90(1)	1, 3"	2		
3	C	45.622			3', 3"	1, 4', 4", 5	
	H'	2.337		3", 4', 4"	3	5	
	H"	1.567		2, 3', 4', 4"	3	2, 5	
4	C	26.415			4', 4"	5	
	H'	1.294		3', 3", 5	4	2, 3, 5	
	H"	1.458		3', 3", 5	4	2, 3, 5	
5	C	17.196			5	3', 3", 4', 4"	
	H2	2.15		4', 4"	5	3, 4	15
6	C	148.067			6	7, 8	
	H	9.863	4.70(7)	7	6	7, 8, 10	1
7	C	124.331			7	6, 9	
	H	6.772	4.70(6)	6, 8	7	6, 9	
8	C	135.778			8	6	
	H	6.925	7.80(9)	7, 9	8	6, 10	
9	C	118.293			9	7	
	H	6.746	7.80(8)	8	9	7, 10, 11	
10	C	151.208				6, 8, 9, 12	
11	C	155.909				9, 12, 13, 15	
12	C	120.602			12	14	
	H	6.598	7.60(13)	13	12	10, 11, 14	
13	C	132.475			13	15	
	H	6.823	7.60(14), 7.60(12)	12, 14	13	11, 15	
14	C	124.719			14	12, 15	
	H	6.244	5.70(15), 7.60(13)	13, 15	14	12, 15	
15	C	147.499			15	13, 14	
	H	8.325	5.70(14)	14	15	11, 13, 14	5

Table S2. Overview over NMR assignments after 1D and 2D NMR analysis:

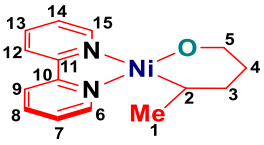

	Atom	*δ (ppm)*	*J (hz)*	*COSY*	*HSQC*	*HMBC*	*ROESY*
1	C	22.958			1		
	H3	1.515	7.00(2)	2	1	2, 3	6
2	C	22.207			2	1	
	H	2.303	7.00(1)	1, 3"	2		6
3	C	35.256			3', 3"	1, 5'	
	H'	0.852		3", 4"	3		
	H"	1.938		2, 3', 4'	3		
4	C	33.971			4', 4"		
	H'	2.24		3", 5"	4		
	H"	2.14		3'	4		
5	C	65.896			5', 5"		
	H'	4.157			5	3	
	H"	4.105		4'	5		
6	C	147.674			6	7	
	H	8.497	5.70(7)	7	6	7, 8, 10	1, 2
7	C	125.261			7	6, 9	
	H	6.336	7.50(8), 5.70(6)	6, 8	7	6, 9	
8	C	132.376			8	6	
	H	6.884	7.50(7)	7, 9	8		
9	C	120.792			9	7	
	H	6.603		8	9	7	
10	C	155.875				6	
11	C	151.327				15	
12	C	118.359			12		
	H	6.746		13	12		
13	C	135.694			13	15	
	H	6.925		12, 14	13		
14	C	124.243			14	15	
	H	6.742	5.00(15)	13, 15	14		
15	C	148.597			15		
	H	9.819	5.00(14)	14	15	11, 13, 14	

BipyNi(OEt)(Et) (1f)

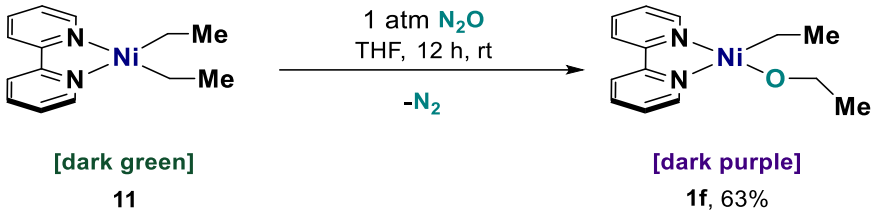

Following a reported procedure,[4] a solution of 520 mg (1.90 mmol, 1 equiv.) of Ni complex **11** in 20 mL of THF was exposed to N_2O atmosphere (about 1atm) for 12 h at 25 °C. The solution changed from deep green to deep violent after 12 h. The purple solution was filtered, through D4 fritte, and the insoluble materials were washed with THF until the filtrate was colorless. The resulting solution was concentrated under high vacuum until about 4 - 5 mL. Pentane was then added (35 mL), allowing further precipitation. The solids were filtered off under argon, through D3 fritte, washed 3 times with pentane (3×10 mL), and residual solvent was removed under high vacuum to afford 345 mg (1.19 mmol, 63% yield) of the complex **1f** as deep purple microcrystalline solid.

Note: The solution in C_6D_6 is deep blue.

^{1}H NMR (600 MHz, C_6D_6, 25 °C) δ 9.80 (dd, *J* = 5.7, 1.8 Hz, 1H, Ar*H*), 8.58 (d, *J* = 5.8 Hz, 1H, Ar*H*), 6.91 (td, *J* = 7.7, 1.7 Hz, 1H, Ar*H*), 6.85 (td, *J* = 7.7, 1.4 Hz, 1H, Ar*H*), 6.74 (ddd, *J* = 7.0, 3.7, 1.8 Hz, 2H, Ar*H*), 6.60 (dt, *J* = 7.9, 1.0 Hz, 1H, Ar*H*), 6.29 (ddd, *J* = 7.3, 5.8, 1.5 Hz, 1H, Ar*H*), 4.11 (q, *J* = 6.7 Hz, 2H, OCH_2), 1.81 (t, *J* = 6.7 Hz, 3H, OCH$_2$CH_3), 1.68 (q, *J* = 7.7 Hz, 2H, NiCH_2), 1.48 (t, *J* = 7.7 Hz, 3H, NiCH$_2$CH_3).

^{13}C NMR (151 MHz, C_6D_6, 25 °C) δ 149.2, 148.3, 136.0, 132.6, 125.4, 124.3, 120.7, 118.3, 61.0, 23.1, 15.9, 10.2.

The characterization data is in accordance with reported literature values.[4]

Impurity: free bipyridine, in *ca.* 10-12%. **^{1}H NMR (600 MHz, C_6D_6, 25 °C)** δ 8.74 (d, *J* = 8.0 Hz, 1H), 8.53 (ddd, *J* = 4.8, 1.8, 1.0 Hz, 2H), 7.20 (td, *J* = 7.7, 1.8 Hz, 2H), 6.68 (ddd, *J* = 7.4, 4.7, 1.2 Hz, 2H).

^{13}C NMR (151 MHz, C_6D_6, 25 °C) δ 156.0, 151.2, 136.6, 123.7, 121.2.

The purity of the oxanickelacycles (**1a-b**, **1f**) was assessed by ^{1}H NMR using acenaphthene as internal standard (unreactive and high solubility in benzene-d_6).

In a typical example, pictures for the synthesis of 1f:

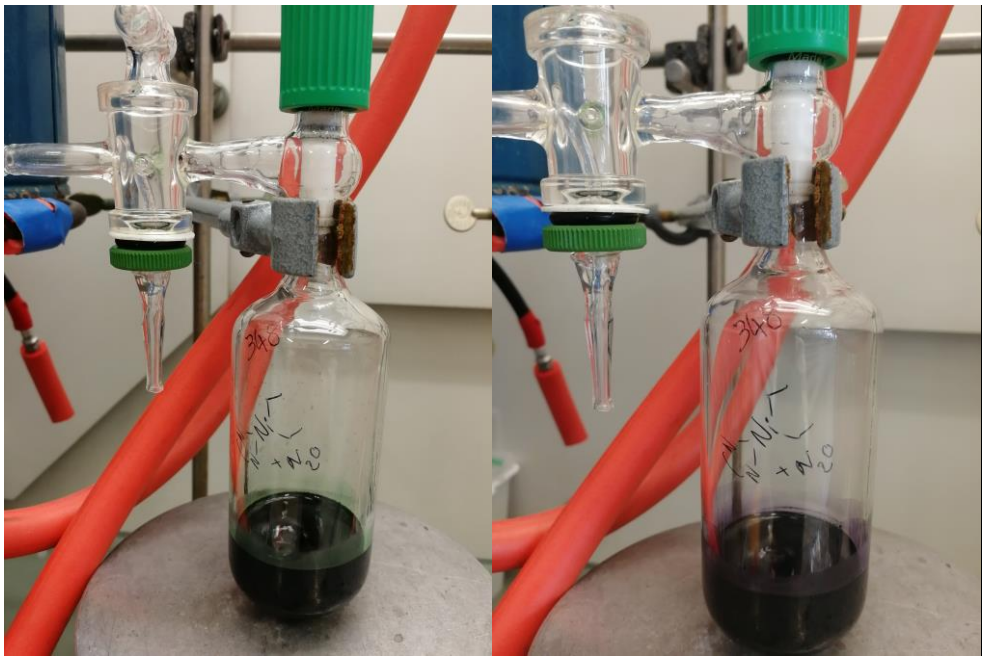

Fig. 1. Left: t = 0 h, green color; right: t = 12 h, purple color.

Fig. 2. Set up for filtration of complex **1f**, before and during.

3. Cyclic voltammetry studies of compound 1b

Cyclic voltammetry (CV) was performed with a Metrohm Autolab PGSTAT101 potentiostat and processed using Metrohm Autolab Nova software 2.1. A cylindrical three-electrode cell was equipped with a glassy carbon working electrode (⌀ 3 mm), a platinum wire as the counter electrode and $Ag/AgNO_3$ (0.01 M) electrode as the reference electrode. The scan rate for a typical experiment was 100 $mV \cdot s^{-1}$. The scan direction was negative. The solution of Ni complex (1.0×10^{-3} M) was prepared in a glovebox, using 5 mL of dry and degassed CD_3CN. The cell was purged with Argon gas for about 10 min. The light purple Ni complex solution was transferred to the cell, and solid *n*-Bu_4NPF_6 was added to reach a concentration of 0.2 M. The cyclic voltammetry was carried out under an Ar gas atmosphere at room temperature. CV of the complex alone was first measured. Then CV of ferrocene was measured, but fast decomposition of the complexes occurred.

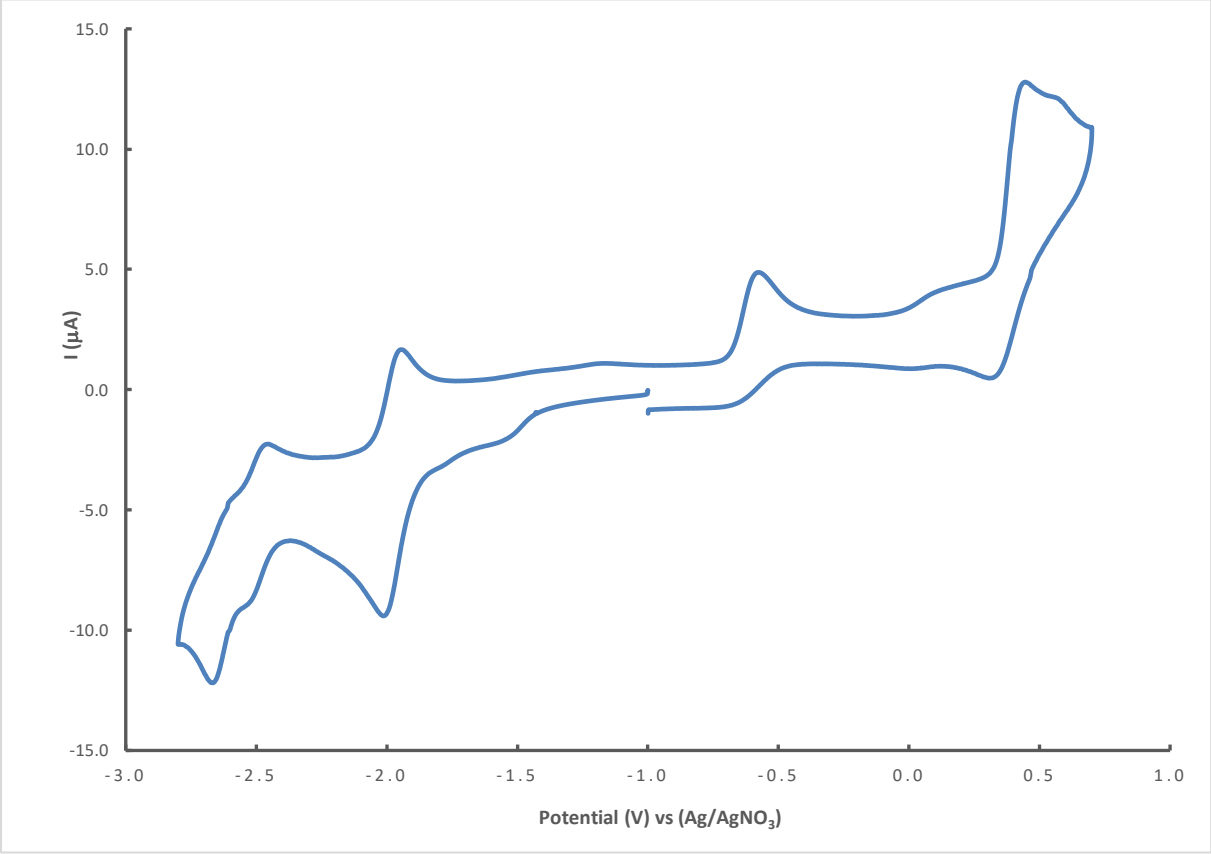

Fig. 3. Full spectra of the cyclic voltammogram for complex **1b** in CD_3CN.

As the reactivity discussed in the manuscript is only based on oxidation, a zoom on the oxidation part is proposed to ensure good reading.

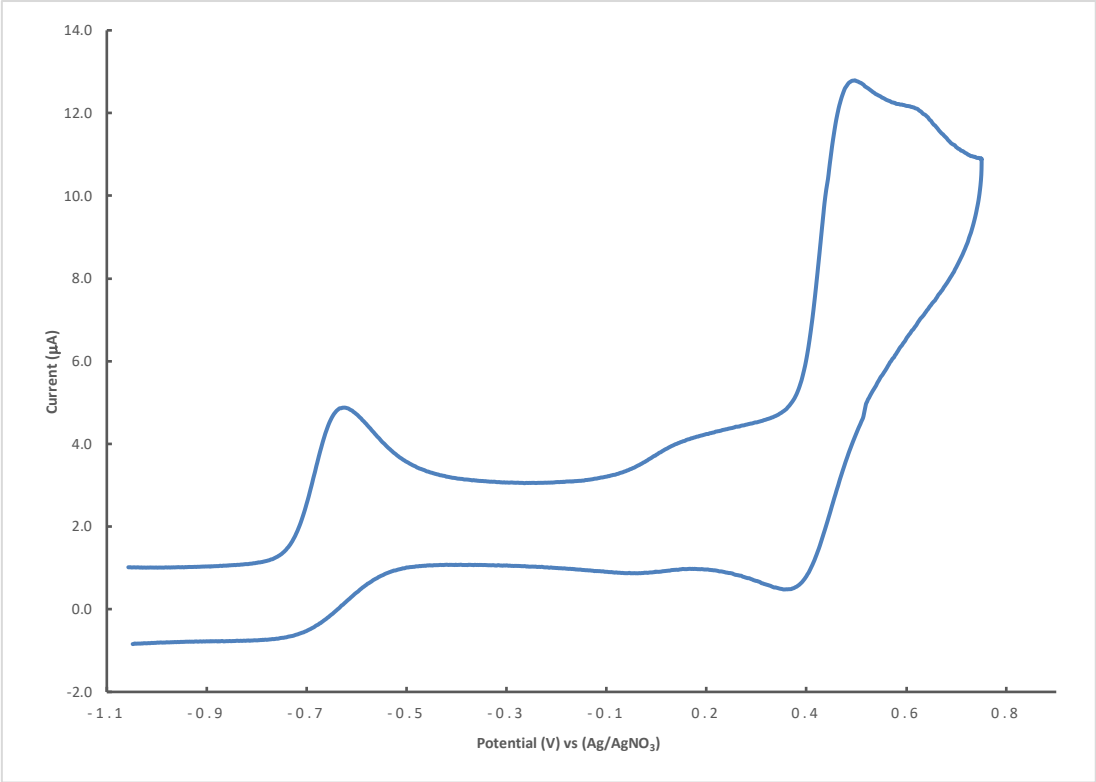

Fig. 4. Zoom on the oxidation window of the cyclic voltammogram for complex **1b** in CD_3CN.

The $E_{1/2}$ value of the ferrocene–ferrocenium (Fc/Fc^+) vs. $Ag/AgNO_3$ in CD_3CN was $E_{1/2}$= 0.106 + 0.045 / 2 = 0.076 V in this measurement. Therefore, the potential against reference are as followed:

For reduction, $E_{1/2}(Ni^{I}/Ni^{II})$ = –1.98 V, $E_{1/2}(Ni^{0}/Ni^{I})$ = –2.63 V;

And for oxidation: $E_{1/2}(Ni^{II}/Ni^{III})$ = –0.63 V, $E_{1/2}(Ni^{III}/Ni^{IV})$ = +0.39 V;

And the potentials against Fc/Fc^+ are as follow:

For reduction, $E_{1/2}(Ni^{I}/Ni^{II})$ = –2.06 V, $E_{1/2}(Ni^{0}/Ni^{I})$ = –2.71 V;

And for oxidation: $E_{1/2}(Ni^{II}/Ni^{III})$ = –0.70 V, $E_{1/2}(Ni^{III}/Ni^{IV})$ = +0.31 V.

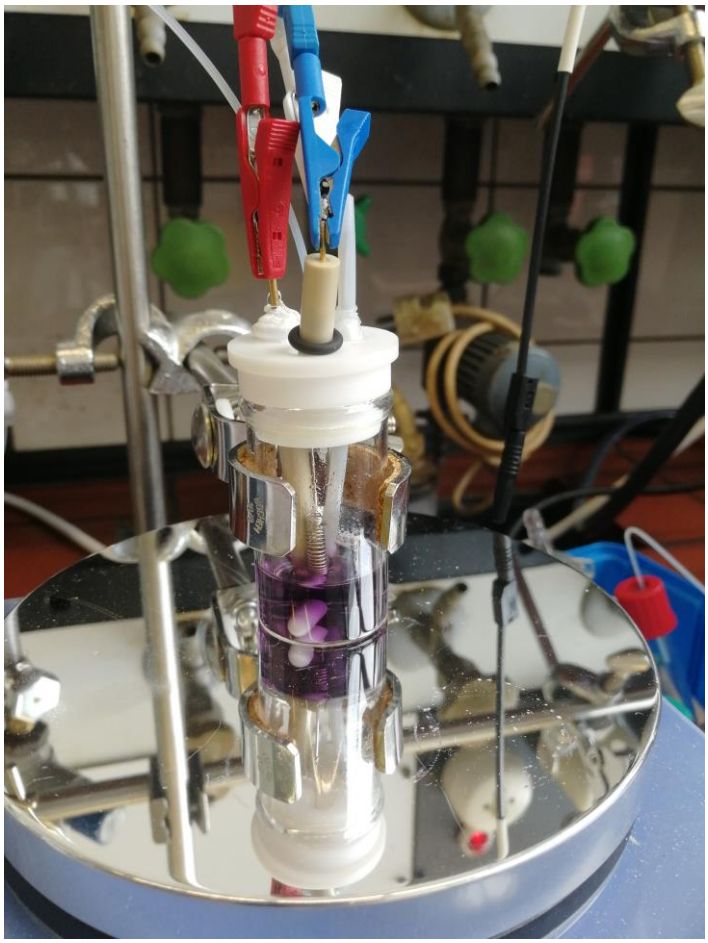

Fig. 5. Set-up of the cell for CV measurements of complex **1b**.

4. Photoredox reactivity

In a typical experiment,[6] in a glovebox filled with argon, Ni complex **1b** (2.0 mg, 6.6 μmol, 1 equiv.) and recrystallized 4CzIPN **5** (2.1 mg, 2.7 μmol, 0.40 equiv.) were introduced in a small vial containing a Teflon coated stir bar. Then, outside the glovebox, under argon flow, 1.5 mL of benzene-d_6 was added in the vial, and the resulting dark but fully soluble solution was stirred for 12 h under blue light irradiation (1 Kessil lamp, closest position, at 25 °C (air stream)). Finally, the solution was transferred into a NMR tube filled with argon for analysis. Alternatively, the reaction was also tested directly in a J-Young NMR tube, using a more concentrated solution (0.8 mL of benzene-d_6 instead of 1.5 mL for vial reaction). Nevertheless, 2-Me-THF (**2b**) was not observed, and the major side product was pent-4-en-2-ol (**6b**). In the reaction run in J-Young NMR tube, the conversion was checked after 2 h and low reactivity was observed with remaining starting material present. We wondered if the photocatalyst was fully soluble and the same experiment was then run in THF-d_8.

Therefore, in a similar manner, the reaction was repeated with THF-d_8 as solvent instead of benzene-d_6 to ensure full solubility of the photocatalyst. In a glovebox filled with argon, Ni complex **1b** (2.0 mg, 6.6 μmol, 1 equiv.) and recrystallized 4CzIPN **5** (2.1 mg, 2.7 μmol, 0.40 equiv.) were introduced in a small vial containing a Teflon coated stir bar. Then, outside the glovebox, under argon flow, 1.5 mL of THF-d_8 was added in the vial, and the resulting dark but fully soluble solution was stirred for 12 h under blue light irradiation (1 Kessil lamp, closest position, at 25 °C (air stream)). Finally, the solution was transferred into a NMR tube filled with argon for analysis. Alternatively, the reaction was also tested directly in a J-Young NMR tube, using a more concentrated solution (0.8 mL of THF-d_8 instead of 1.5 mL for vial reaction). Nevertheless, 2-Me-THF (**2b**) was not observed, and the major side product was pent-4-en-2-ol (**6b**).

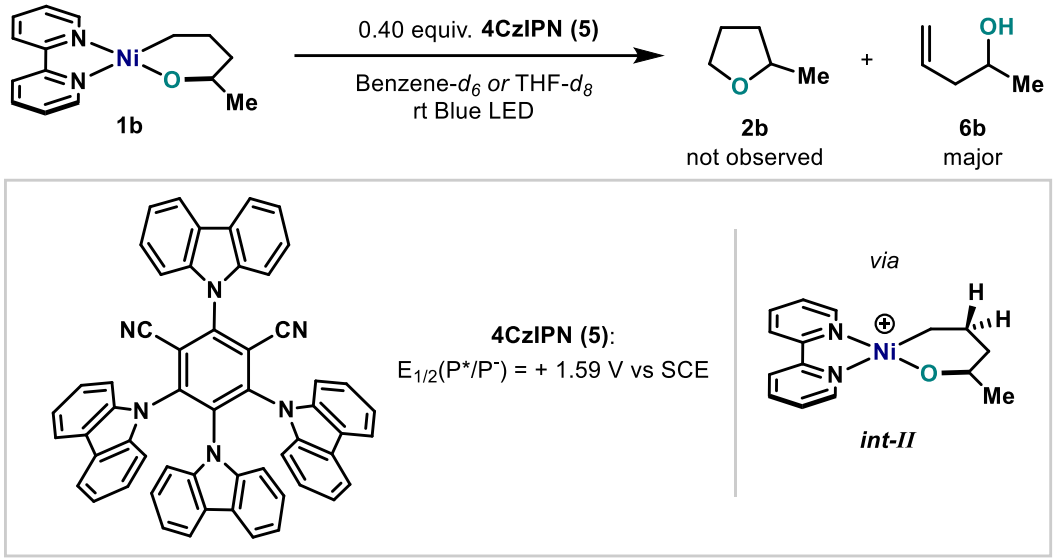

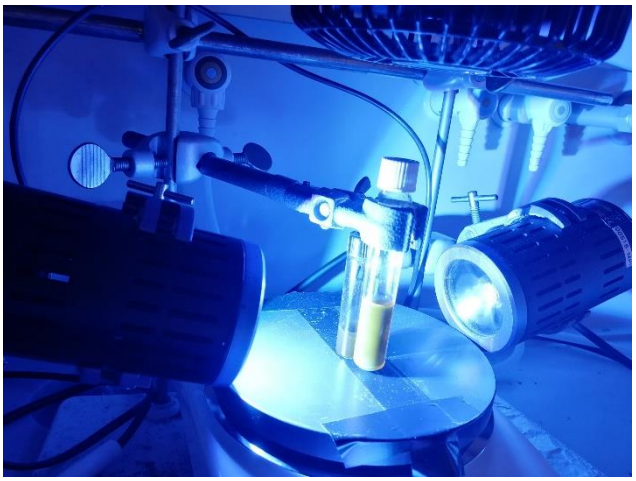

Fig. 6. Set-up used for trials of photoredox catalysis, only one lamp is turned on.

5. Reactivity with iodine

5.1 Product distribution:

5.1.1. Reaction of 1a with iodine:

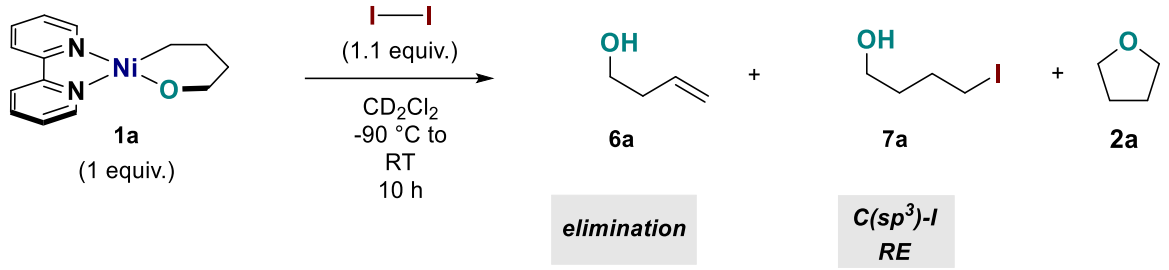

In a glovebox, oxanickelacycle **1a** (8.6 mg, 0.030 mmol, 1 equiv) is inserted in a J-Young NMR tube. Then, outside of the glovebox, a precooled solution of 0.4 mL of iodine (8.4 mg, 0.033 mmol, 1.1 equiv., under argon) in CD_2Cl_2 is added to a solution of **1a** in 0.2 mL of CD_2Cl_2 (in the NMR tube, in dry ice). The reaction is then transferred in a NMR probe, which was precooled at –90 °C, and the NMR is recorded at several temperatures, increasing every 10 °C. A paramagnetic dimer **9a** is observed, which evolved quickly at temperature higher than –10 °C (*See section 5.2.1.1*). At the end of the process (about 5 hours), no more Ni^{III} is observed. Precipitation on the side wall of the tube led to the loss of the shim. In the last NMR at 25 °C, the crude mixture indicates possible presence of the 4-iodobutan-1-ol[7] (**7a**) along with but-3-en-1-ol[8] (**6a**) and traces of THF (**2a**). After 10 h standing in the NMR tube, the mixture is filtered through an HPLC filter, and the proposed product distribution is confirmed by NMR spectroscopy. This sample was also submitted to HRMS, which confirmed the presence of iodoalcohol **7a**.

HRMS (ESI) calcd for $C_4H_9IO^+$ $[M+H]^+$ 199.96926; found 199.96928.

The following HSQC is measured after filtration of the reaction after 10 h in a NMR tube at 25 °C. In the blue square, cross-peaks confirmed that the peaks at 3.20 ppm in ^1H NMR corresponds to the peaks at 7.3 ppm in the ^{13}C NMR, and can be attributed to the CH_2–I of **7a**. THF **4a** and byproduct **6a** are also confirmed in this NMR experiment by cross-peaks.

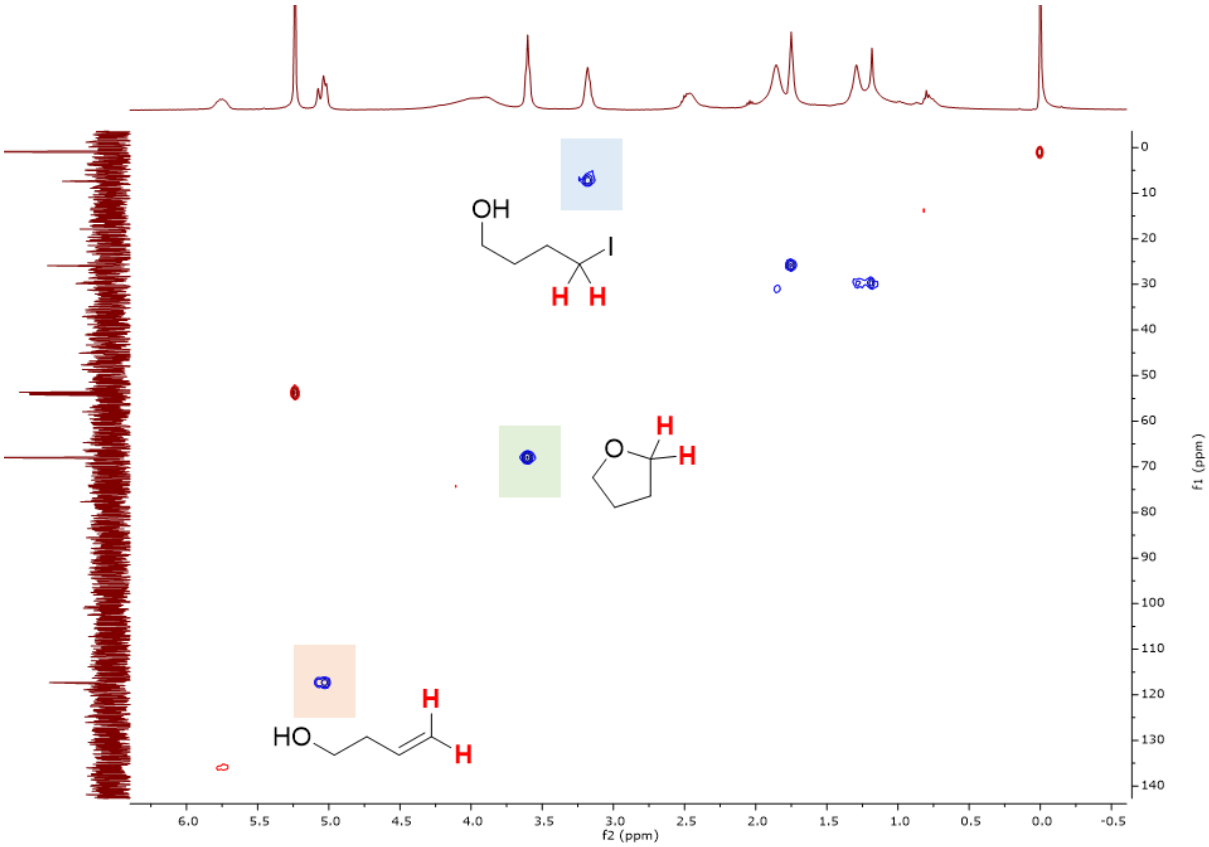

Fig. 7. HSQC of the crude mixture after filtration through HPLC filter, after 10 h.

5.1.1. Reaction of 1b with iodine:

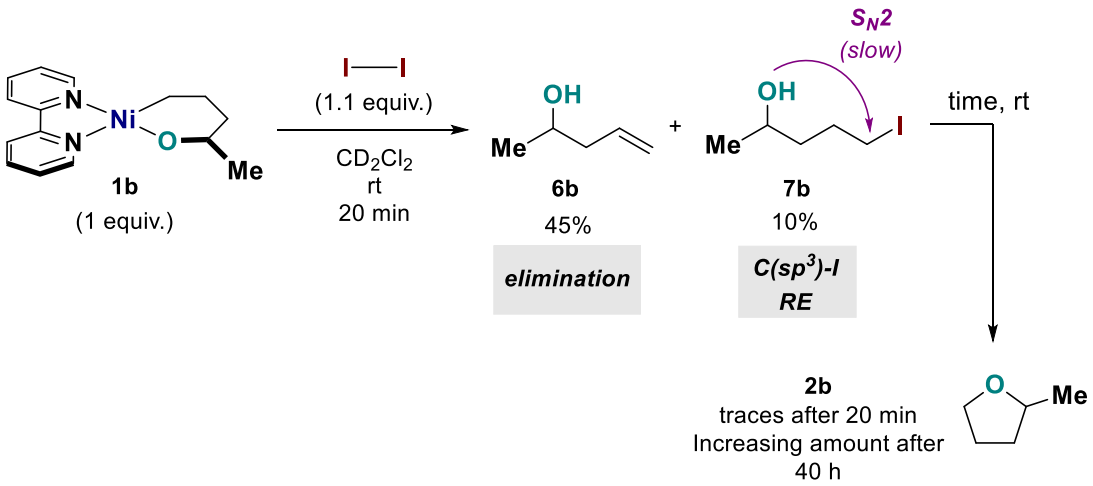

In a glovebox, oxanickelacycle **1b** (5.0 mg, 0.017 mmol, 1 equiv.) is introduced in a vial with a Teflon coated stir bar, and dissolved in 0.4 mL of CD_2Cl_2 at RT. Then, to this solution of **1b** is added a solution of 0.3 mL of iodine (4.2 mg, 0.017 mmol, 1 equiv.) in CD_2Cl_2 at 25 °C. The reaction is stirred for 20 min, during which the color quickly change from deep purple to dark

orange to light brown. This solution is then filtered using HPLC filter, directly in a NMR tube, thus giving a solution suitable for analysis by NMR. Internal standard *para*-fluoronitrobenzene (2.0 mg, 0.0142 mmol, 0.85 equiv.) is added and the product distribution is observed in figure 8.

The experiment was also repeated as followed: In a glovebox, oxanickelacycle **1b** (9.0 mg, 0.030 mmol, 1 equiv.) is introduced in a J-Young NMR tube. Then, outside of the glovebox, a precooled solution of 0.4 mL of iodine (8.4 mg, 0.033 mmol, 1.1 equiv., under argon) in CD_2Cl_2 is added to a solution of **1b** in 0.2 mL of CD_2Cl_2 (in the NMR tube, in dry ice). The reaction is then transferred in a NMR probe, which was precooled at –90 °C. And the NMR is recorded at several temperatures, increasing every 10 °C. A paramagnetic dimer **9b** is observed which evolved quickly at temperature higher than 0 °C (*See section 5.2.1.2*). At the end of the process (about 5 hours), no more Ni^{III} is observed. Precipitation on the side wall of the tube led to the loss of the shim. In the last NMR at 25 °C, the crude mixture indicates possible presence of the 5-iodopentan-2-ol[9] (**7b**) along with pent-4-en-2-ol[10] (**6b**) and very small traces of THF (**2b**). After 10 h standing in the NMR tube, the mixture is filtered through an HPLC filter, and the proposed product distribution is confirmed by NMR spectroscopy. This sample was also submitted to GC-MS, which confirmed the presence of iodoalcohol **7b**.

Only ^{13}C shift are listed below, as most of the ^{1}H shifts are overlapping. (*vide infra*)

For **7b**: **^{13}C NMR (151 MHz, CD_2Cl_2)** δ 67.4, 40.3, 30.4, 23.9, 7.6.

For **6b**: **^{13}C NMR (151 MHz, CD_2Cl_2)** δ 135.5, 117.8, 67.3, 44.2, 23.0.

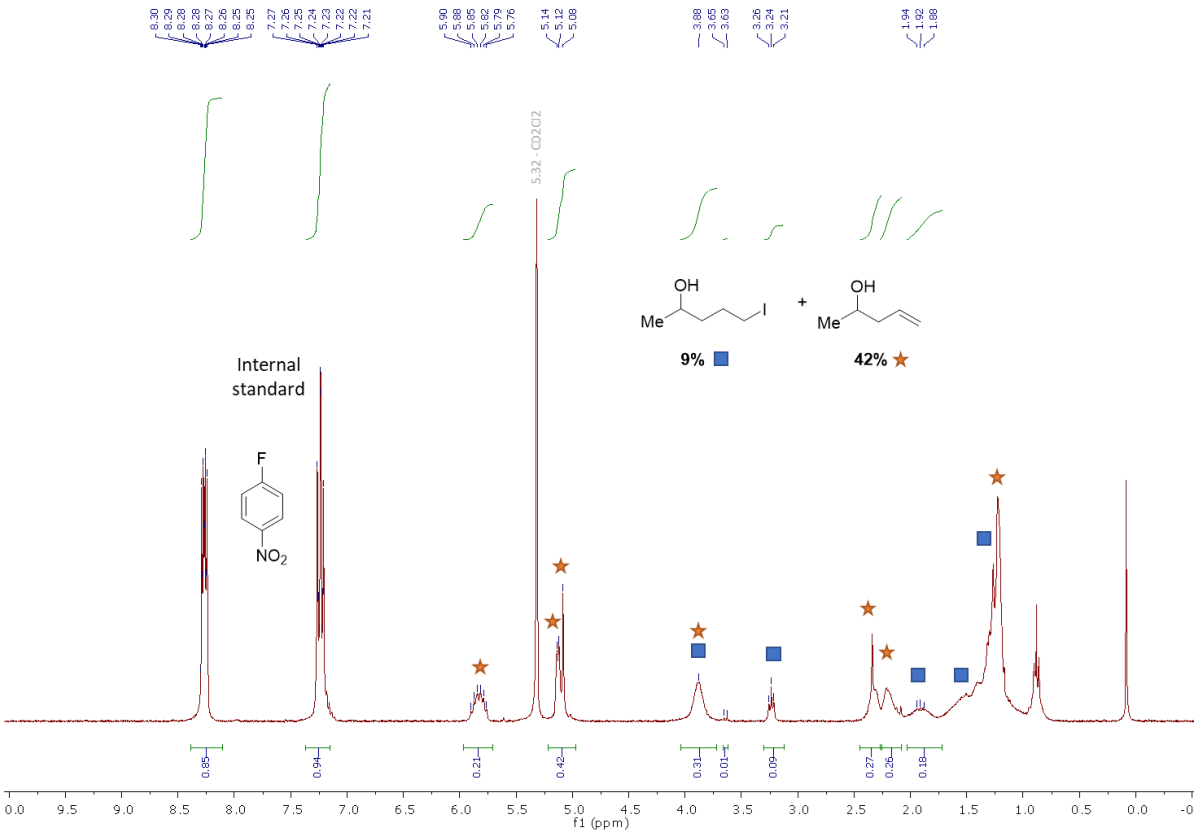

Fig. 8. Reaction of **1b** with iodine, stopped after 20 min, followed by filtration.

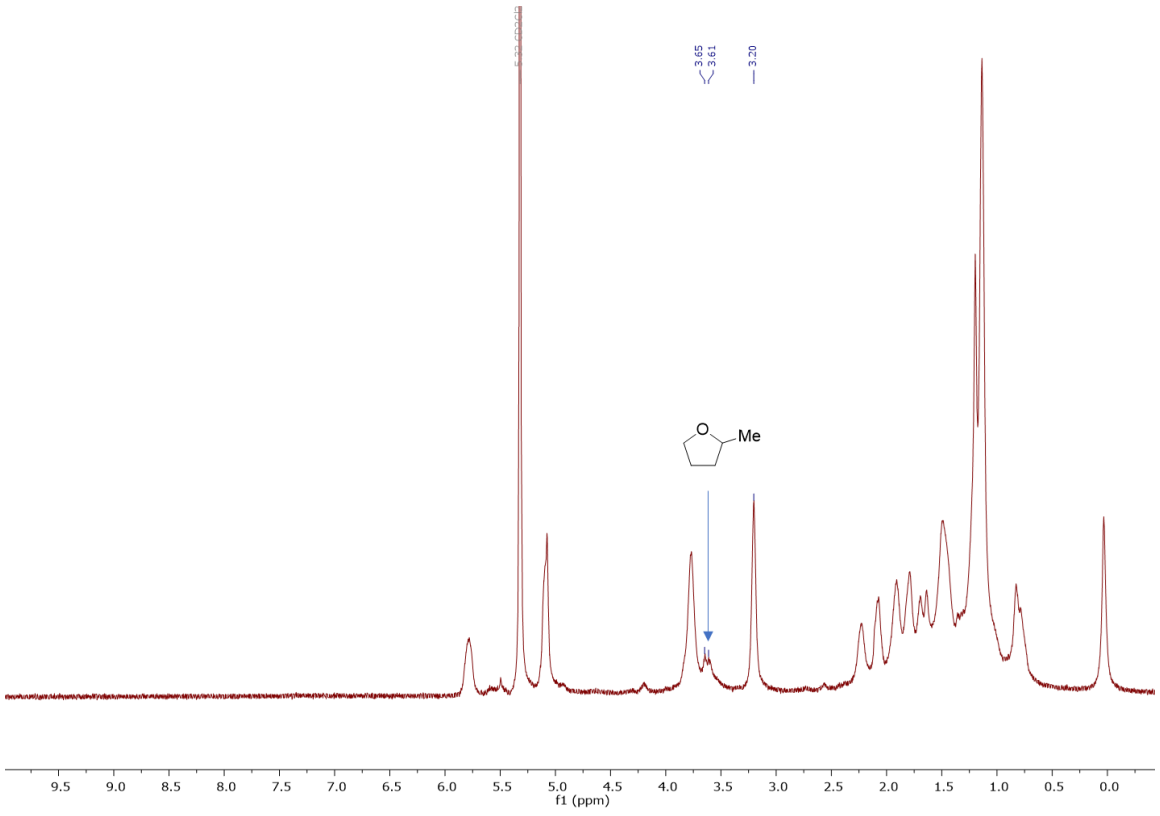

Fig. 9. Reaction of **1b** with iodine in NMR tube for 40 h, followed by filtration.

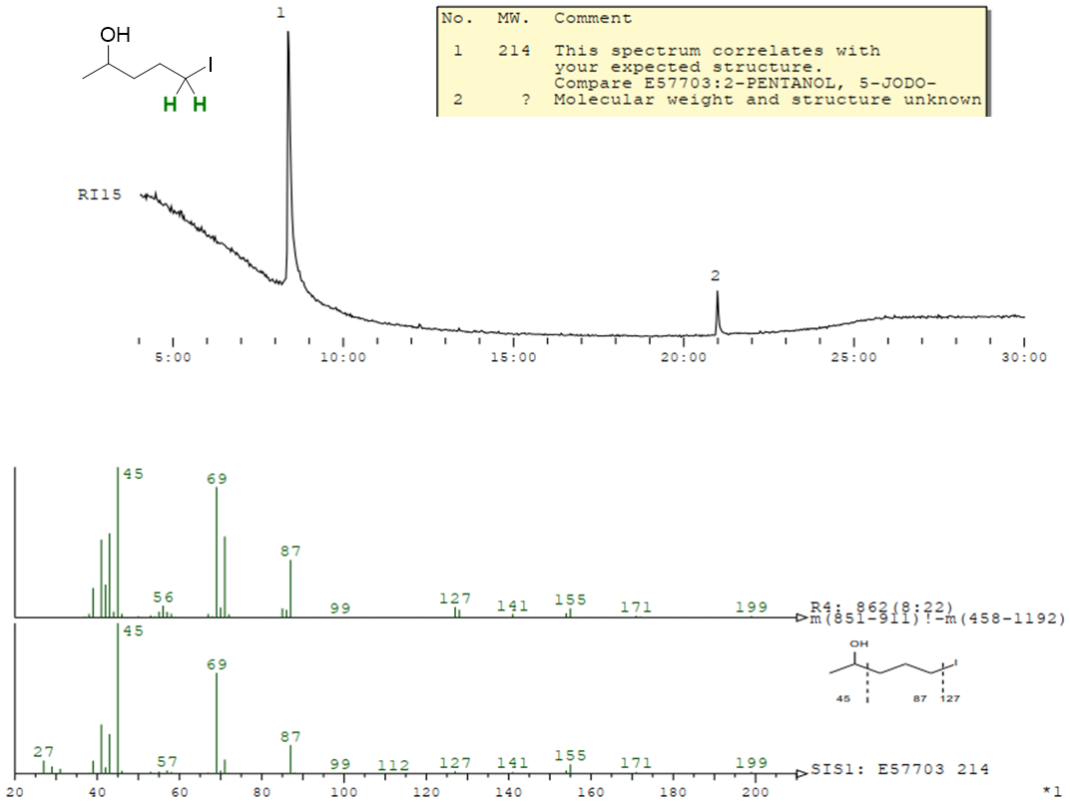

Fig. 10. GS-MS spectra of the crude reaction mixture of **1b** with iodine, stopped after 20 min.

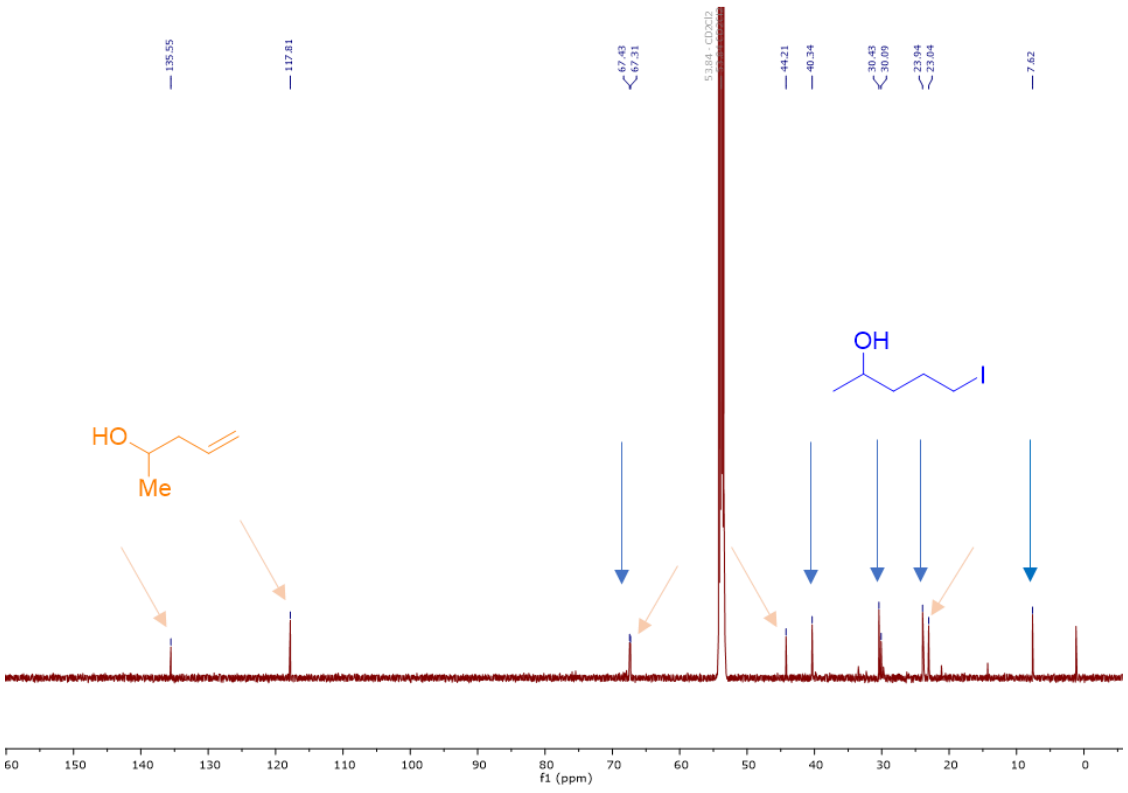

Fig. 11. ^{13}C NMR spectrum of the crude mixture after filtration using HPLC filter, after 40 h.

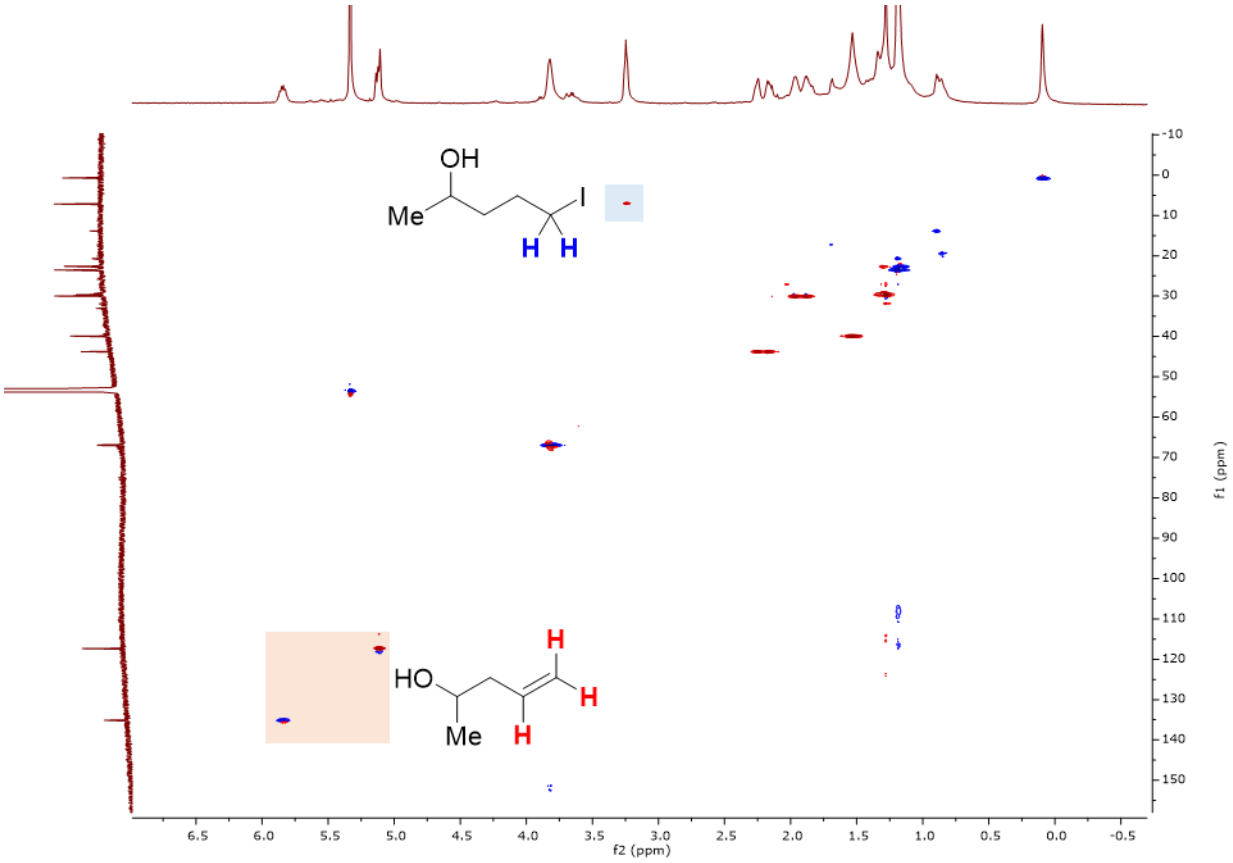

Fig. 12. HSQC of the crude mixture after filtration using HPLC filter, after 40 h.

To further support the presence of iodoalcohols in crude mixture, a comparison with an authentic sample of 1-iodooctane in CD_2Cl_2 was undertaken. Figure 13 revealed that triplet around 3.20−3.25 ppm is a good indication of RCH_2CH_2–I.

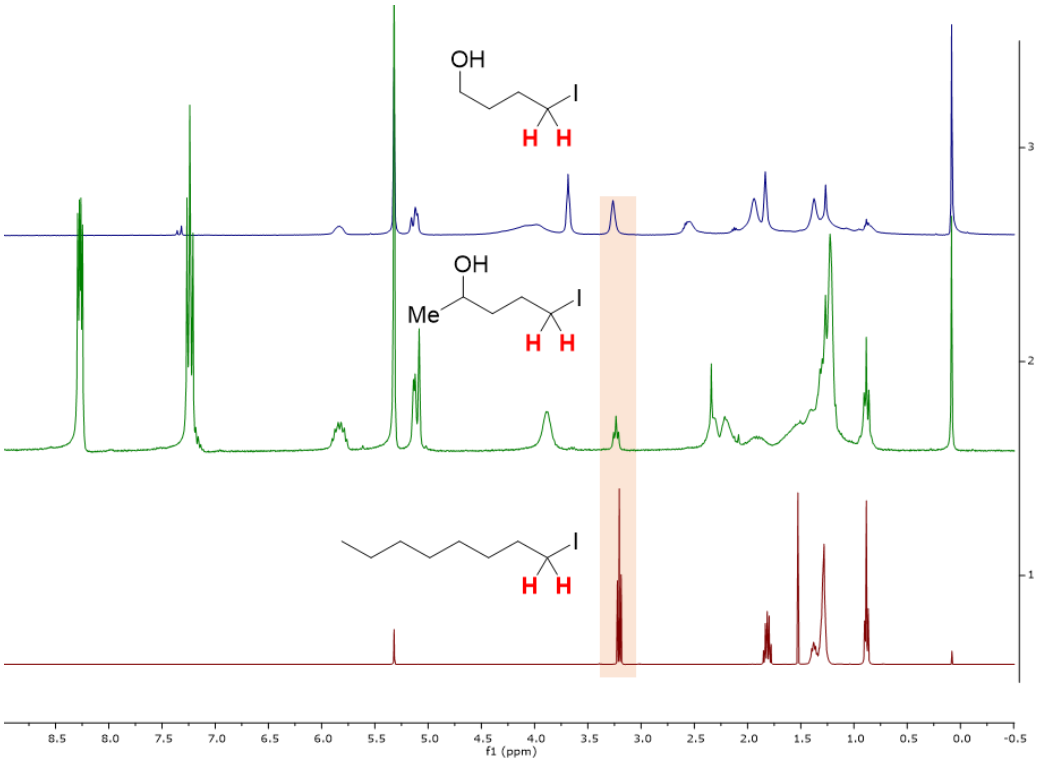

Fig. 13. Comparison of ^{1}H NMR in CD_2Cl_2 of crude mixtures containing iodoalcohol **7a** (top), **7b** (middle) and an authentic sample of 1-iodooctane (bottom)

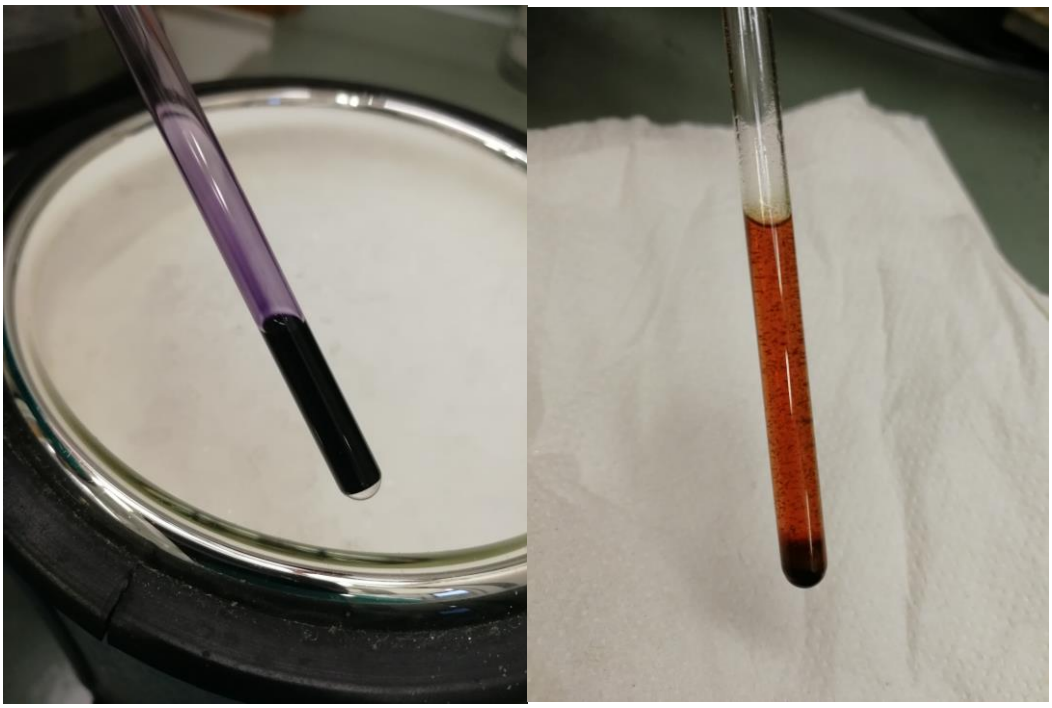

Fig. 14. Typical color of CD_2Cl_2 solutions of oxanickelacyclohexane complexes before (left) and after (right) addition of iodine solution.

5.2. Characterization of dimeric Ni^{III}-Ni^{III} complex

5.2.1 NMR Measurements

5.2.1.1 Using substrate 1a: Ni^{III}-Ni^{III} complex (9a)

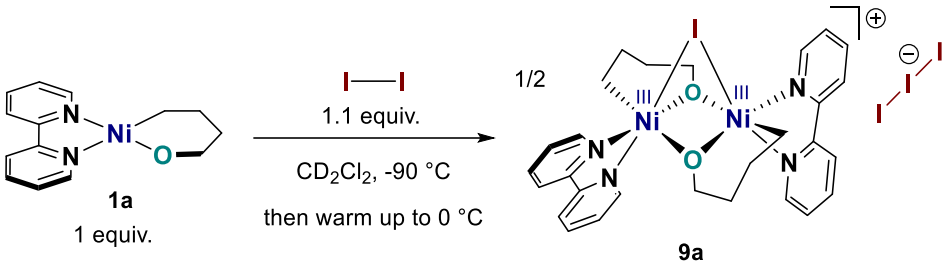

In a glovebox, oxanickelacycle **1a** (8.6 mg, 0.030 mmol, 1 equiv.) is introduced in a J-Young NMR tube. Then, outside of the glovebox, in dry ice, a precooled solution of 0.4 mL of iodine (8.4 mg, 0.033 mmol, 1.1 equiv., under argon) in CD_2Cl_2 is added to a solution of **1a** in 0.2 mL of CD_2Cl_2 (in the NMR tube). The reaction is then transferred in a NMR probe, which was precooled at –90 °C. And the NMR is recorded at several temperatures, increasing every 10 °C up to 25 °C. ^{1}H NMR characterization was possible at low temperature. Attempts for 2D characterization or ^{13}C proved unsuccessful due to the high paramagnetic nature of this intermediate. This dimer rapidly evolved and decomposed at temperatures higher than 0 °C. This led to precipitation of solid particles on the wall of the NMR tube, thus rendering NMR analysis completely impossible. (broad waves only).

^{1}H NMR (400 MHz, CD_2Cl_2, –90 °C) δ 237.3 (s, 1H), 109.2 (s, 1H), 104.6 (s, 1H), 95.5 (s, 1H), 68.2 (s, 1H), 60.3 (s, 1H), 38.8 (s, 1H), 36.2 (s, 1H), 30.7 (s, 1H), 22.0 (s, 1H), 18.9 (s, 1H), 15.2 (s, 1H), 11.0 (s, 1H), 3.3 (s, 1H), –98.0 (s, 1H), –932.5 (s, 1H).

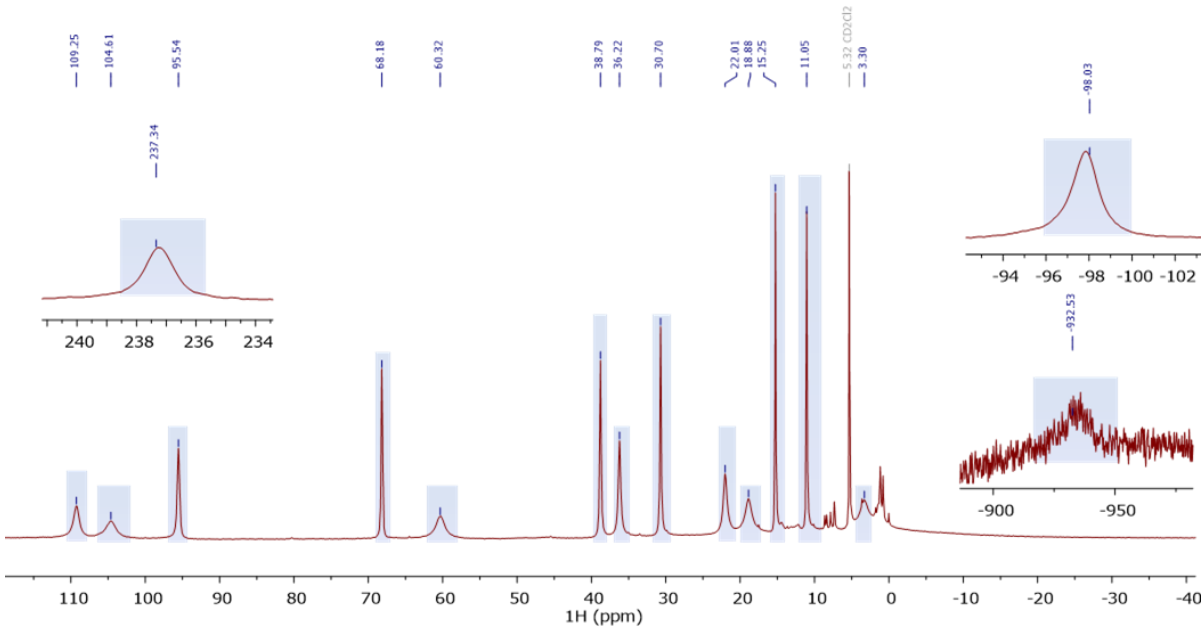

Fig. 15. ^{1}H NMR spectrum of dimer complex **9a** at –90 °C in CD_2Cl_2.

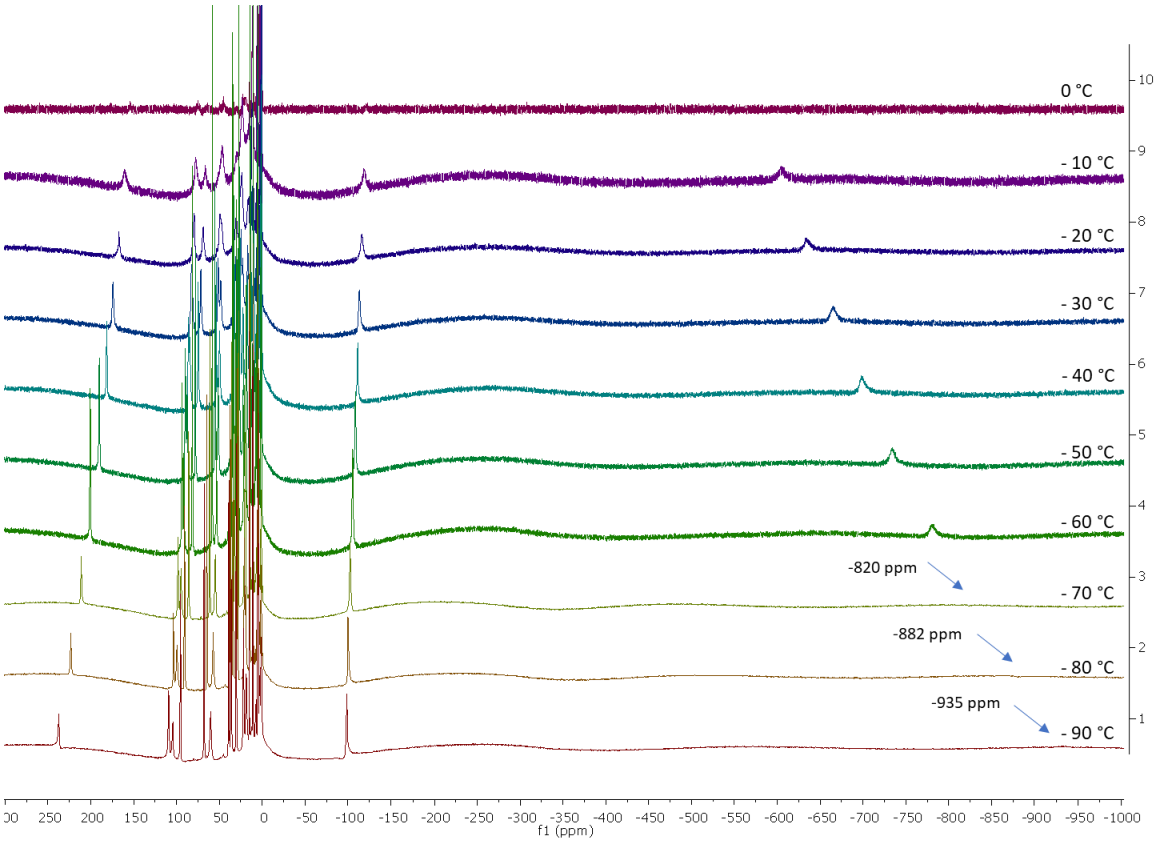

Fig. 16. VT ^{1}H NMR spectra of dimer complex **9a** in CD_2Cl_2 from –90 to 0 °C.

Interestingly, it is possible to plot the shifts vs 1/T (in K^{-1}) and to verify that our system actually follows Curie´s paramagnetism law with a linear relationship. 3 examples are shown below.

For the peaks between 0 and +110 ppm, it can be possible to do the same plot, but from -90 to –40 °C only, as at –30 °C or higher there is overlapping of several peaks.

See below for 3 examples, between –90 and –10 °C, before full decomposition:

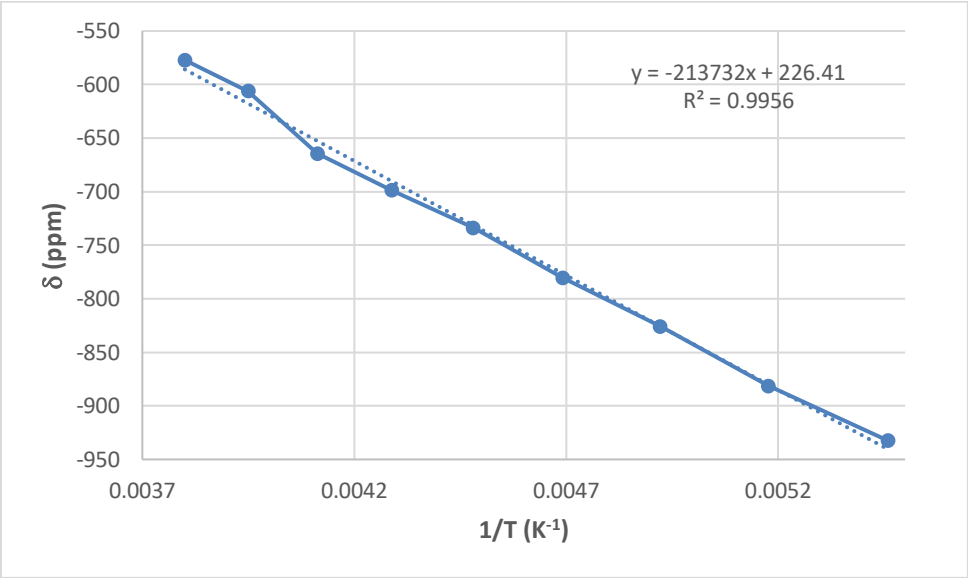

Fig. 17. VT ^{1}H NMR shift vs 1/T (K^{-1}) for the proton at –932.5 ppm, between –90 and –10 °C.

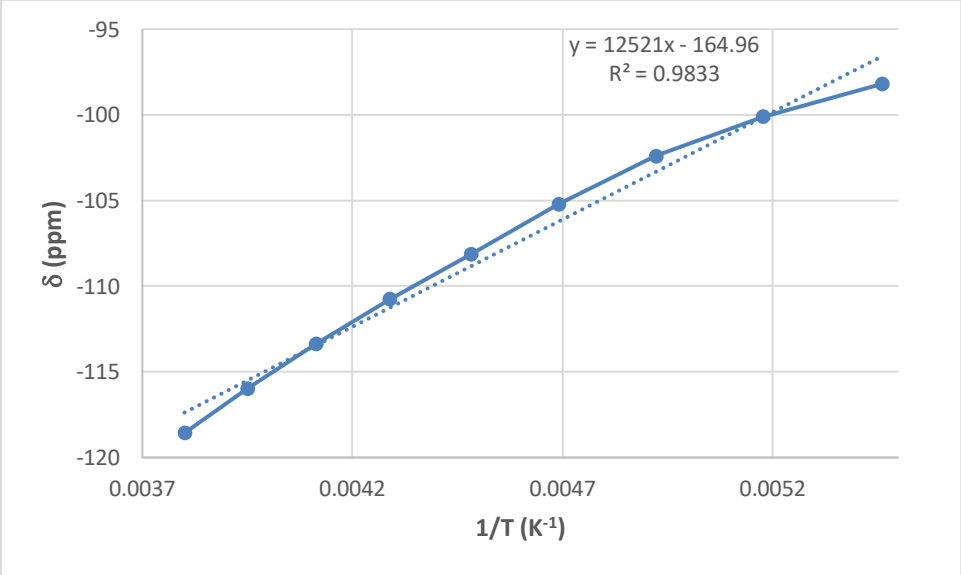

Fig. 18. VT ^{1}H NMR shift vs 1/T (K^{-1}) for the proton at –98.2 ppm, between –90 and –10 °C.

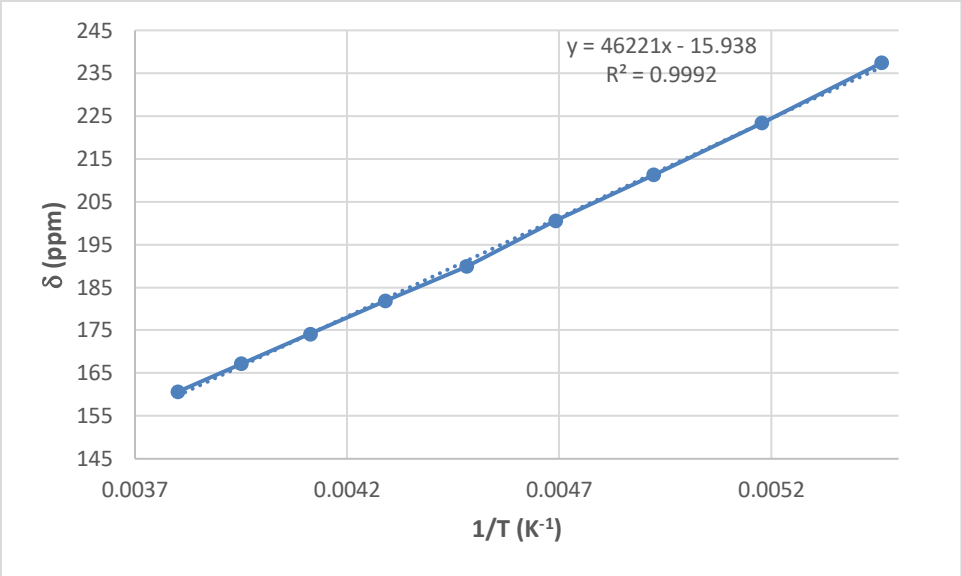

Fig. 19. VT ^{1}H NMR shift vs 1/T (K^{-1}) for the proton at +237.4 ppm, between –90 and –10 °C.

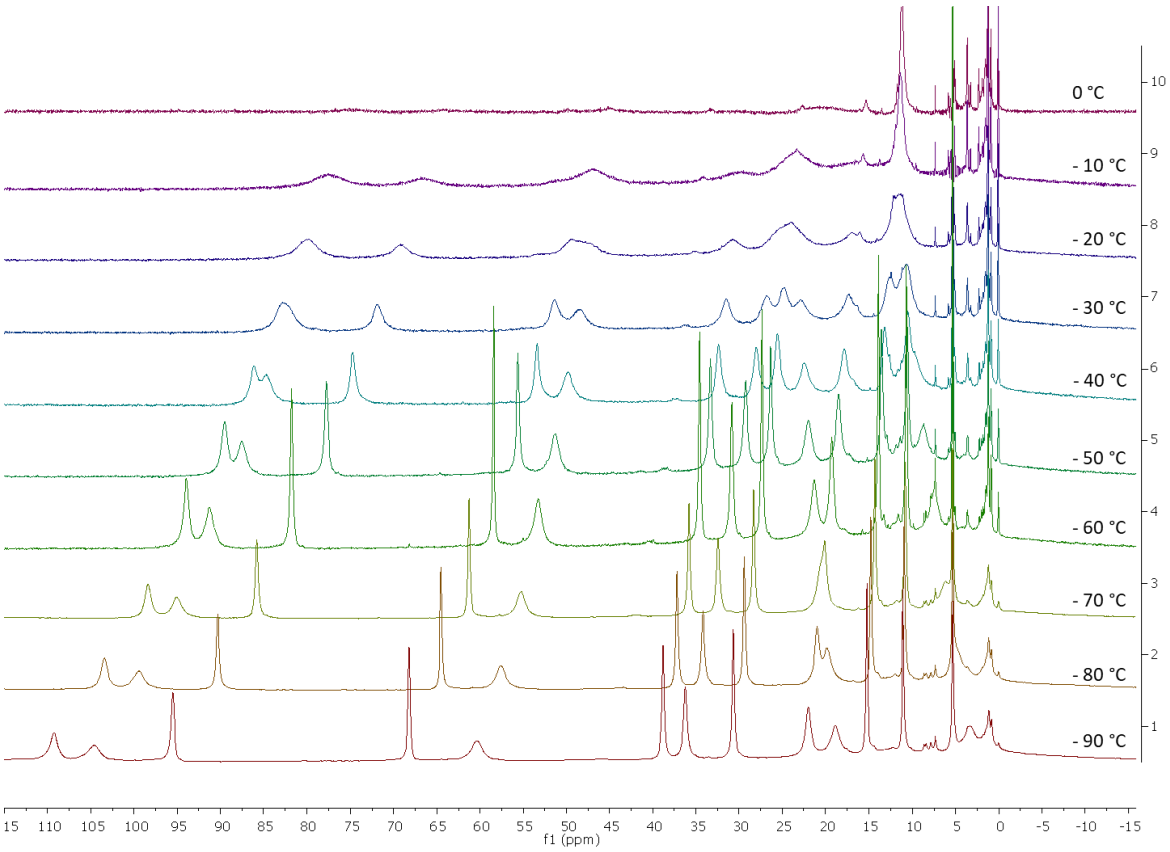

Fig. 20. Zoom in the region –15 / +115 ppm of the VT ^{1}H NMR spectra of dimer complex **9a** in CD_2Cl_2.

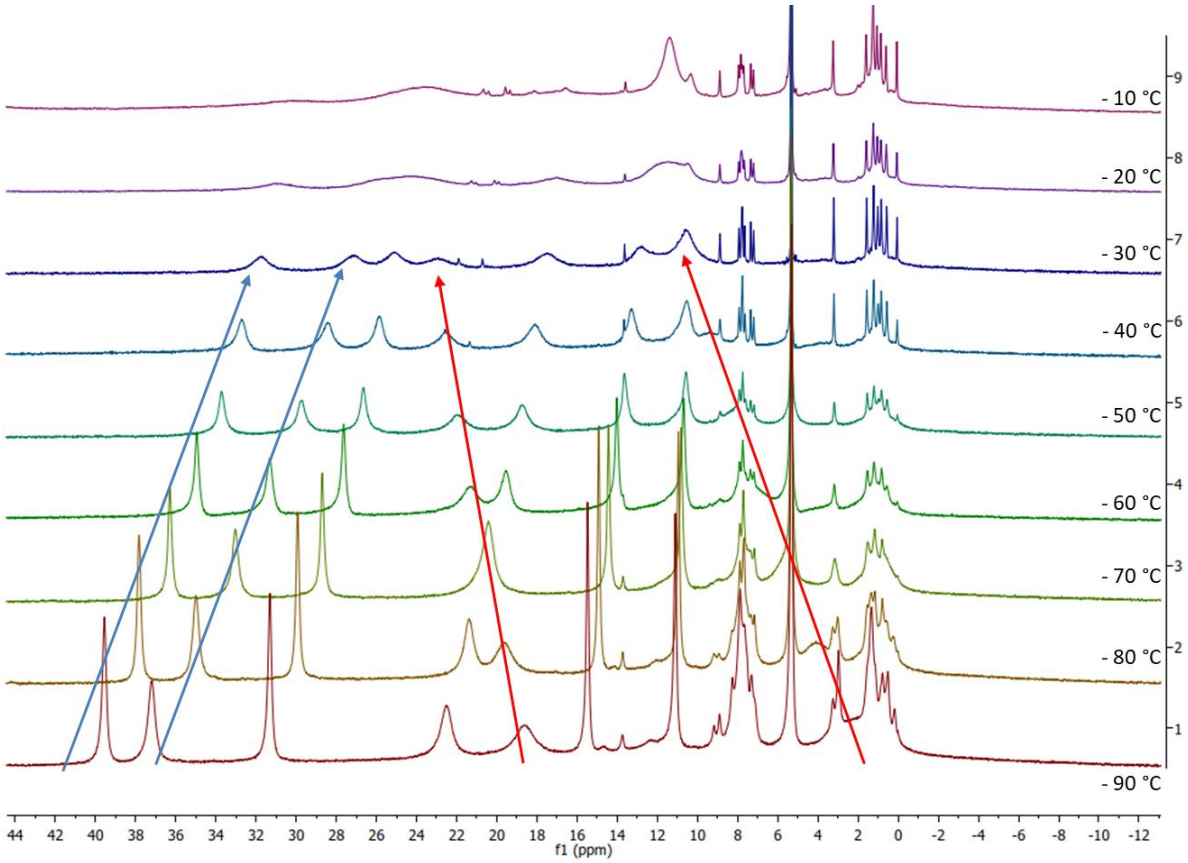

Fig. 21. Zoom in the region –12 / +45 ppm of the VT ^{1}H NMR spectra of dimer complex **9a** in CD_2Cl_2. Different temperature-dependence shifts are observed: most of the peaks followed the blue trend (decreasing ppm value with higher T) whereas only several peaks followed the red trend (increasing ppm value with higher T)

Evans methods:

To further characterize complex **9a**, we calculated its magnetic susceptibility μ_{eff} (in Bohr magneton). An identical NMR sample was then prepared with a J-Young tube containing a sealed capillary charged with DCM. To get more insights, we repeated the measurement every 10 °C, from –80 °C to room temperature. By analyzing the difference between the DCM peaks (residual and capillary) we were able to correlate them to the magnetic susceptibility at each temperature, according to the Evans method.[11,12]

Then, depending the structure (dimer vs monomer), we obtained a magnetic susceptibility μ_{eff}(dimer) = 2.96 to 3.08, and μ_{eff} (monomer)= 2.06 to 2.15. Interestingly, μ_{eff} (dimer) is in good agreement with a theoretical value of 2.83 for two unpaired electrons, while μ_{eff}

(monomer) is in agreement with a theoretical value of 1.73 for a single unpaired electron. The difference between μ_{eff} (dimer) and the closest theoretical value (average=0.15) is lower than the one between μ_{eff}(monomer) and its closest theoretical value (average = 0.36). Hence, these results point out that the oxidation state of the nickel complex is +3; however, the Evans method can not help to fully rule out the monomeric structure.

Table S3. Theoretical value for the magnetic susceptibility depending of unpaired electrons.

$n_{(unpaired\ e-)}$	**1**	**2**	**3**	**4**
$\mu_{eff(theoretical)}$	1.73	2.83	3.87	4.90

During the Evans measurement, we recorded the evolution of the magnetic susceptibility over a gradient of temperature. The graphic below does not show significant change of magnetic behavior within the range of temperature screened (Fig. 22).

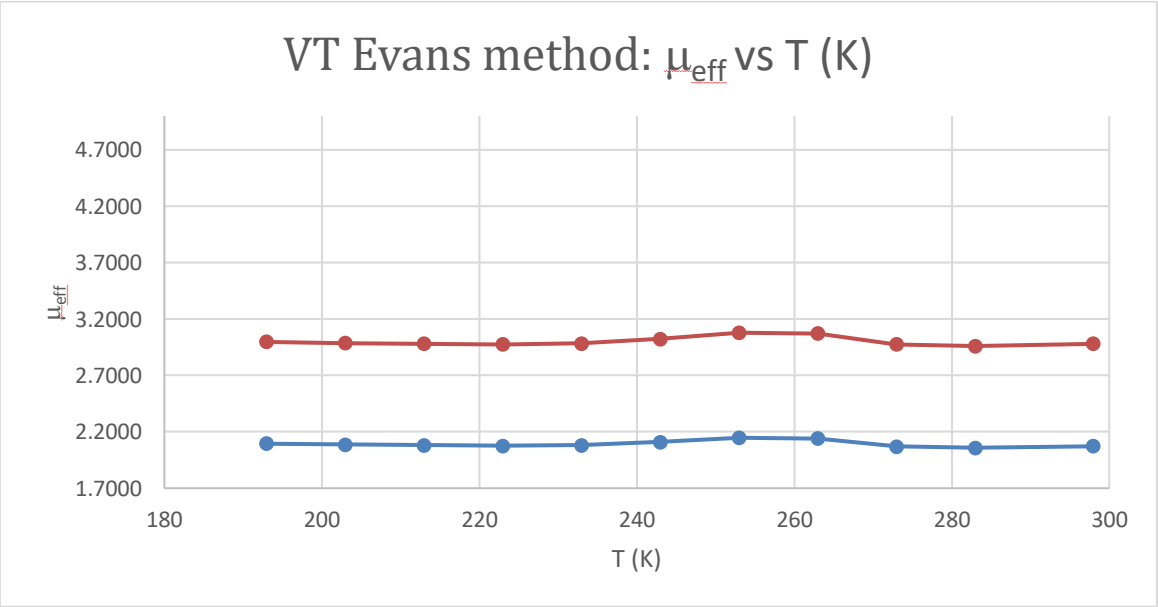

Fig. 22. VT of the magnetic susceptibility from 193 K to 298 K.

5.2.1.2. Using substrate 1b: Ni(III) dimer 9b

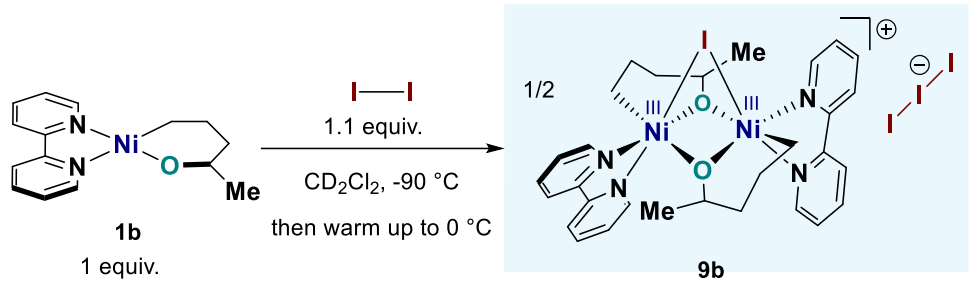

In a glovebox, oxanickelacycle **1b** (9.0 mg, 0.030 mmol, 1 equiv.) is introduced in a J-Young NMR tube. Then, outside of the glovebox, in dry ice, a precooled solution of 0.4 mL of iodine(8.4 mg, 0.033 mmol 1.1 equiv., under argon) in CD_2Cl_2 is added to a solution of **1b** in 0.2 mL of CD_2Cl_2 (in the NMR tube, in dry ice). The reaction is then transferred in a NMR probe, which was precooled at –90 °C. And the NMR is recorded at several temperature, increasing every 10 °C up to 25 °C. ^{1}H NMR characterization was possible at low temperature. Attempts for 2D characterization or ^{13}C proved unsuccessful due to the high paramagnetic nature of this intermediate. This dimer rapidly evolved and decomposed at temperature higher than 0 °C. This led to precipitation of solid particles on the wall of the NMR tube, thus rendering NMR analysis completely impossible (broad waves only).

At the end of the process (about 5 hours), no more Ni^{III} is observed. Precipitation on the side wall of the tube led to the loss of the shim. In the last NMR at RT, the crude mixture indicates the product distribution obtained after the reaction at RT in 20 min: 5-iodopentan-2-ol (**7b**) and pent-4-en-2-ol **6b**, with only very small traces of THF **2b**.

^{1}H NMR (400 MHz, CD_2Cl_2, –40 °C) δ 176.9 (s, 1H), 93.7 (s, 1H), 84.5 (s, 1H), 73.0 (s, 1H), 51.9 (s, 1H), 45.5 (s, 1H), 34.4 (s, 1H), 26.5 (s, 1H), 24.6 (s, 1H), 19.4 (s, 1H), 18.4 (s, 1H), 16.2 (s, 3H), 13.8 (s, 1H), 10.9 (s, 1H), –89.5 (s, 1H), –752.3 (s, 1H).

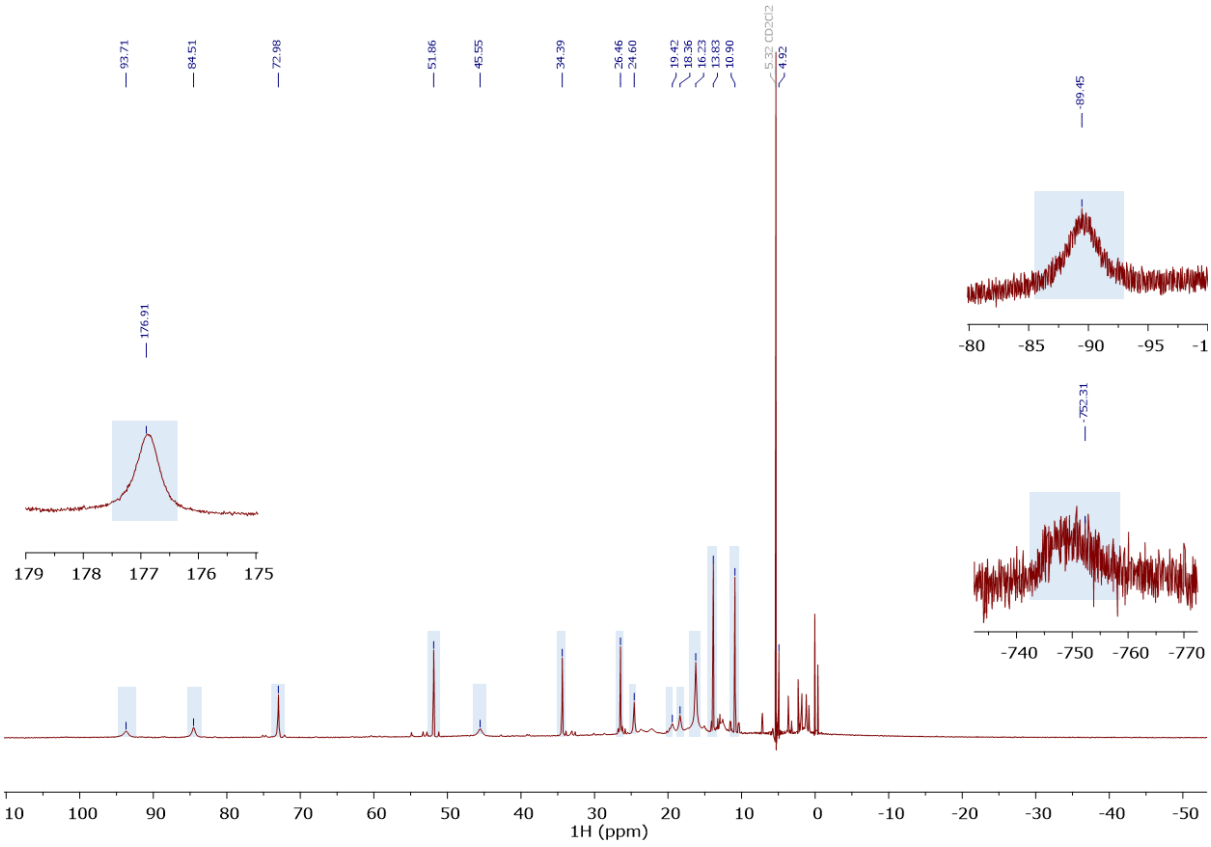

Fig. 23. ^{1}H NMR spectrum of dimer complex **9b** at –40 °C in CD_2Cl_2.

The NMR spectra of dimer **9b** is also highly paramagnetic with similar range of peaks, which is consistent with the NMR spectra obtained for **9a**. The VT NMR spectra of dimer **9b** exhibits fluxional behavior. Indeed, between –90 and –50 °C, it seems that there are 2 sets of peaks. At higher temperature, only one set of peaks is observed; however, cooling down again the reaction mixture allowed the 2nd set of peaks to appear again. A possible explanation is a match-mistmatch of the dimerisation at lower T due to the chiral center at the methyl position.

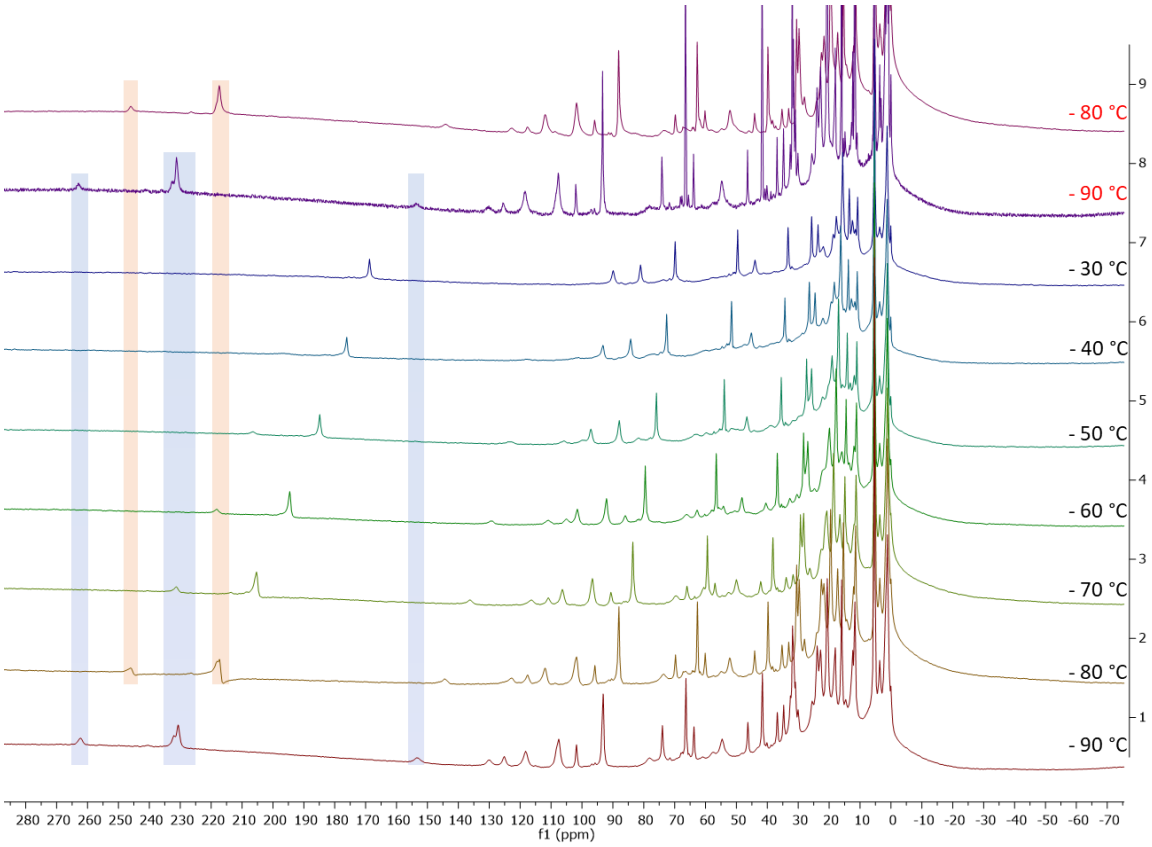

Fig. 24. VT ^{1}H NMR spectra of dimer complex **9b** in CD_2Cl_2 from –90 to –30 °C, then cooled down again to –90 and –80 °C.

5.2.2. HRMS Measurements

5.2.2.1. HRMS Measurement of dimer 9a

A precooled pink solution of iodine (8.4 mg, 0.033 mmol, 1.1 equiv., under argon) in 0.5 mL of CD_2Cl_2 was added to a deep purple solution of oxanickelacycle **1a** (8.6 mg, 0.030 mmol, 1 equiv.) in 0.5 mL of CD_2Cl_2 in a Schlenk at –78 °C under positive argon pressure. The resulting solution turned quickly dark yellow. After 10 min stirring, an aliquot of the mother liquor was then filtered and introduced in a new Schlenk kept at –78 °C. This solution was quickly analyzed by HRMS at room temperature.

HRMS (ESI) calcd for $C_{28}H_{32}IN_4Ni_2O_2^+$ $[M\text{-}I_3]^+$ 699.02714; found 699.02655. ESI negative revealed the presence of I_3^- at 380.7.

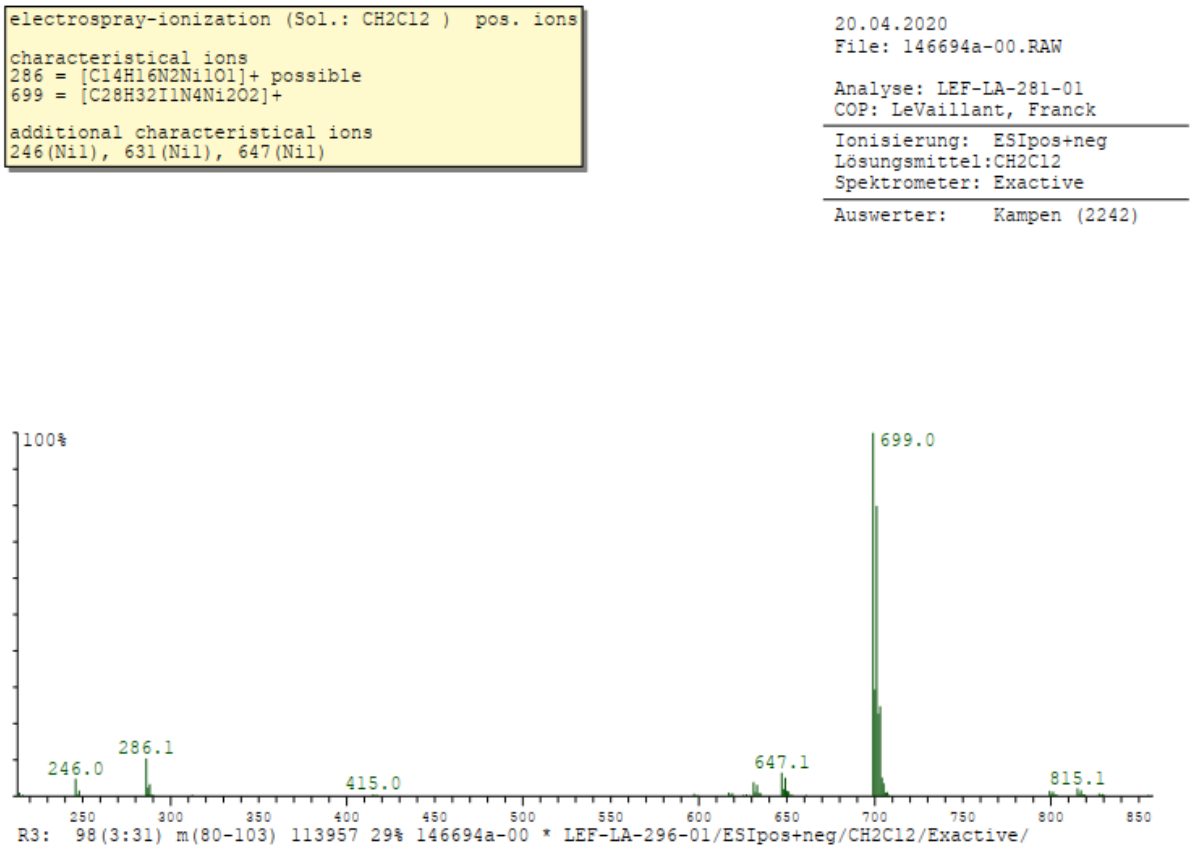

Fig. 25. HRMS analysis of a crude reaction mixture using **1a** and I_2 at –78 °C in CD_2Cl_2, showing a peak corresponding to [***9a***-I_3^-] in ESI^+ mode.

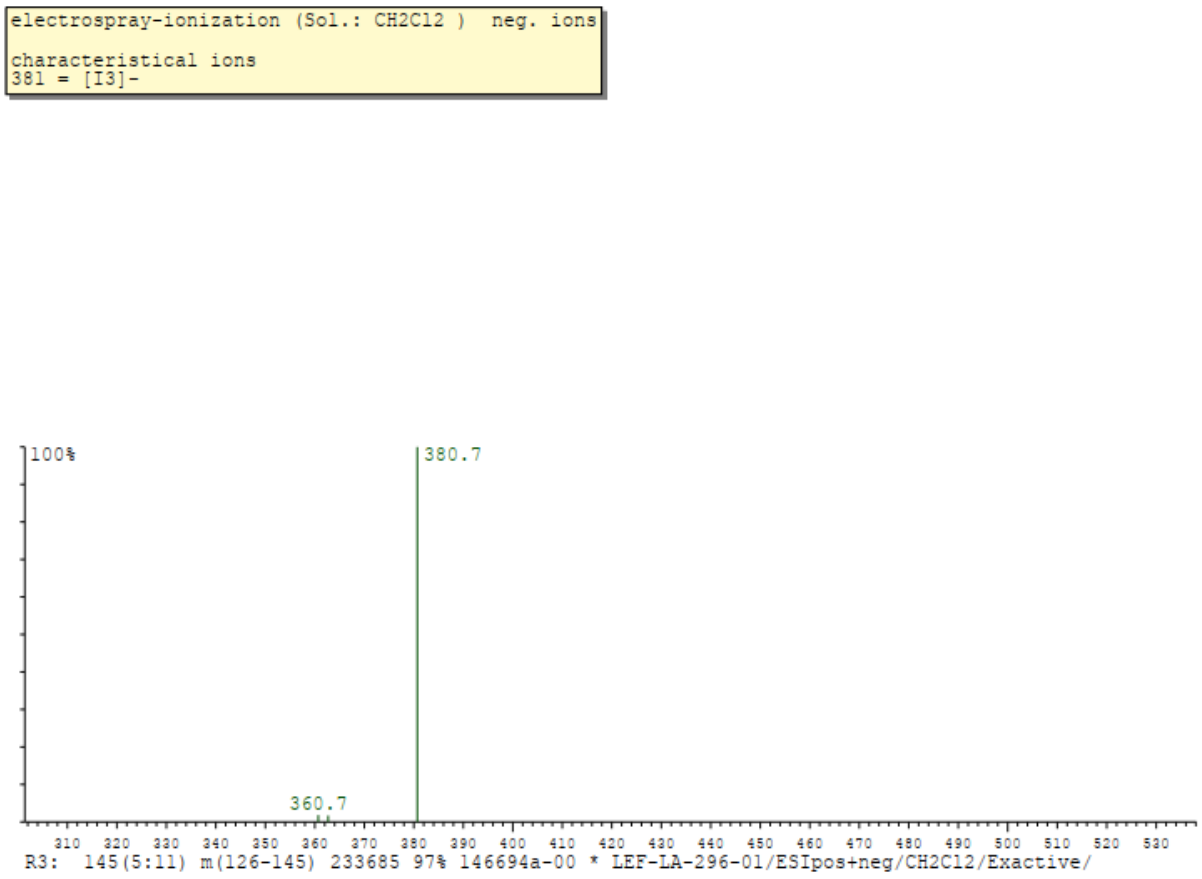

Fig. 26. HRMS analysis of a crude reaction mixture using **1a** and I_2 at –78 °C in CD_2Cl_2, showing a peak corresponding to [I_3^-] in ESI$^-$ mode.

5.2.2.2. HRMS Measurement of dimer 9b

A precooled dark pink solution of iodine (8.4 mg, 0.033 mmol, 1.1 equiv.) in 0.5 mL of CD_2Cl_2 was added to a cold deep purple solution of oxanickelacycle **1b** (9.0 mg, 0.030 mmol, 1 equiv.) in 0.5 mL of CD_2Cl_2 in a Schlenk at –78 °C under positive argon pressure. The resulting solution turned quickly dark yellow. After 10 min stirring, an aliquot of the mother liquor was then filtered and introduced in a new Schlenk kept at –78 °C. This solution was quickly analyzed by HRMS at room temperature.

HRMS (ESI) calcd for $C_{30}H_{36}IN_4Ni_2O_2^+$ $[M\text{-}I_3]^+$ 727.05882; found 727.05844. ESI negative revealed the presence of I_3^- at 380.7.

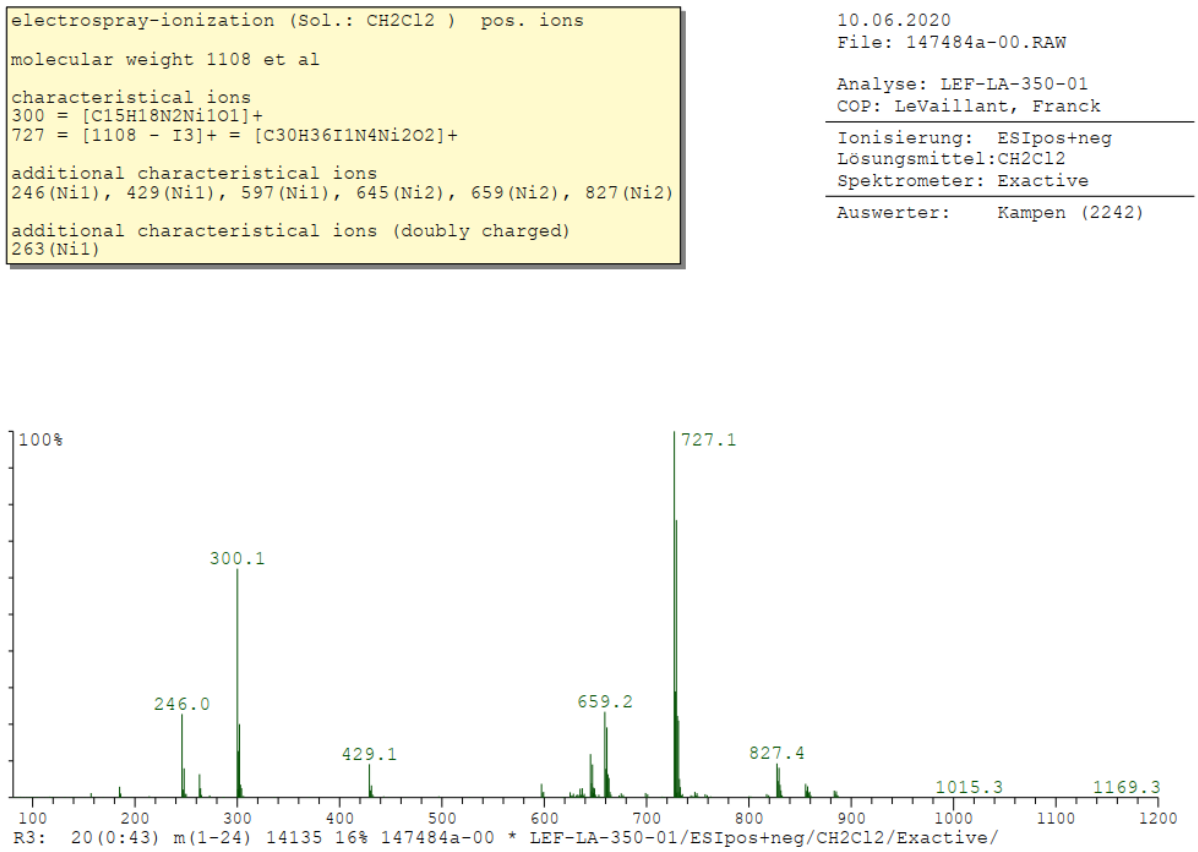

Fig. 27. HRMS analysis of a crude reaction mixture using **1b** and I_2 at –78 °C in CD_2Cl_2, showing a peak corresponding to [***9b***-I_3^-] in ESI^+ mode.

5.2.3. X-Ray structural analysis:

5.2.3.1. X-Ray analysis of polymeric $[bipyNiI_2]_n$ (8)

Using a sample prepared for the low-T NMR studies of dimer **9a**, the solution in the J-Young NMR tube was warmed up to 25 °C. The supernatant was discarded and the brown solid was washed several times with benzene-d_6 before being solubilized with DCM, transferred in clean NMR tube, and placed in a freezer at –20 °C. Small crystals grown and were suitable for X-ray analysis, revealing a polymeric structure of $[bipyNiI_2]_n$ (Figure 28). Iodine atoms are relatively disordered, and the disordered atoms are removed from the picture for clarity.

N.B.: in some cases, green solids were found in the J-Young NMR tube, and possibly attributed to monomeric bipyNiI₂. However, attempts to isolate the green solids in order to grow crystals always resulted in the formation of brown solids, most likely upon polymerization to give polymeric [(bipy)NiI₂]ₙ.

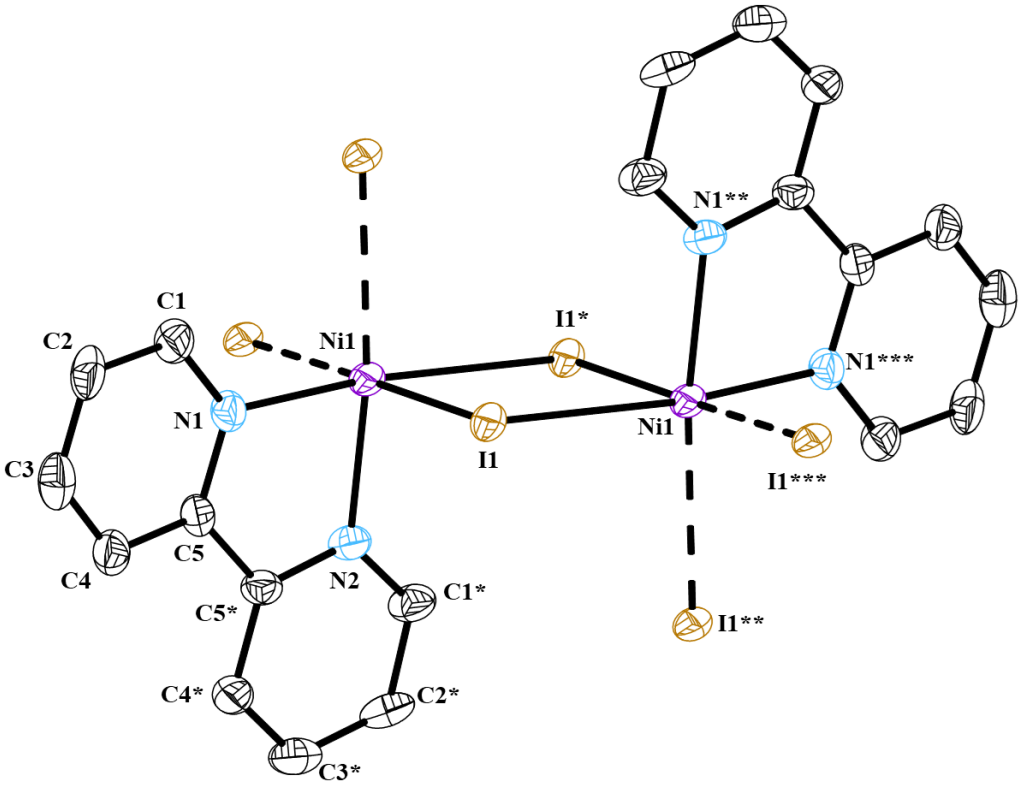

Fig. 28. X-Ray structure of **8** (Disordered iodine atoms are omitted for clarity).

5.2.3.2. X-Ray analysis of Ni^{III}-Ni^{III} complex

A precooled pink solution of iodine (2.6 mg, 0.011 mmol, 1.1 equiv., under argon) in 1.5 mL of Toluene/CD_2Cl_2 (30/70) was added to a deep purple solution of oxanickelacycle **1a** (2.9 mg, 0.010 mmol, 1 equiv.) in 1.5 mL of Toluene/CD_2Cl_2 (30/70) in a Schlenk under argon at –78 °C. The resulting solution turned quickly light yellow. This solution is stable for weeks in dry-ice and red crystals of **9a** can be obtained after several days in a freezer at –35 °C (Figure 29).

Attempts to get crystals of **9b** did not meet success (various solvents tested, at different temperatures).

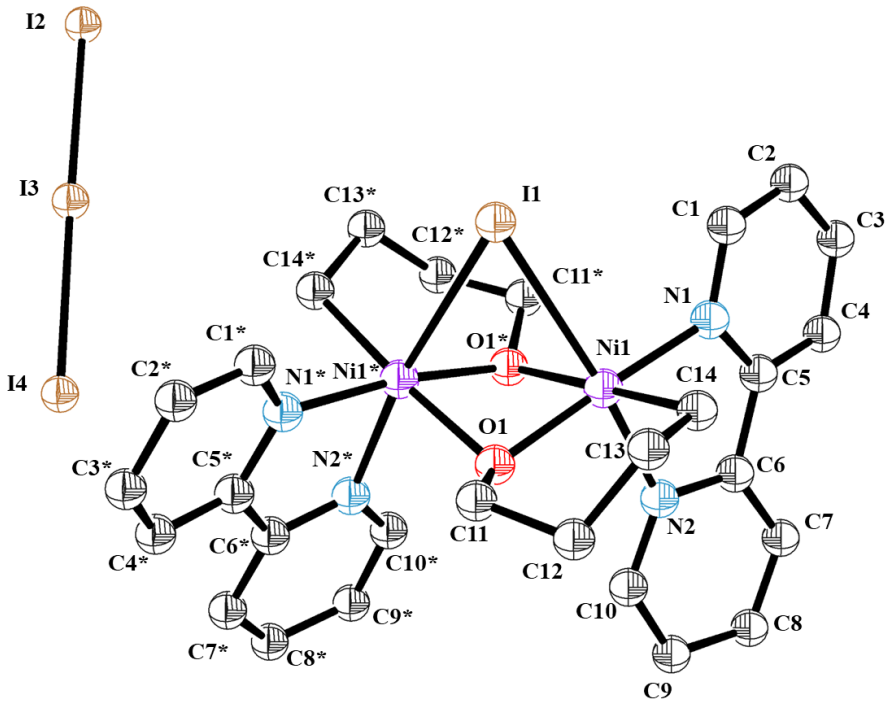

Fig. 29. X-Ray structure of **9a.**

(Disordered iodine atoms in the triiodide counterion are omitted for clarity)

5.2.4. EPR measurement: In situ characterization of Ni^{III}–Ni^{III} dimer 9a-b

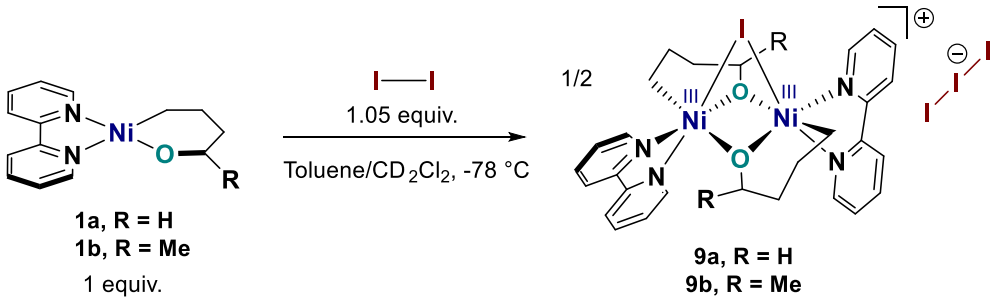

A precooled pink solution of iodine (2.6 mg, 0.010 mmol, 1.05 equiv., under argon) in 2.4 mL of Toluene was added to a deep purple solution of oxanickelacycle **1b** (2.9 mg, 0.0096 mmol, 1 equiv.) in 2.5 mL of CD_2Cl_2 (30/70) in a Schlenk at –78 °C. The resulting solution was stirred for 5 minutes and turned quickly light yellow. An aliquot of the mother liquor (0.30 mL) was then filtered and introduced in long NMR tube under positive argon flow. This tube was flame-sealed before being frozen in liquid N_2 for analysis of **9b**. A background analysis of an empty tube was realized to ensure that the observed signals do not count for the tube.

EPR sample for **9a** was prepared in the same manner. However, **9a** is more sensitive to temperature, and partial decomposition might have occurred during transfer, resulting in a lower quality EPR spectra. Still, the signal observed is strong and similar to the one obtained for **9b**.

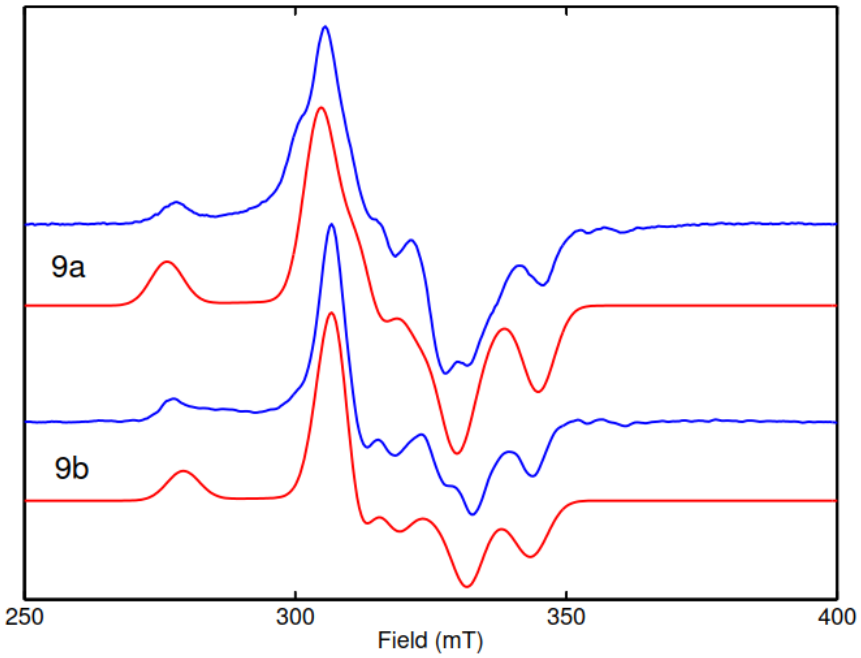

Fig. 30. X-band EPR of complex **9a** and **9b** recorded at 30K (blue traces). Experimental parameters: 1 mW, 100kHz 7.5 Gauss Field modulation. The red traces represent the Easyspin (esfit) simulation with the following parameters: g(**9a**)= (2.081, 2.155, 2.279); g(**9b**)= (2.084,

2.144, 2.287). Dipolar interaction D(**9b**) = 517 MHz; D(**9a**) = 550 MHz. *J*-coupling = 50 MHz. Complete list of parameters is collected in table S6.

The EPR of **9a** and **9b** (Fig. 30) were recorded 30K. The spectra are not consistent with a regular Ni^{III} *S*=1/2 monomer species and show multiple splittings pointing to an electron-electron spin-spin interaction. The crystal structure of **9a** (orthorhombic space group Pbcm) indicates that the two Ni^{III} centers are related to each other by a two-fold axis through the Iodide atom and normal to the axis connecting the two Ni atoms as well as the axis connecting the two bridging Oxygen atoms, i.e. parallel to the a-axis of the unit cell (Fig. 31). The axis connecting the two Ni atoms is considered as the dipolar axis and points approximately along the c-axis. Using these constraints considerably reduces the number of fitting parameters for the EPR spectrum. Thanks to the orthorhombic unit cell, the a-, b-, and c-axes can be directly used as axis frame for the EPR simulations. The spin Hamiltonian used to analyze the EPR spectrum is written as:

$$H = \beta B g_A S_A + \beta B g_B S_B + J S_A S_B + S_A D S_B$$

Where β is the Bohr magneton, B is the magnetic field, S_A and S_B are spin operators referring to the two Ni^{III} *S*=1/2 centers and g_A, g_B are the corresponding g-matrices. J represents the (isotropic) exchange parameter and D is the (traceless) dipolar interaction tensor. The orientations of the two g-matrices are unknown but, according to the symmetry found in the crystal structure of **9a**, their relative orientations are related by two fold symmetry along the x-axis (crystal a-vector). Therefore, since the two Ni^{III} are chemically identical, the parameters (3 principle values and 3 Euler angles) of only one of the g-matrices needs to be varied in the fitting procedure. In addition, the two parameters of the dipolar interaction D are varied: The principal values of the D-tensor (Dx, Dy, Dz) are given as (1+d, 1-d, -2)×D. Here "D" is the dipolar parameter and "d" (-1<d<1) the "rhombicity" parameter. By assuming a J-value of 50 MHz (very weak anti-ferromagnetic coupling) and varying the 8 parameters specified above a convincing fit to the EPR spectra was obtained as displayed in figure 27. A complete list of parameters is collected in table S4, and a comparison with ***int-I*** in table S6.

The very weak J-coupling between the two Ni^{III} centers is consistent with the magnetic behavior of the dimer in liquid state as observed in NMR. Effectively, the NMR experiment is observing "uncoupled" Ni^{III} centers and the dimer complex is evaluated as two independent S=1/2 systems (see Evans method, *in section 5.2.1.*).

Table S4. EPR g-parameters extracted for complexes **9a** and **9b**. (Euler angles with respect to the crystal axis in degrees).

Complex	gx	gy	gz	α	β	γ	J (MHz)	D (MHz)	d
9a	2.081	2.155	2.279	12	-167	99	50	550	-0.11
9b	2.084	2.144	2.287	-36	163	52	50	517	-0.12

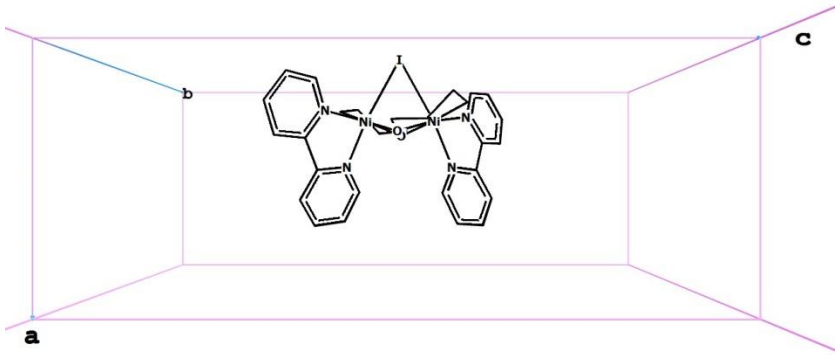

Fig. 31. Orientation of **9a** in its orthorhombic unit cell (Pbcm). The two Ni^{III} centers and their surrounding are related by a two-fold axis through the Iodine atom along the a-axis.

5.2.5. DFT calculations on Ni^{III}–Ni^{III} dimer 9a

Density Functional Theory (DFT) calculations were performed in ORCA 4.2.1 on the coordinates of **9a** using the B3LYP as well as the TPSSh functional in combination with the zora-def2-TZVP basis set including atom pairwise dispersion correction as well as relativistic effects.[13-23] Broken Symmetry calculations using various combinations of functionals (B3LYP/TPSSh) and basis sets (zora-def2-TZVP/def2-TZVP) provided estimates of the exchange interaction between the two Ni^{III} centers (i.e. the energy difference between the S=1 and S=0 configuration) scattering around 0 eV. The lowest value of 0.0009 eV (B3LYP/def2-TZVP) is within the numerical accuracy of the employed DFT methods. Therefore, for most practical purposes, one is lead to assume that there is no spin delocalization between the two Ni^{III} centers and that the Ni^{III} dimer behaves as two independent Ni^{III} complexes. To verify this model, an additional DFT calculation was carried out on a model in which one of the Ni^{III} centers was replaced by a Ga^{III} center thus introducing a closed shell system (S=0) on one of the monomer units. Figure 32 shows a comparison between the spin density distribution of the

Ni^{III}–Ni^{III} dimer and the Ni^{III}–Ga^{III} complex. The spin density is concentrated on the Ni^{III} center itself as well as on the coordinating carbene carbon and the bridging oxo moieties. Interestingly, for the Ni−Ga complex no spin density is found on the Ga side of the complex (apart from a small contribution on the bridging oxo-moieties) suggesting that the metal centers on both sides are not connected by spin delocalization.

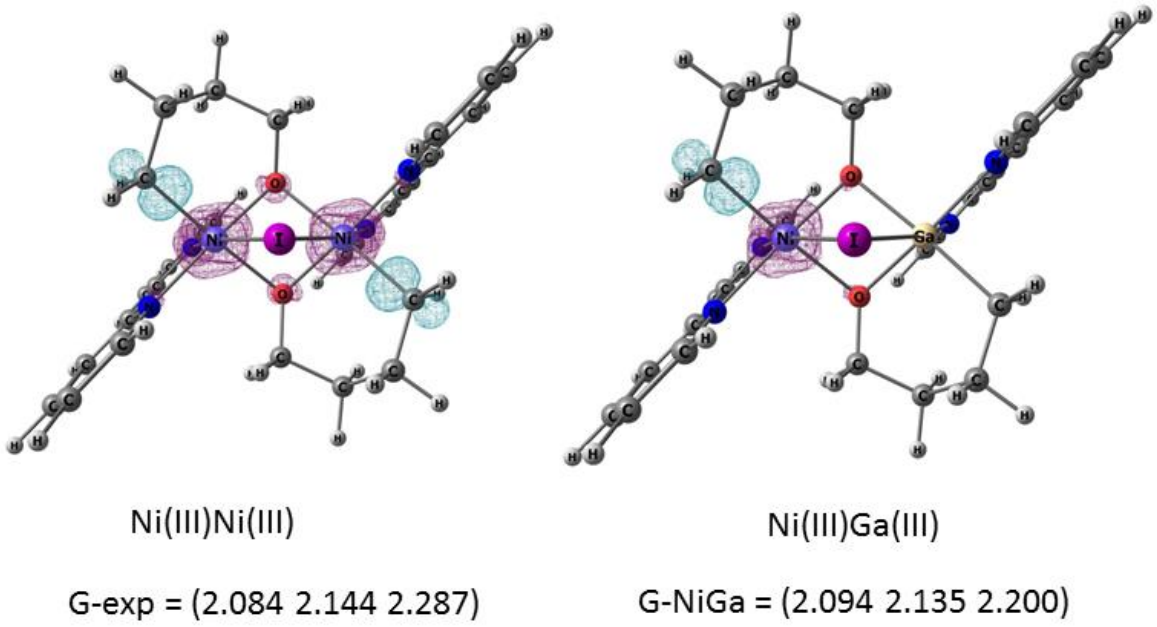

Fig. 32. Spin density over complex **9a** (left) and the analogous Ni^{III}–Ga^{III} complex (right). The complexes are viewed along the 2 fold axis so that the bipy ligands are perpendicular to the plane of the picture. The experimental g-tensor is provided for the Ni^{III}–Ni^{III} dimer whereas the calculated g-tensor is listed for the Ni^{III}–Ga^{III} complex.

For the Ni^{III}–Ga^{III} complex also the g-tensor as well as the ^{1}H hyperfine interactions were calculated (Table S5). The calculated g-tensor (2.094 2.135 2.200) corresponds quite well to the experimental g-tensor (2.084 2.144 2.287) which, in turn is very similar to that of mono Ni^{III} complex with a related structure (2.03, 2.14, 2.20).[24] The isotropic hyperfine interactions of the protons in the alkyl ligand span a large range (−50MHz to +3 MHz). It is likely that these protons are observed in the ^{1}H NMR having large paramagnetic shifts. A major contribution to the paramagnetic shift is the Fermi contact interaction which is proportional to the isotropic hyperfine interaction for the corresponding proton. For a spin-system with isotropic g-tensor the expression is relatively simple:

$$\delta_{FC} = \frac{A_{iso} g \beta S(S+1)}{3\gamma_N \hbar k T} \qquad (1.1)$$

At a temperature of –30 °C the δ_{FC} is around 30 ppm/MHz. Only a few protons show a large negative paramagnetic shift (–50 to –100 ppm) with anti-Curie behavior. These could be assigned to protons #3, #31 and/or #34 (Table S5).

Table S5. Proton isotropic hyperfine interactions calculated for Ni^{III}-Ga^{III} complex. Preliminary assignment to protons observed in ^{1}H NMR (Fig. 15)

proton	A(iso) MHz	δ_{FC} (ppm) calc (30/MHz)	δ (ppm) exp
13	+2.25	+68	
23	+1.70	+51	
31	-2.77	-83	-98
02	+1.09	+33	
03	-56.2	-1686	-932
34	-2.88	-86	-98
37	+2.96	+89	

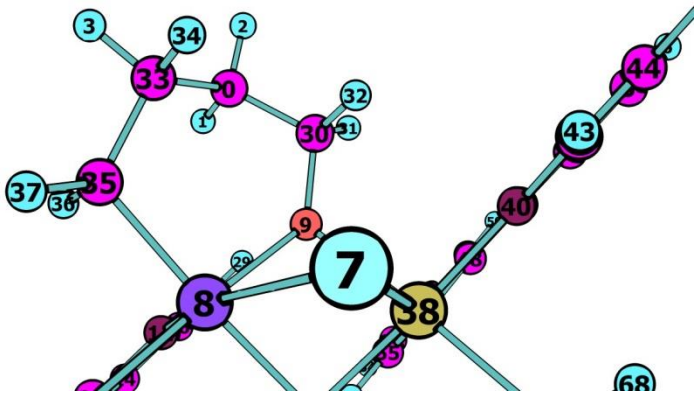

Fig. 33. Atom numbering of Ni^{III}-Ga^{III} model in Figure 32 referring to the proton numbering in Table S5.

6. Reactivity with other oxidants

6.1. Screening of oxidants

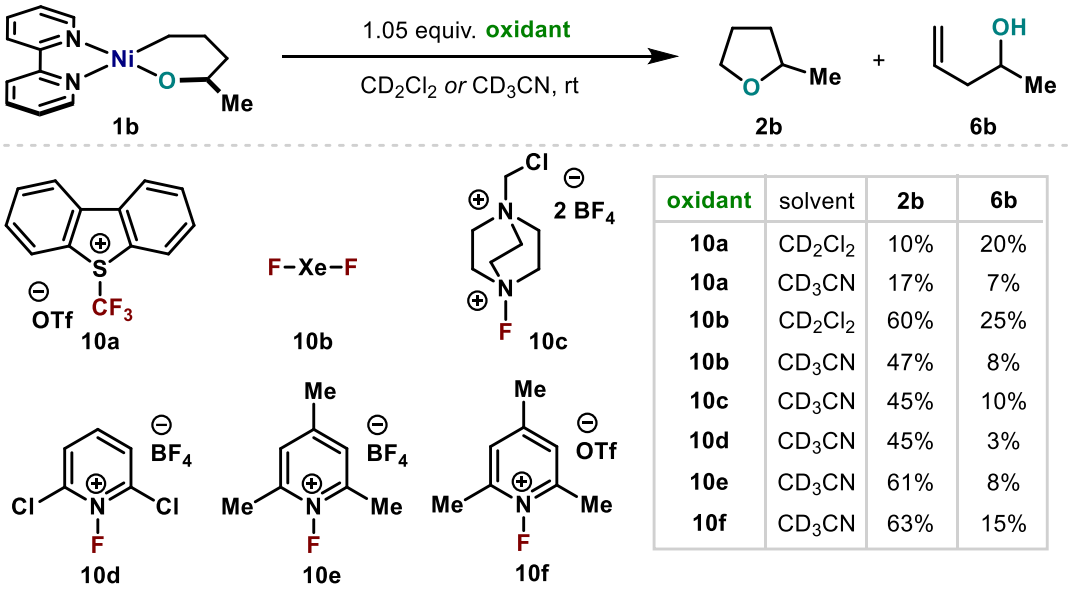

oxidant	solvent	2b	6b
10a	CD_2Cl_2	10%	20%
10a	CD_3CN	17%	7%
10b	CD_2Cl_2	60%	25%
10b	CD_3CN	47%	8%
10c	CD_3CN	45%	10%
10d	CD_3CN	45%	3%
10e	CD_3CN	61%	8%
10f	CD_3CN	63%	15%

General procedure

In a glovebox, oxanickelacycle **1b** (9.0 mg, 0.030 mmol, 1 equiv.) is introduced in a J-Young NMR tube. 0.5 mL of dry and degassed CD_3CN is added by syringe, then internal standard (mesitylene, 3.50 µL, 3.02 mg, 0.0252 mmol, 0.839 equiv.) is added. The NMR tube is then capped and shaken to homogenize the purple solution of **1b**. To this solution oxidant (**10a-f)** (0.0315 mmol 1.05 equiv.) is added as solid. The NMR tube is capped again, shaken (the reaction happens usually in less than 1 min), and removed from the glovebox for direct NMR measurement at room-temperature. 2-Me-THF **2b** and byproduct **6a** are observed by NMR and the NMR yield is measured versus mesitylene.

6.1.1. Details for the reaction using Umemoto´s reagent and oxanickelacycle 1a:

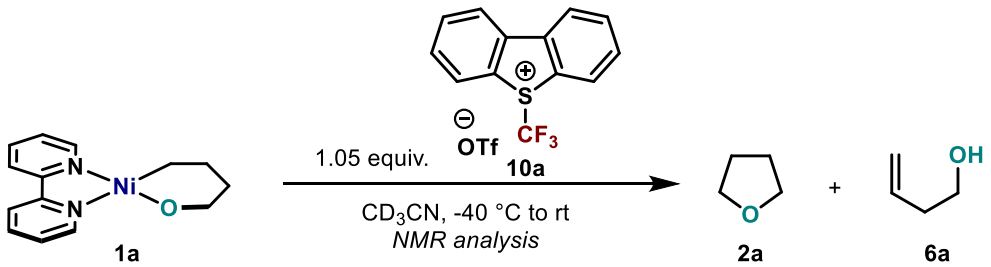

In a glovebox, oxanickelacycle **1a** (8.6 mg, 0.030 mmol, 1 equiv.) is introduced in a J-Young NMR tube. 0.2 mL of dry and degassed CD_3CN is added by syringe, before capping the NMR tube and shaking slowly to homogenize the purple solution of **1b**. A solution of Umemoto's

reagent (12.7 mg. 0.0315 mmol, 1.05 equiv.) is then prepared in a vial using 0.2 mL of dry and degassed CD_3CN. Outside the glovebox, under an argon flow in acetonitrile-dry ice bath, the cold solution of **10a** is introduced quickly by syringe, and the vial is washed with 0.10 ml of CD_3CN. The NMR tube is capped again, and shaken only just before putting it in the NMR probe (precooled at −40 °C) for direct NMR measurement between at −40 °C and 25 °C.

This reaction was followed by NMR to see whether $Ni^{IV}–CF_3$ intermediate could be observed. Even at −40 °C in CD_3CN, no highly shifted signal was detected in ^{19}F NMR. Expected product THF **2a** and side product **6a** are obtained in rather low amount. Residual amount of reagent can be observed. Finally, formation of HCF_3 is confirmed both in ^1H and ^{19}F spectra (Fig. 34-36), and seems to be increasing in the same manner as **6a**, thus suggesting the possible existence of (bipy)$NiHCF_3$ that may reductively eliminate. Paramagnetic nickel species can be also detected (peaks > 13 ppm), and seems to indicate the presence of high-spin Ni^{II} complexes after reductive elimination.

For fluoroform HCF_3, **^{1}H NMR (400 MHz, CD_3CN)** δ 6.82 (q, *J* = 79.4 Hz, 1H).

^{19}F NMR (376 MHz, CD_3CN) δ –79.87.

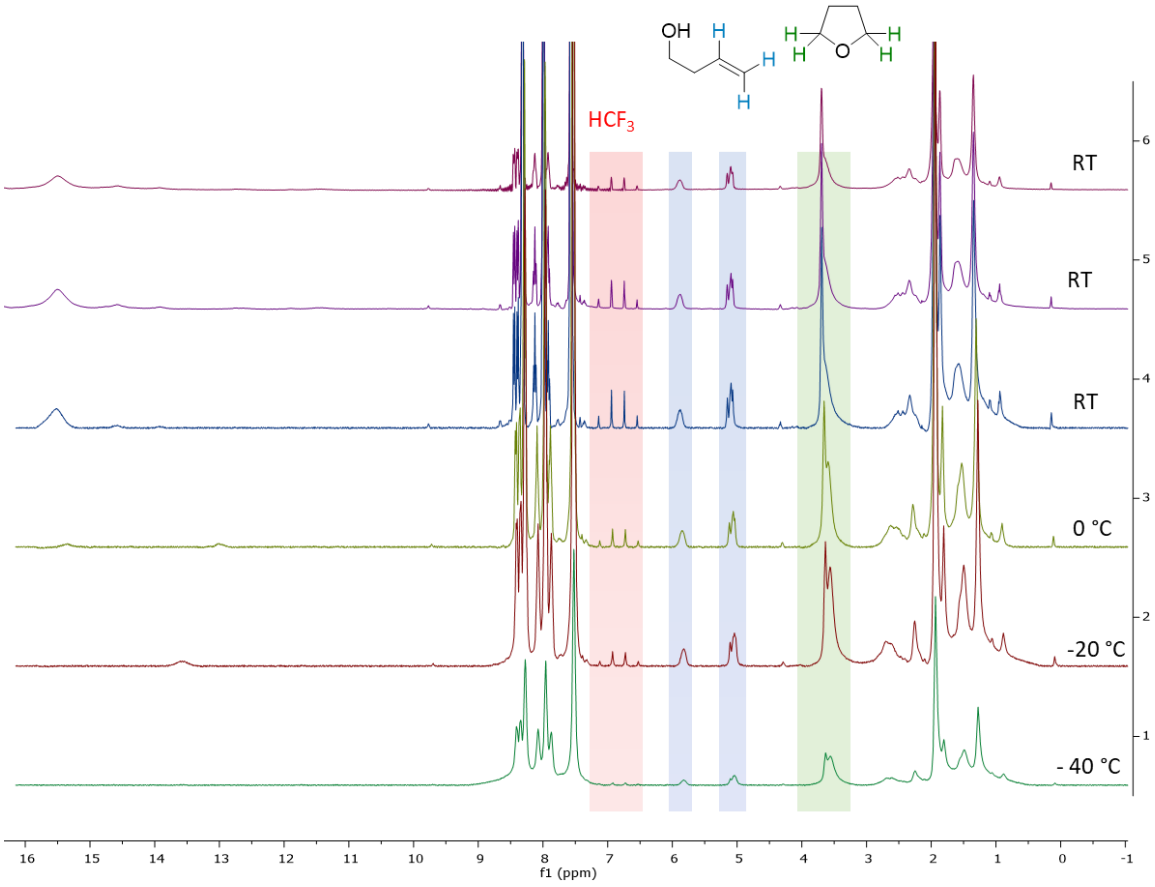

Fig. 34. VT ^1H NMR spectra of the formation of HCF_3 in CD_3CN.

The formation of 5,5,5-trifluoropentan-1-ol is suggested by both ^{1}H NMR (see peaks at 3.5 ppm and 2.3 ppm) and in ^{19}F spectra (see peaks at −67 ppm confirming the C−CF_3)

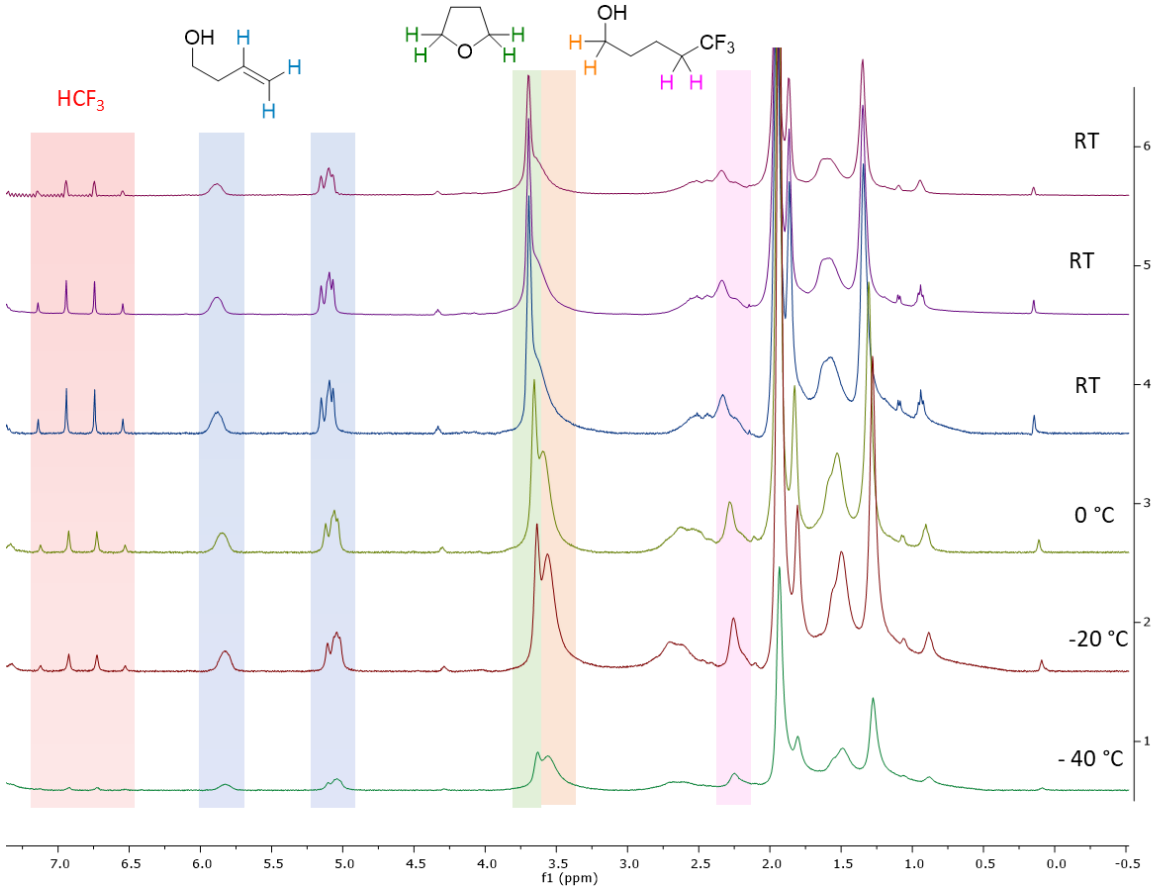

Fig. 35. VT ^{1}H NMR spectra of the formation of HCF_3 and 5,5,5-trifluoropentan-1-ol in CD_3CN.

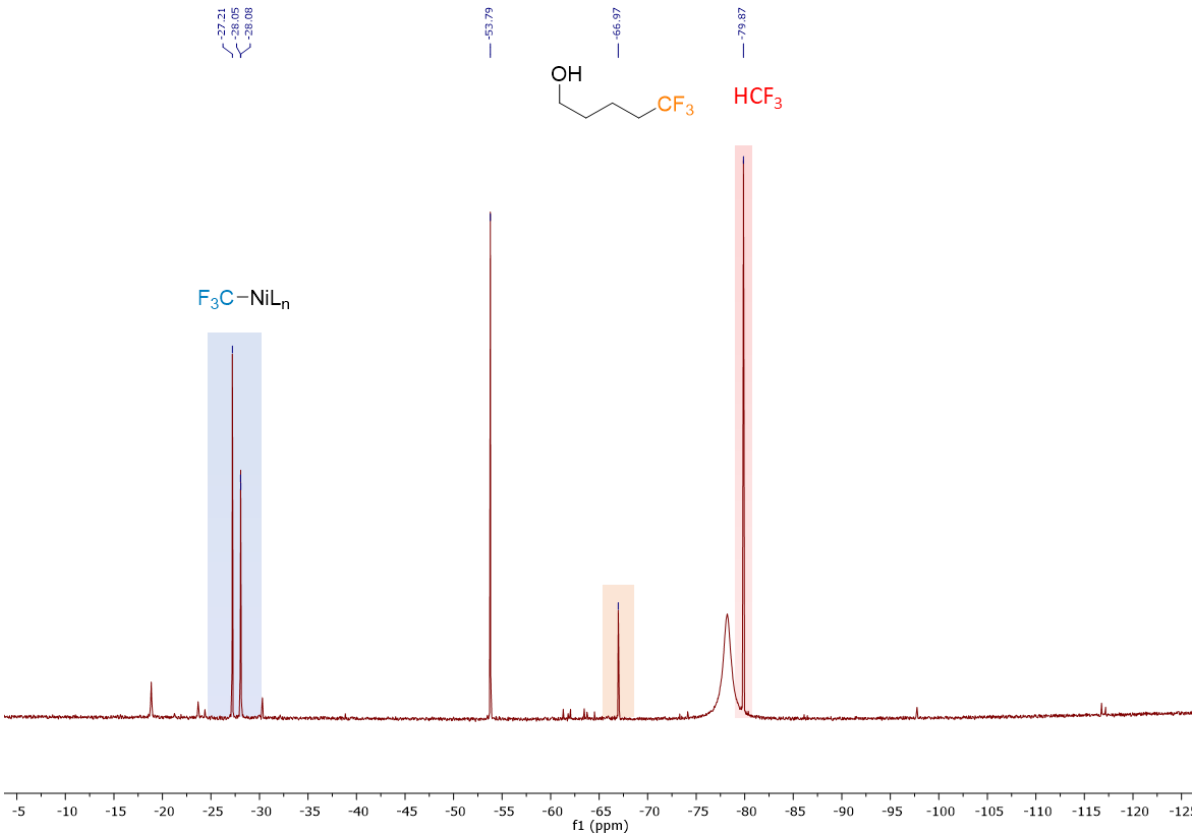

Fig. 36. ^{19}F NMR spectrum of the formation of HCF_3 and 5,5,5-trifluoropentan-1-ol in CD_3CN at 25 °C.

6.1.2. Details for the reaction using XeF_2 in CD_2Cl_2:

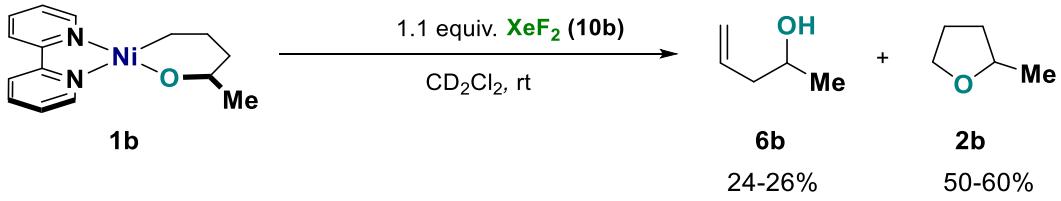

1b **6b** 24-26% **2b** 50-60%

In a glovebox, oxanickelacycle **1b** (3.5 mg, 0.012 mmol, 1 equiv.) is introduced in a vial containing a small Teflon-coated stir bar. To this vial is added 0.6 mL of dry and degassed CD_2Cl_2 by syringe. To this dark purple solution is added XeF_2 (**10b**) (2.2 mg, 0.013 mmol 1.1 equiv.) is added as solid, and the resulting solution is stirred for 2 min, during which the purple color faded from deep purple to very light purple. This solution is then transferred in a NMR tube using a HPLC filter to remove the inorganic salts. The NMR tube is capped, removed from the glovebox, then internal standard (*para*-fluoronitrobenzene, 1.7 µL, 2.2 mg, 0.0156 mmol, 1.34 equiv.) is added, right before NMR measurement at 25 °C. 2-Me-THF **2b** is observed by NMR in 50-60% yield, along with 25% of **6b**.

Note: this reaction cannot be performed directly in a NMR tube because the precipitation of insoluble nickel salts after reductive elimination prevents a good analysis. Switching to CD_3CN allowed direct reaction in NMR tube without the need for filtration.

Comparison of an authentic sample of 2-Me-THF with the outcome of the reaction using XeF_2 confirmed the C-O bond formation: 2-Me-THF was observed in both ^{1}H NMR and ^{13}C NMR.

Crude reaction mixture **2b**: **^{1}H NMR (400 MHz, CD_2Cl_2)** δ 3.94 – 3.80 (m, 2H), 3.64 (q, *J* = 7.5 Hz, 1H), 2.03 – 1.75 (m, 3H), 1.37 (dq, *J* = 11.5, 7.9 Hz, 1H), 1.18 (d, *J* = 6.0 Hz, 3H).

^{13}C NMR (101 MHz, CD_2Cl_2) δ 75.5, 67.9, 33.4, 26.2, 21.1.

From authentic sample **2b**:[25]

^{1}H NMR (300 MHz, CD_2Cl_2) δ 3.97 – 3.77 (m, 2H), 3.69 – 3.58 (m, 1H), 2.05 – 1.75 (m, 3H), 1.47 – 1.31 (m, 1H), 1.18 (d, *J* = 6.1 Hz, 3H).

^{13}C NMR (75 MHz, CD_2Cl_2) δ 75.4, 67.9, 33.5, 26.3, 21.1.

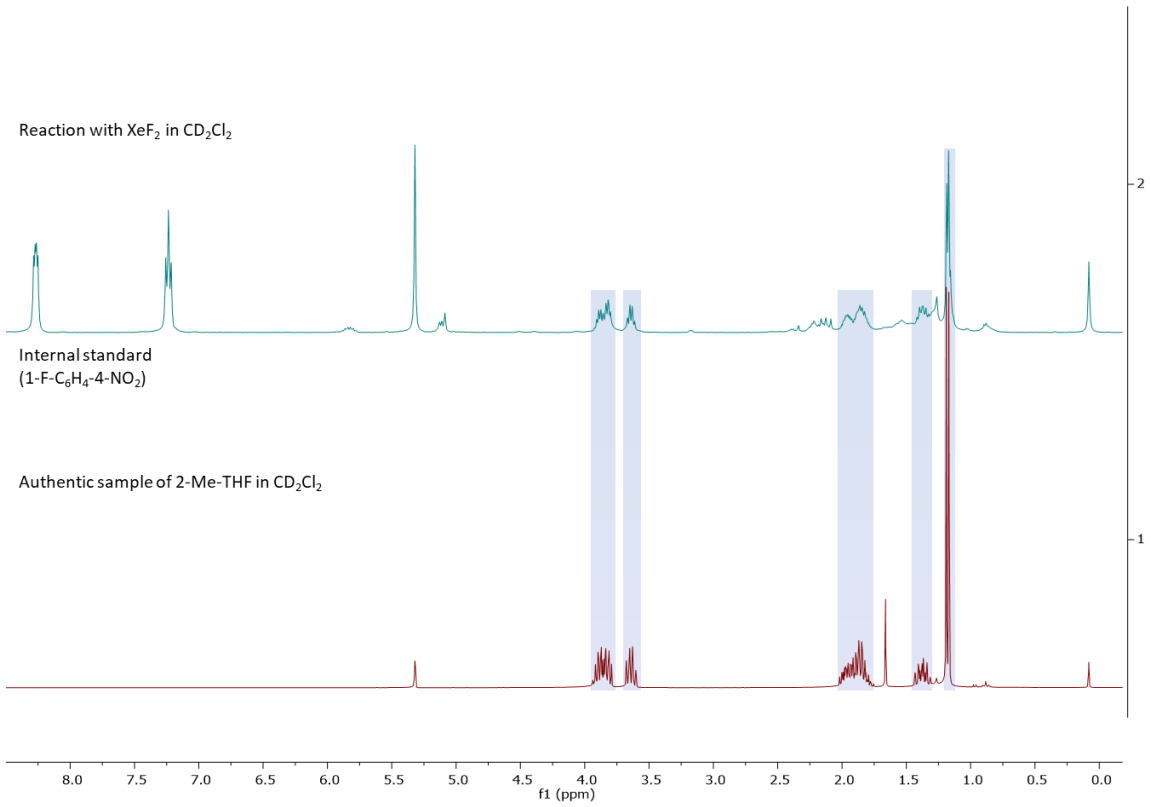

Fig. 37. Comparison between ^{1}H NMR spectra of the reaction of **1b** with **XeF_2** to make **2b**, with an authentic sample of **2b**.

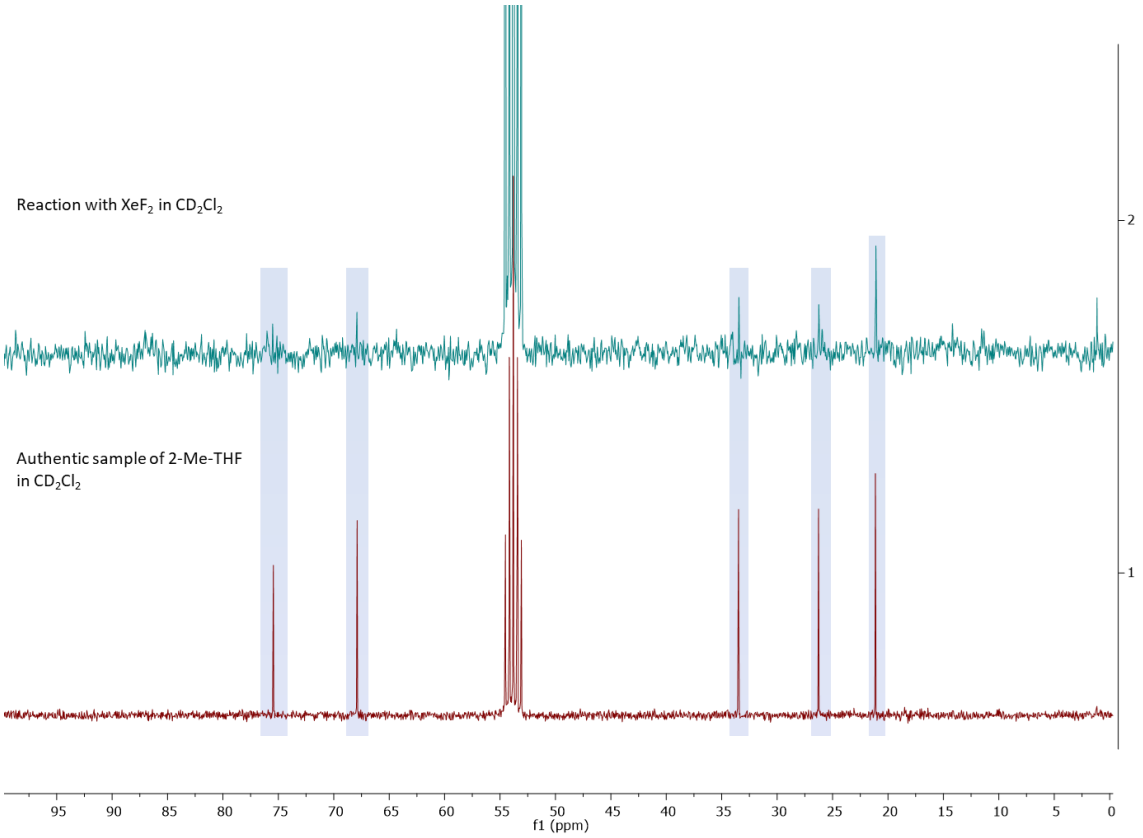

Fig. 38. Comparison between ^{13}C NMR spectra of the reaction of **1b** with **XeF_2** to make **2b**, with an authentic sample of **2b**.

NMR yields are calculated versus *para*-fluoro-nitrobenzene as internal standard. The yield of alkene **6b** is 24-26%, and the yield of 2-Me-THF **2b** is in the range of 50-60%. (Integration indicates 72-84%, which is an over integration due to the presence of one proton from the side product). It is difficult to get a cleaner spectra due to the volatility of the organic products.

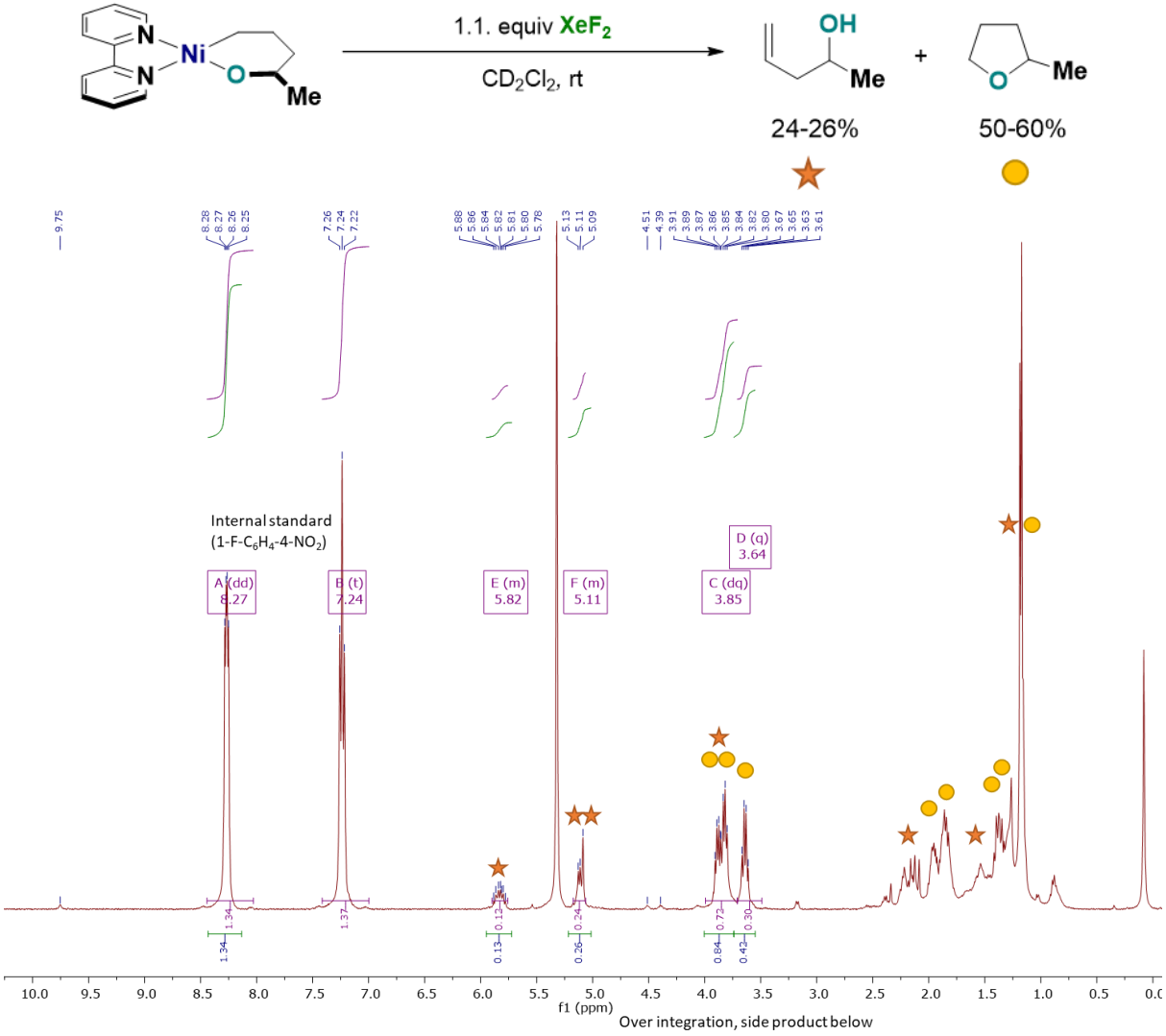

Fig. 39. ^{1}H NMR spectrum of the reaction of **1b** with **XeF_2** to make **2b** with internal standard.

6.1.3. Details for the reaction using reagent 10e and oxanickelacycle 1a:

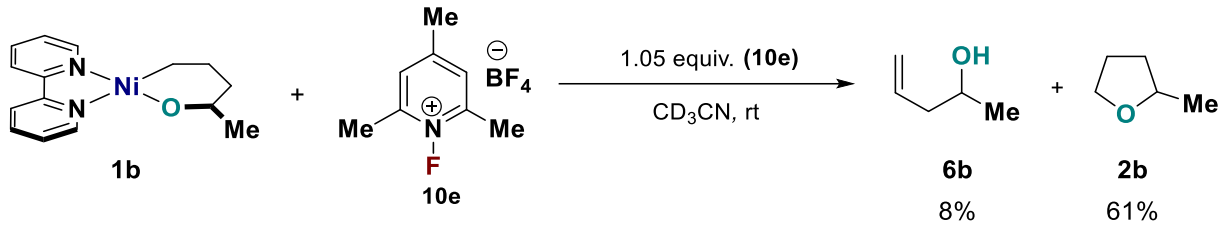

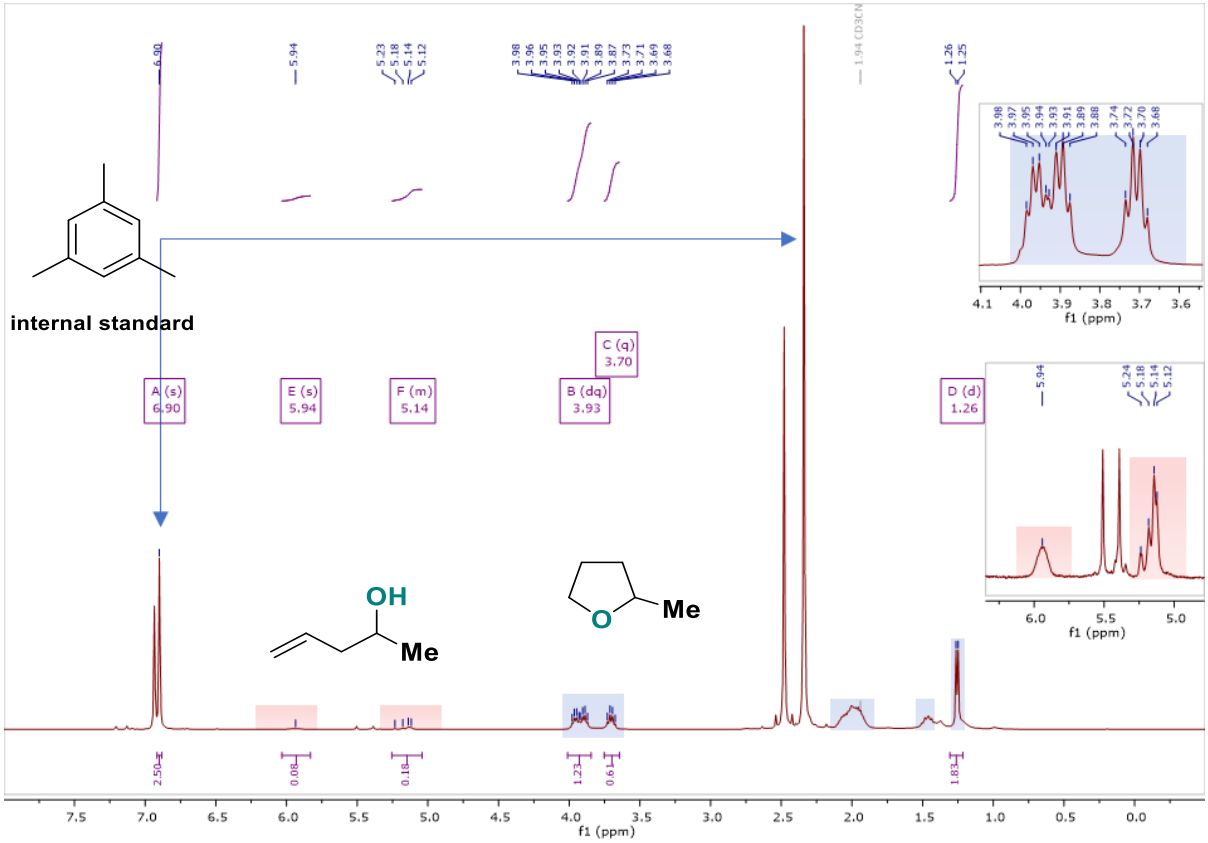

Fig. 40. ^{1}H NMR spectrum of the reaction of **1b** with **10e** to make **2b** with internal standard**.**

6.2. Synthesis of THF

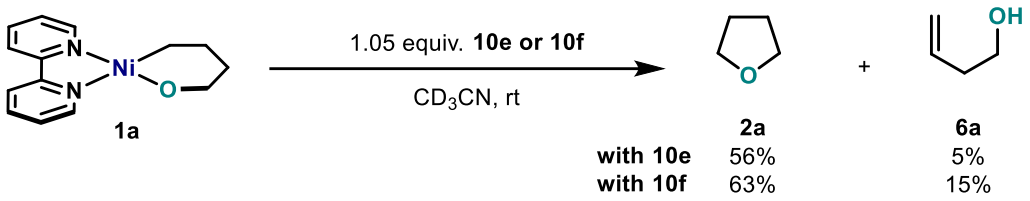

In a glovebox, oxanickelacycle **1a** (8.6 mg, 0.030 mmol, 1 equiv.) is introduced in a J-Young NMR tube. 0.5 mL of dry and degassed CD_3CN is added by syringe, then internal standard (mesitylene, 3.50 μL, 3.02 mg, 0.0252 mmol, 0.839 equiv.) is added. The NMR tube is then capped and shaken to homogenize the purple solution of Ni(II) complex. To this solution NFTPB (**10e**, N-fluoro-2,4,6-trimethylpyridinium tetrafluoroborate) (7.2 mg, 0.032 mmol 1.05 equiv.) is added as solid. The NMR tube is capped again, shaken (the reaction happens in less than 30 seconds to give a pale brown yellow color), and removed from the glovebox for direct NMR measurement at room-temperature. THF **2a** is observed by NMR in 56% yield, along with 5% of **6a**. Similar reactivity is observed using NFTPT (**10f**, N-fluoro-2,4,6-trimethylpyridinium triflate) affording THF **2a** in 63% along with 15% of byproduct **6a**.

^{1}H NMR (400 MHz, CD_3CN) δ 3.66 (m, 2H), 1.85 (m, 2H).

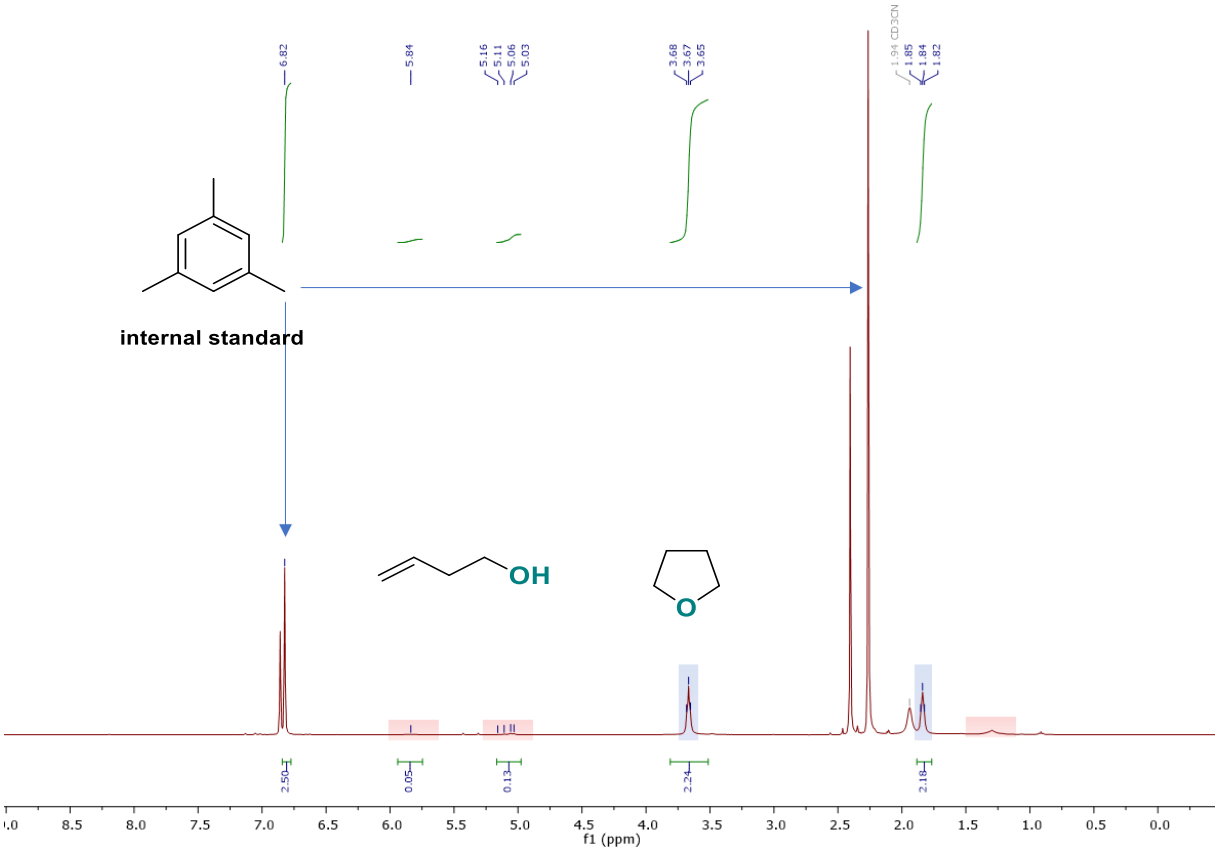

Fig. 41. NMR spectrum of the crude after reaction of **1a** and **10e** at 25 °C in CD_3CN forming THF (**2a**, 56%) and **6a** (5%).

6.3. Synthesis of diethyl ether

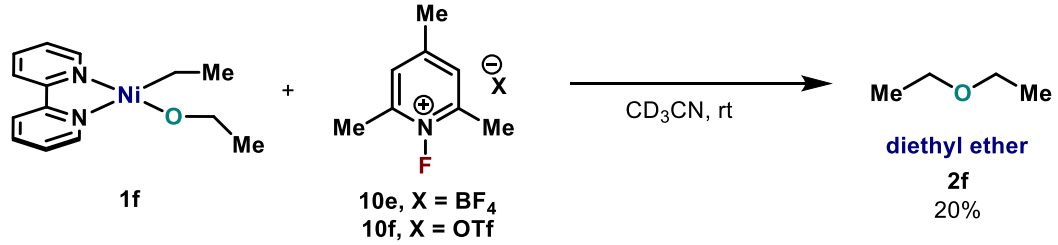

In a glovebox, oxanickelacycle **1f** (9.6 mg, 90% purity, 0.030 mmol, 1 equiv.) is introduced in a J-Young NMR tube. 0.5 mL of dry and degassed CD_3CN is added by syringe, then internal standard (mesitylene, 3.50 μL, 3.02 mg, 0.0252 mmol, 0.839 equiv.) is added. The NMR tube is then capped and shaken to homogenize the purple solution of Ni(II) complex. To this solution NFTPB (**10e**, N-fluoro-2,4,6-trimethylpyridinium tetrafluoroborate) (7.2 mg, 0.032 mmol 1.05 equiv.) is added as solid. The NMR tube is capped again, shaken (the reaction happens in less than 30 seconds to give a pale brown yellow color), and removed from the glovebox for direct NMR measurement at room-temperature. Diethylether **2f** is observed by NMR in 20% yield. Similar reactivity is observed using NFTPT (**10f**, N-fluoro-2,4,6-trimethylpyridinium triflate).

^{1}H NMR (400 MHz, CD_3CN) δ 3.46 (q, *J* = 6.9 Hz, 4H), 1.17 (t, *J* = 6.8 Hz, 6H).

^{13}C NMR (101 MHz, CD_3CN) δ 65.8, 13.7.

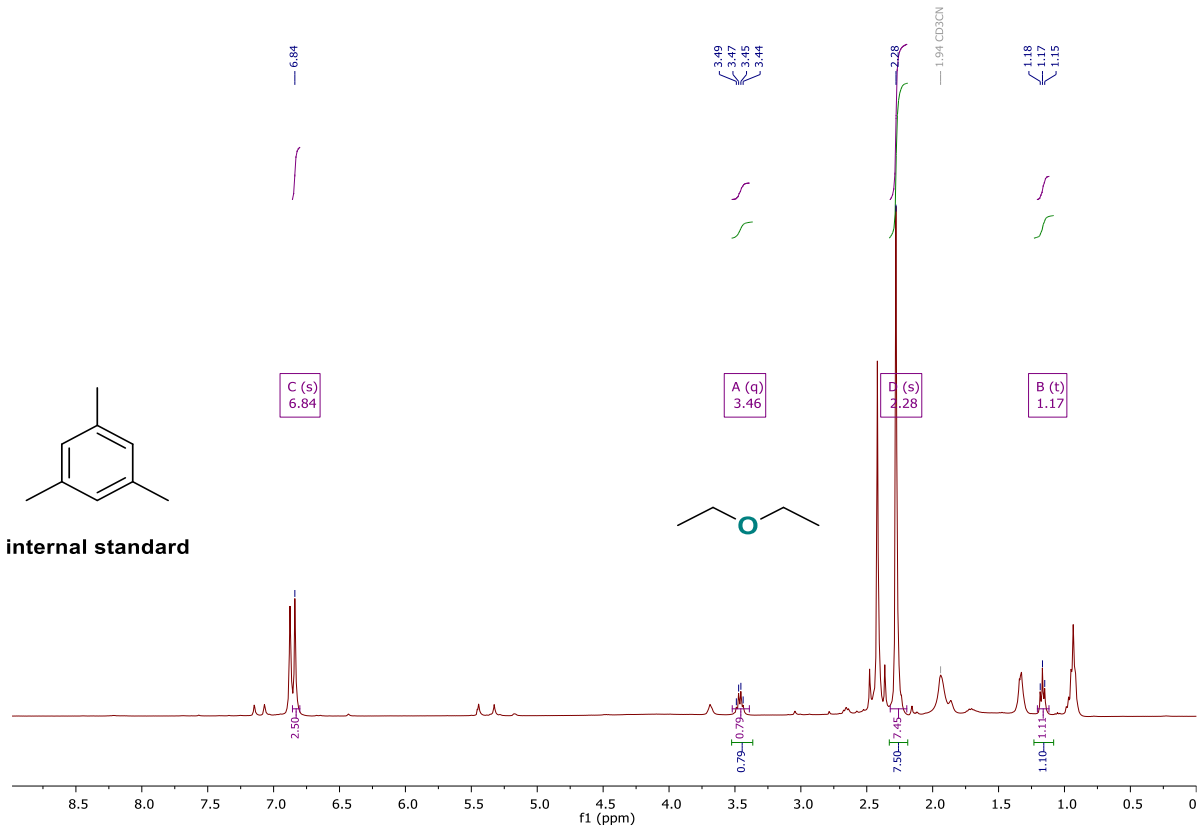

Fig. 42. ^{1}H NMR spectrum of the crude after reaction of **1f** and **10e** at 25 °C in CD_3CN forming Et_2O (**2f**, 20%)

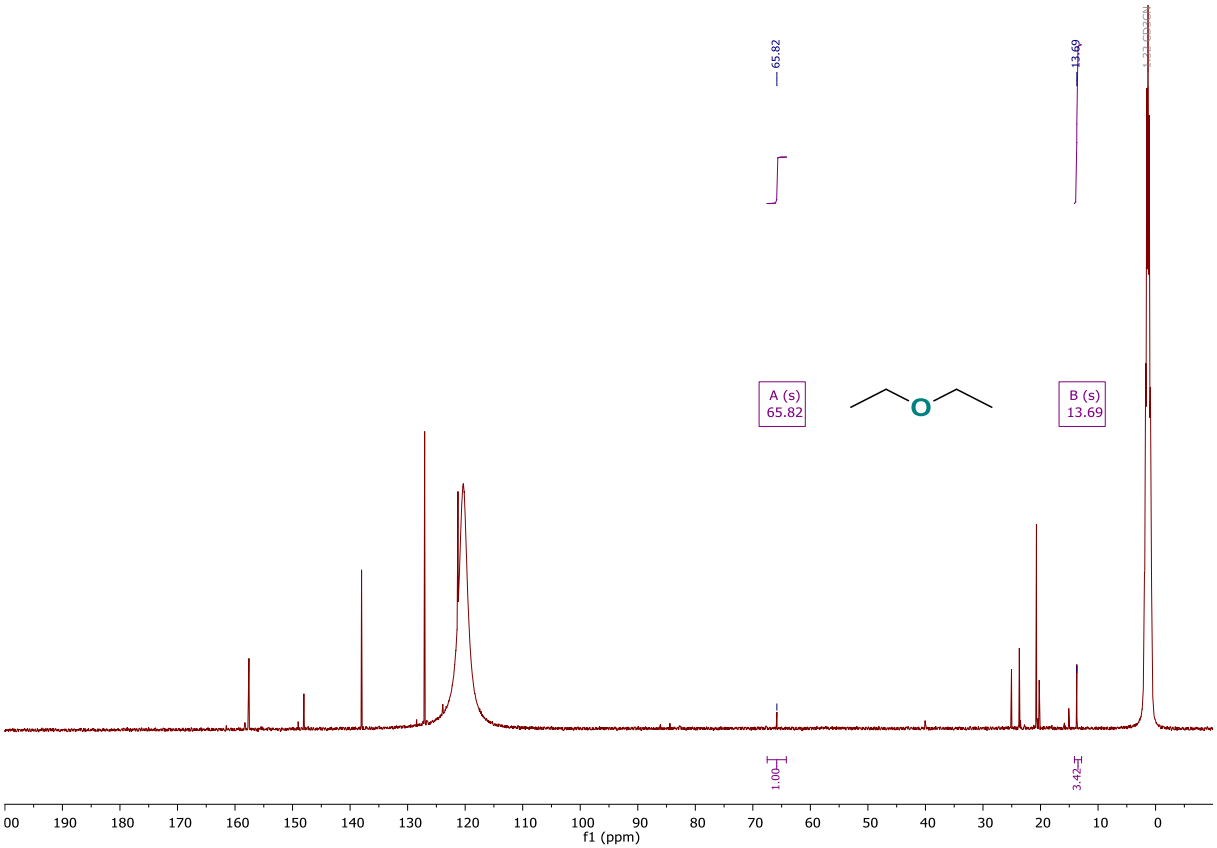

Fig. 43. ^{13}C NMR spectrum of the crude after reaction of **1f** and **10e** at 25 °C in CD_3CN forming Et_2O (**2f**, 20%).

6.4. Mechanistic details of the reaction with F^+ oxidants

6.4.1. Fate of the nickel complex using XeF_2

After the reaction of **1b** at 25 °C in a Schlenk with XeF_2 (**10b**), the solid was isolated by removing all the volatiles under high-vaccum. HRMS analysis using MeOH as solvent revealed the presence of several nickel complexes which are in concordance for *in situ* formation of bipyNiF_2.[26] Formation of such (bipy)NiF_2 via Ni^{IV} bearing two fluoride ligands (*path c*) appeared to be more likely than the alternative pathway consisting in a monomeric Ni^{III}-F (*path a*) giving a Ni^{I}-F after RE which would be then reoxidized to Ni^{II}-F_2. Finally, a mono- or bimetallic RE (*path b)* from dinuclear complex can not be ruled out at this stage, and could also afford such Ni complexes distribution.

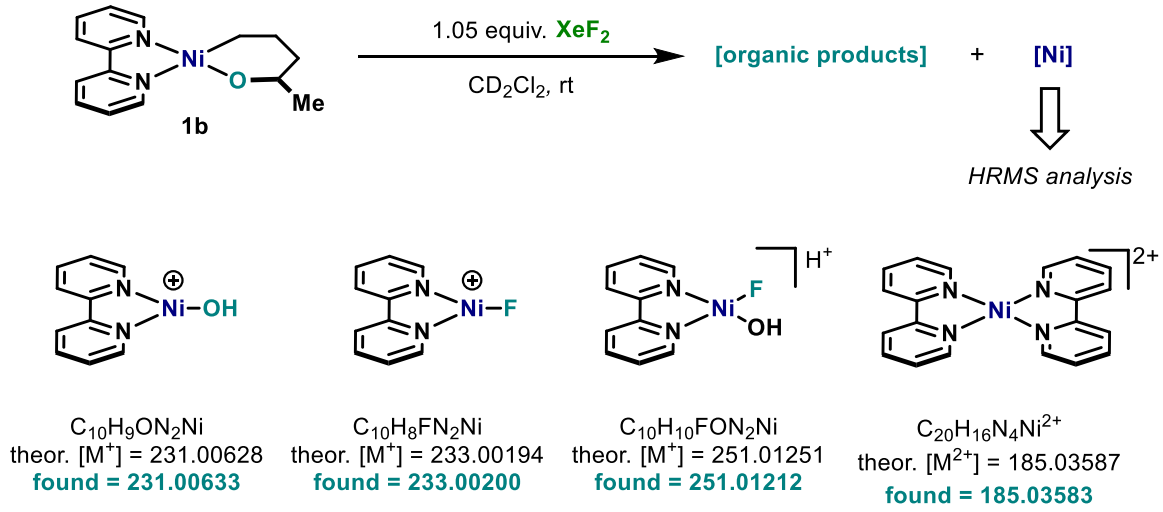

Fig. 44. HRMS analysis of the fate of Ni complex in the reaction of **1b** and **10b** at 25 °C in CD_2Cl_2.

The solids exhibited paramagnetic behavior in NMR. Attempts to observe signals by EPR did not meet any success, thus considering the samples as EPR-silent. This is actually consistent with bipy$Ni^{II}F_2$ complex being tetrahedral high spin complexes.

6.4.2. Attempts towards spectroscopic observations of Ni^{III} or Ni^{IV} intermediates

All attempts to observe potential Ni^{III} or Ni^{IV} complexes bearing simple bipy ligand were unsuccessful, even at –90 °C in the NMR probe. The observed reactivity was either too fast (< 1 min) or facing stirring / solubility issues (Fig. 45). The use of N-fluoropyridinium salts **10e-**

f, XeF_2 (**10b**), SelectFluor (**10c**), or addition of coordinating ligands such as pyridine or DMAP to further stabilize the putative Ni species formed did not lead to any detectable intermediate neither in the diamagnetic nor the paramagnetic region by ^{1}H or ^{19}F NMR (peaks below –250 ppm for Ni^{IV}).

Additionally, we envisaged that in situ release of one equivalent of pyridine could stabilize a high valent Ni intermediate. To do so, the use of the unsubstituted N-fluoropyridinium was tested; however this strong oxidant also gave a very fast reaction without detection of intermediates.

General procedure:

In a glovebox, oxanickelacycle **1b** (9.0 mg, 0.030 mmol, 1 equiv.) is introduced in a J-Young NMR tube. 0.25 mL of dry and degassed solvent is added by syringe. The NMR tube is then capped and shaken to homogenize the purple solution of **1b**. The solution is then cooled in dry ice. To this solution, oxidant (**10b-f**) (0.0315 mmol 1.05 equiv.) is added as a solution in 0.25 mL of solvent, under argon. The NMR tube is capped again, shaken slowly still inside of the dry ice-bath and brought for direct NMR measurement at the indicated temperature. In all the cases below, no intermediates was observed, while the efficient formation of 2-Me-THF **2b** is always confirmed.

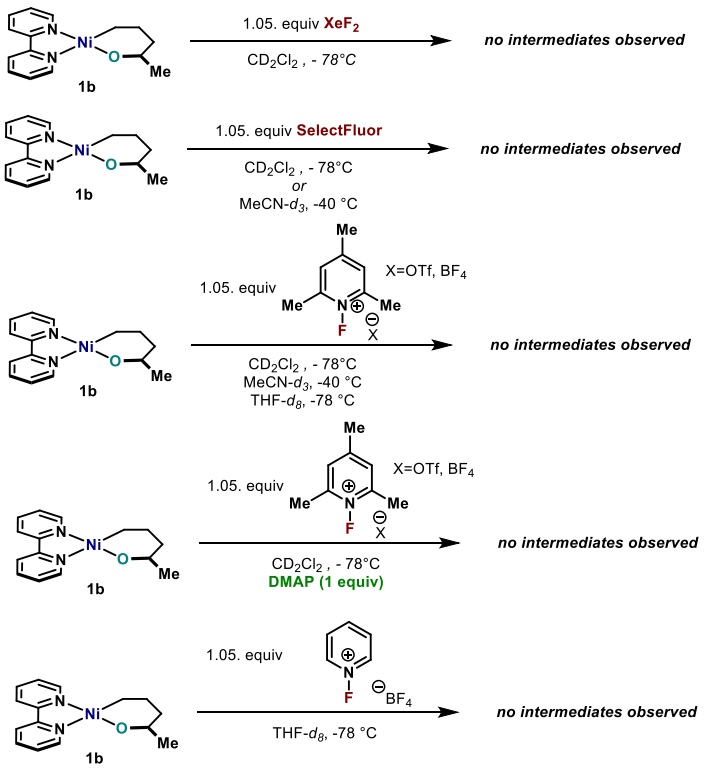

Fig. 45. Summary of attempts to observe by NMR reactive high valent nickel intermediates using F^+ oxidants at low temperature

For **10b** and **10c** in CD_2Cl_2, the oxidant is placed as solid at the bottom of the NMR tube, and then 0.25 mL of solvent is added. This resulting mixture is shaken, and placed in dry ice. Then, 0.25 mL cold solution of **1b** is added before going to the NMR.

For **10e-f**, when the reaction takes places in CD_2Cl_2 or THF-d_8, **10e-f** are added as 0.15 mL CD_3CN solution to a 0.35 mL solution of of **1b** in CD_2Cl_2 or THF-d_8. This ensure a good solubility of the oxidant. The reverse addition order (as for **10b-c**) was tested but without greater success.

Finally DMAP was added as solid inside the glovebox, at the same time of addition of **1b**.

6.4.3. Detection of C(sp^3)-F bond formation

Interestingly, during these experiments we often detected a very minor peak at –220 ppm by ^{19}F NMR, which seems to belong to a stable species and it does not evolve overtime. Furthermore, in the coupled ^{19}F NMR, it is a triplet. This peak would be consistent with a CH_2F group. We therefore assign this peak to traces of formation of C(sp^3)-F. Such bond formation is most certainly suggestion of the involvement of high-valent nickel species.

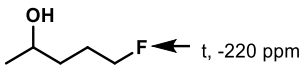

6.4.4. Attempts of in situ formation of Ni^{III}–F species

We also decided to check the outcome of the oxidation of oxanickelacycle **1b** with $FcBF_4$ (1.0 equiv.) in the absence or presence of CsF (Fig. 43). It was envisaged that if a cationic Ni^{III} is formed, subsequent trapping of the F anion would ensure the formation of a putative Ni^{III}–F, which can then undergo reductive elimination. However, when the reaction was performed, only traces (<5%) of **2b** were obtained, with unidentified byproducts being dominant. This experiment does not rule out the presence of Ni^{III} species but certainly indicates that F- is still a good base to eliminate olefin via an E2 mechanism. Importantly, no C(sp^3)–F bond formation was observed. This result point out at the involvement of other species than Ni^{III} in the C–O bond forming event.

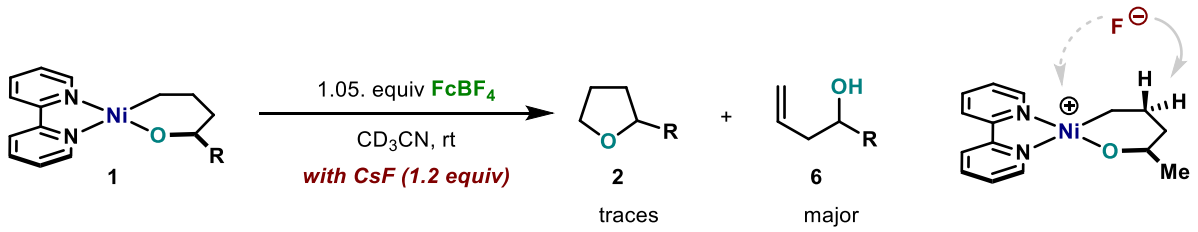

Fig. 46. Reaction between **1b** and $FcBF_4$, in presence of CsF, and possible reaction pathways.

Another experiment we performed is the addition of CsF or AgF to the in situ generated Ni^{III} dimer **9b** (Fig. 47.). In the case of CsF, C-I bond formation is still dominating at short conversion while C-O bond formation remain low. In the case of AgF, 18% of the 2-Me-THF is observed, and C-I bond formation is barely detected. However, major decomposition happens, hence the overall low yield of this reaction. It is unclear yet if the AgF-reaction occurred via halogen exchange (via *in situ* generation of cationic fluorinated bimetallic ***int-I***) or by oxidation to Ni^{IV} species.

Reaction procedure:

In a glovebox, oxanickelacycle **1b** (9.0 mg, 0.030 mmol, 1 equiv.) is introduced in a flame dried Schlenk equipped with a teflon coated stir bar. Then, outside of the glovebox, a precooled solution of 0.5 mL of iodine (7.6 mg, 0.030 mmol, 1.0 equiv., under argon) in CD_2Cl_2 is added to a stirring solution of **1b** in 0.5 mL of CD_2Cl_2 (in the Schlenk, in dry ice). The reaction is kept stirring for 5 min to ensure the formation of paramagnetic dimer **9b** (dark yellow brown color). At this stage, under argon flow, at –78°C, solid CsF (11.4 mg, 0.0750 mmol, 2.5 equiv.) or AgF (9.5 mg, 0.075 mmol, 2.5 equiv.) is added all at once. After 5 min stirring at –78°C, the reaction is allowed to warm up to room temperature and kept stirring for additional 30 min. In the case of CsF, some precipitations occurred, but the solutions was still brown. However, in the case of AgF, the solution became colorless and major precipitations (grey solids) occurred. To this mixture was added internal standard mesitylene (3.5 μL, 0.025 mmol), followed by filtration using HPLC filter in a NMR tube. The results are indicated below.

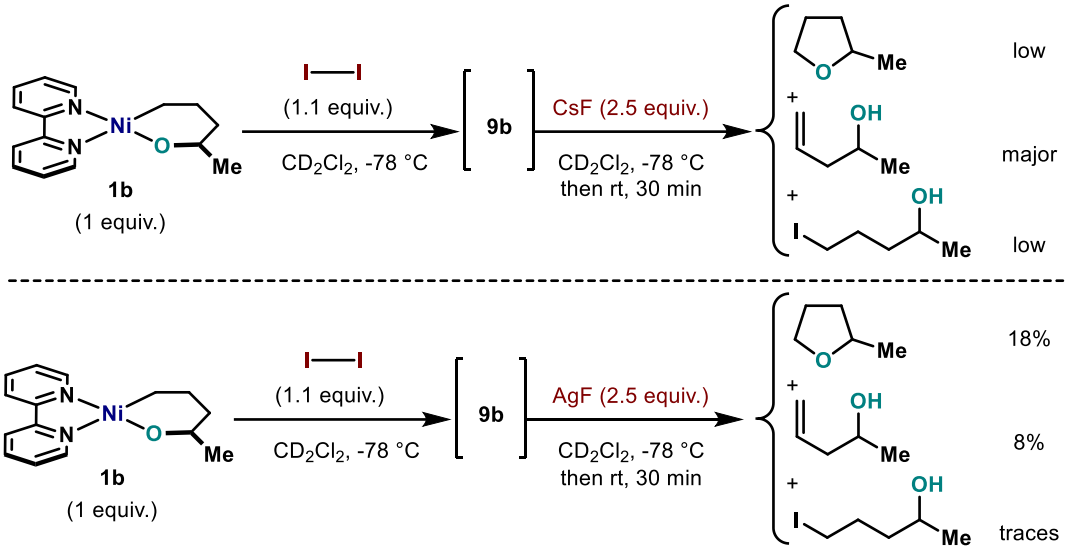

Fig. 47. Reactions of in situ formed **9b** with CsF and AgF.

6.4.5. Low temperature HRMS analysis of intermediates in the reaction using 10f

HRMS is a good tool to detect reactive intermediates in low amount. Quick analysis of a reaction mixture at –78 °C, in CD_2Cl_2 to ensure low solubility of **10f** (added as solid, with only a quick shake before the measurement) and therefore lower reaction rate, allowed the observation of several species (intermediates and final products complexes, Fig. 48). At this stage, it is unclear if ***int-II*** is obtained from oxidation of remaining starting material due to the measurement, or if it is from dissociation of the dimer ***int-I***.

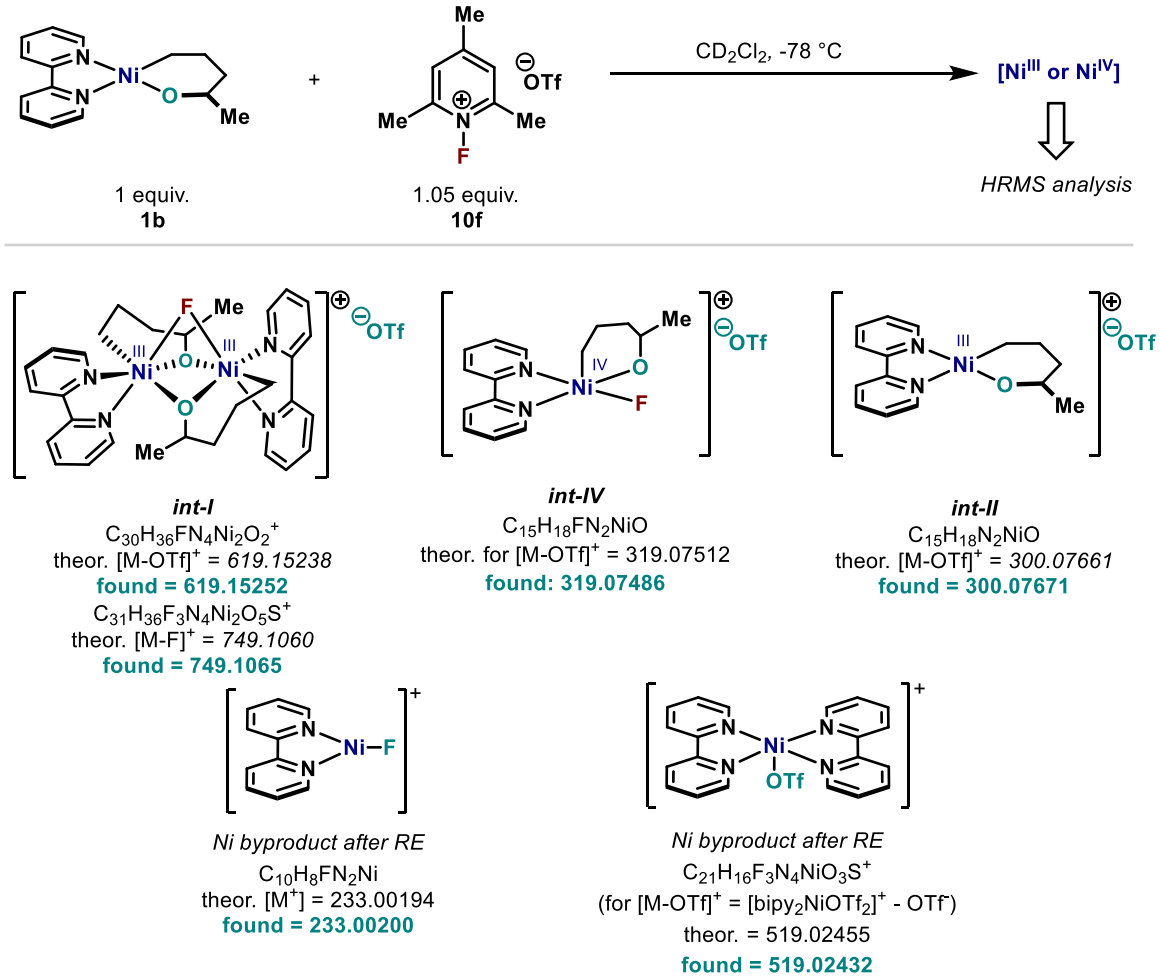

Fig. 48. HRMS analysis of the fate of Ni complex in the reaction of **1b** and **10f** at –78 °C in CD_2Cl_2.

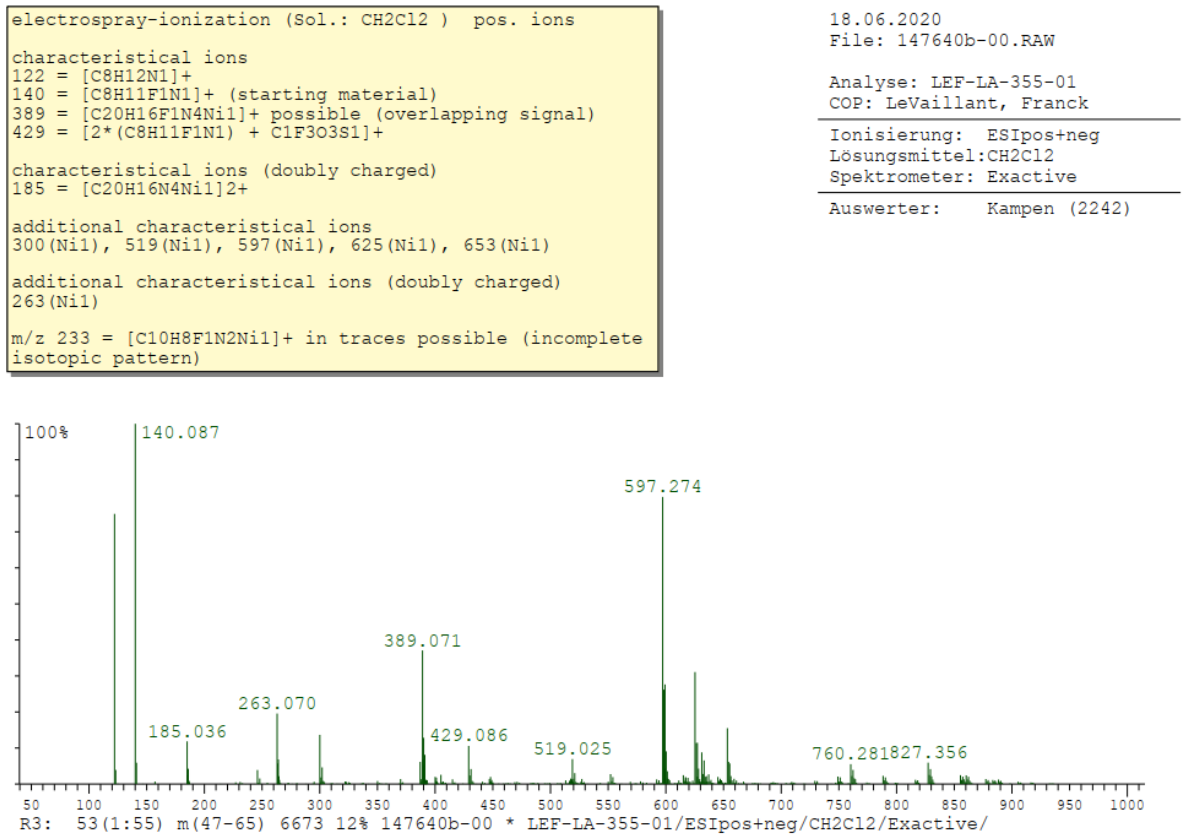

Fig. 49. HRMS analysis of a crude reaction mixture using **1b** and **10f** at –78 °C in CD_2Cl_2.

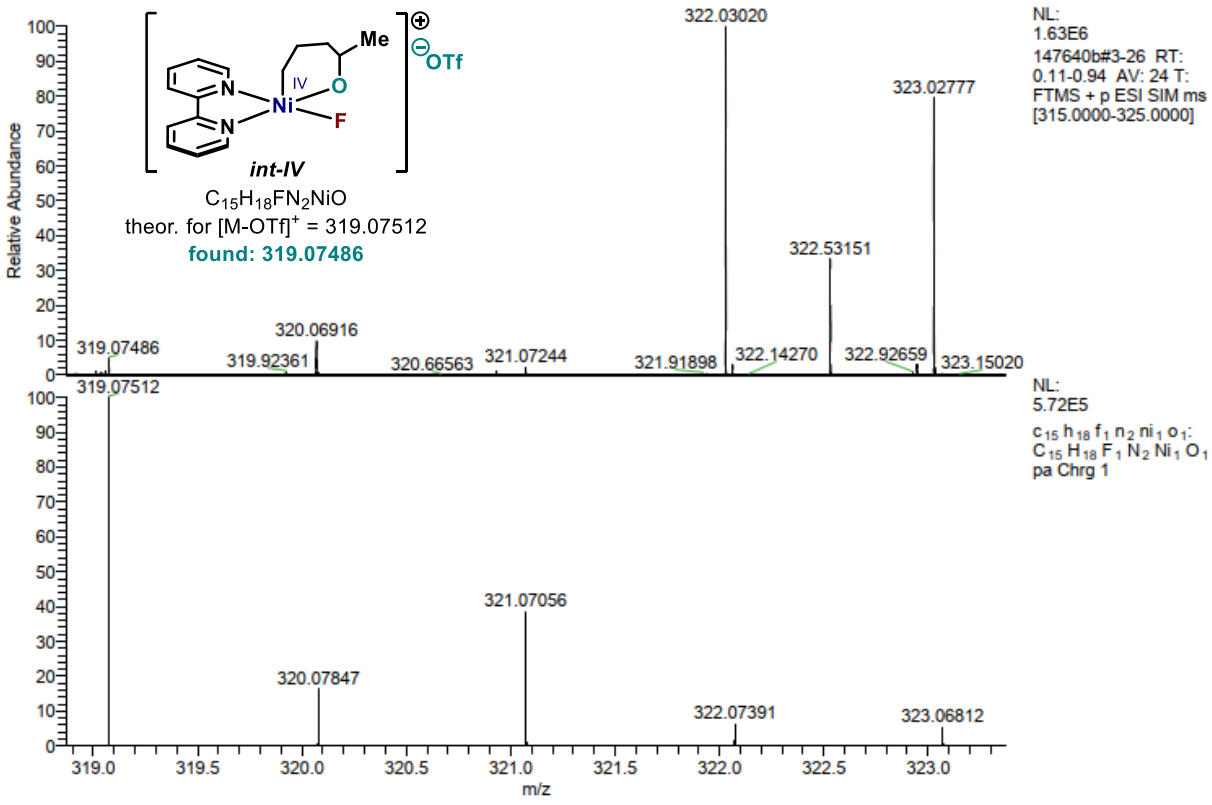

Fig. 50. HRMS analysis of a crude reaction mixture using **1b** and **10f** at –78 °C in CD_2Cl_2,

showing a peak corresponding to [***int-IV***-*OTf*]+; theoretical *m/z* of the peak corresponding to [***int-IV***-*OTf*]+ (bottom).

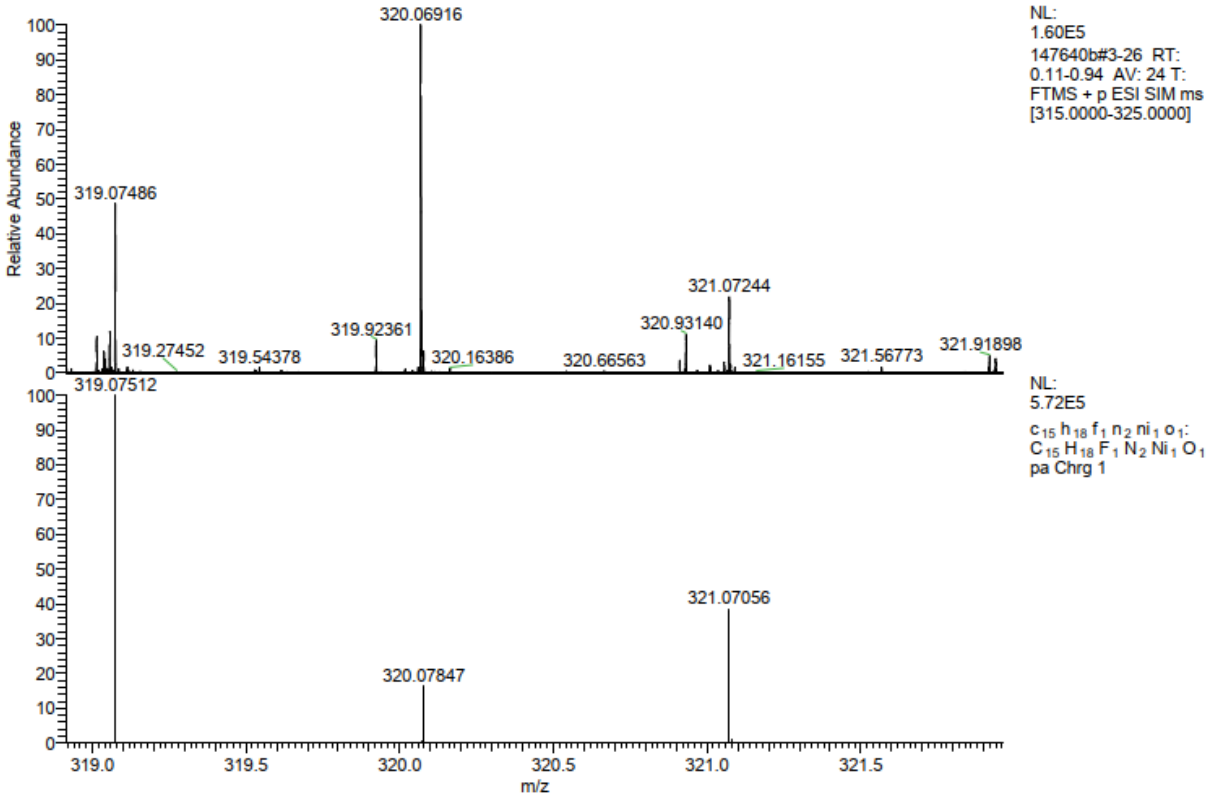

Fig. 51. HRMS analysis of a crude reaction mixture using **1b** and **10f** at –78 °C in CD_2Cl_2, showing a peak corresponding to [***int-IV***-*OTf*]+; theoretical *m/z* of the peak corresponding to [***int-IV***-*OTf*]+ (bottom).

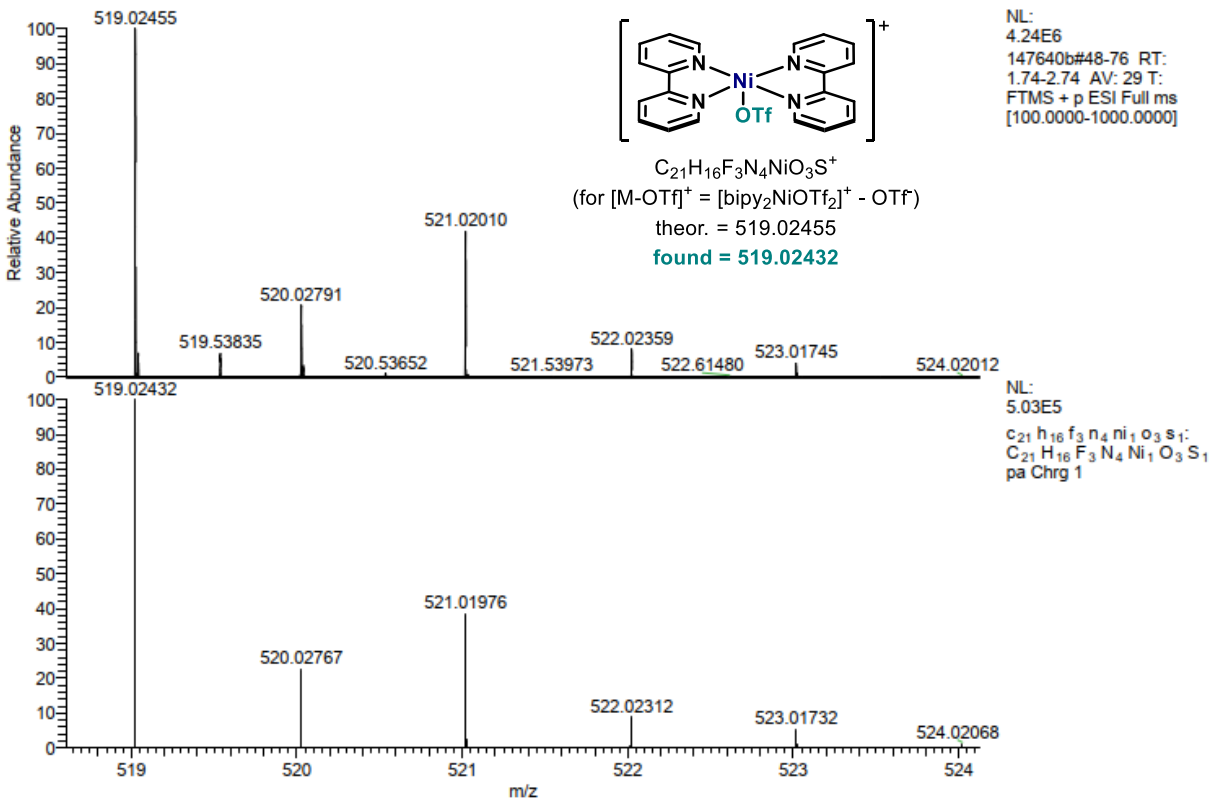

Fig. 52. HRMS analysis of a crude reaction mixture using **1b** and **10f** at –78 °C in CD_2Cl_2, showing a peak corresponding to [***S1****-OTf*]+; theoretical *m/z* of the peak corresponding to [***S1****-OTf*]+ (bottom).

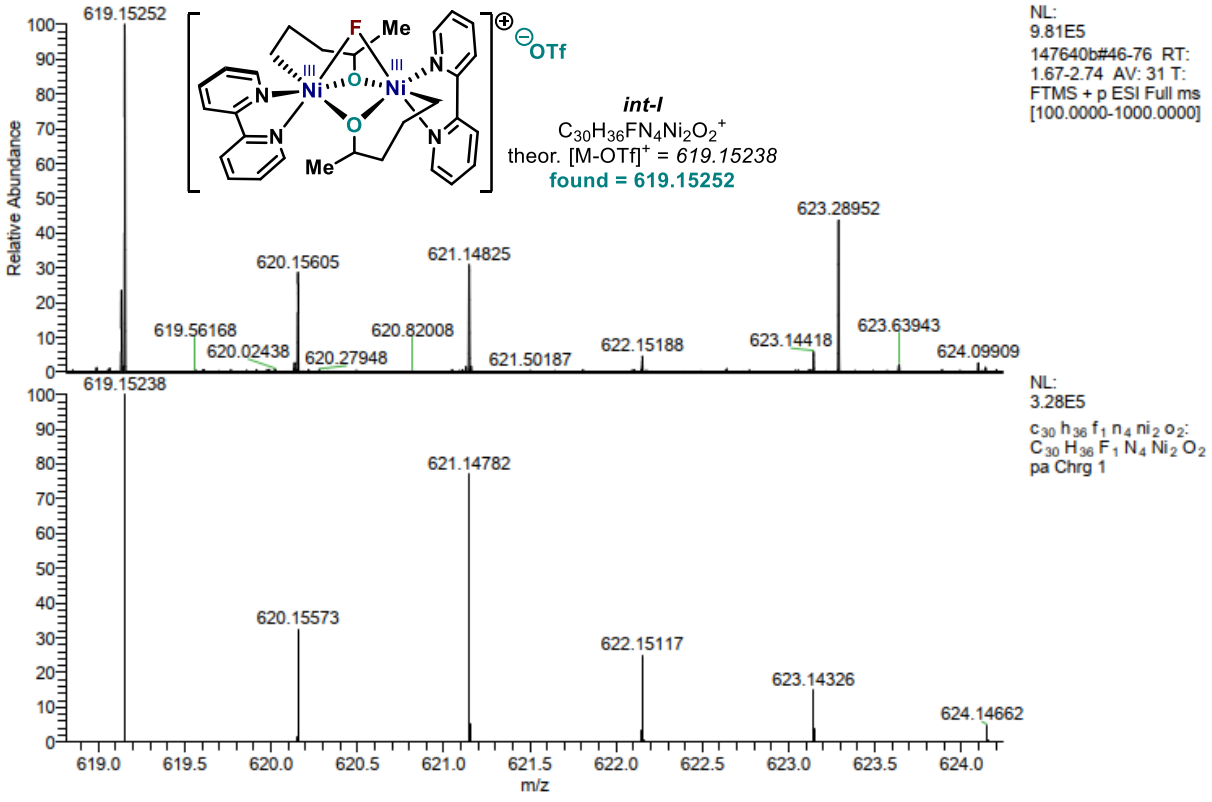

Fig. 53. HRMS analysis of a crude reaction mixture using **1b** and **10f** at –78 °C in CD_2Cl_2, showing a peak corresponding to [***int-I***-*OTf*]+; theoretical *m/z* of the peak corresponding to [***int-I***-*OTf*]+ (bottom).

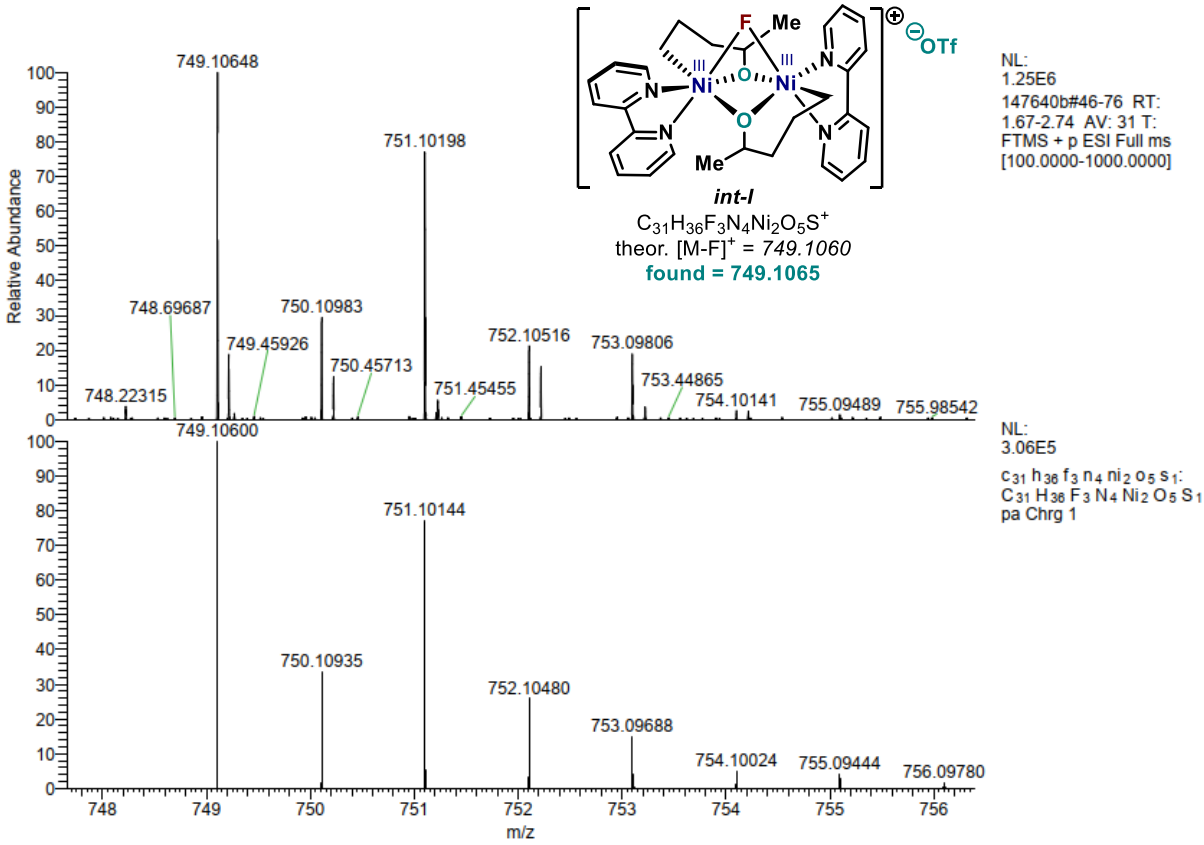

Fig. 54. HRMS analysis of a crude reaction mixture using **1b** and **10f** at –78 °C in CD_2Cl_2, showing a peak corresponding to [***int-I***-*F*]+; theoretical *m/z* of the peak corresponding to [***int-I***-*F*]+ (bottom).

6.4.6. EPR measurement: In situ characterization of Ni^{III}–Ni^{III} dimer *Int-I*

Since Ni^{III} intermediates can not be ruled out based on our current data, we have placed extra effort in trying to intercept paramagnetic species by EPR. Due to low solubility of N-fluoropyridinium at low temperatures, the need for a glass for the analysis and the fast reaction rates, sample preparation for EPR analysis became a major challenge. Transferring a solution from a reaction occurring in a Schlenk resulted in decomposition and messy EPR spectra. Therefore, we attempted the reaction of a frozen solution of **1b** in toluene with a slowly added solution of N-fluoropyridinium in DCM at –95 °C (see the procedure below) directly inside the quartz tube. In this way, we aimed at intercepting any Ni^{III}–F formed at the interface between both solid solutions that slowly react upon shaking.

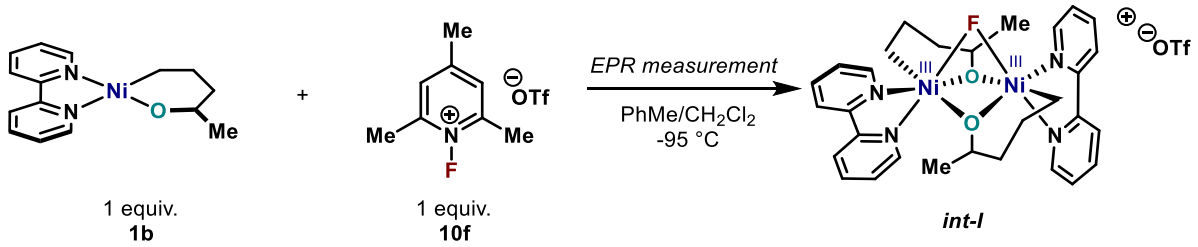

In a glovebox, oxanickelacycle **1b** (3.0 mg, 0.010 mmol, 1 equiv.) is introduced in a flame dried Schlenk equipped with a Teflon coated stir bar. Outside of the glovebox, under argon, 1.0 mL of dry and degassed tolune is then added by syringe, and the resulting deep blue solution is stirred to homogenize it. Separately, a solution of NFTPT (**10f**, N-fluoro-2,4,6-trimethylpyridinium triflate) (2.9 mg, 0.010 mmol 1.0 equiv.) in 0.50 mL of dry and degassed DCM is prepared in a vial under argon.

Then, a dry long EPR tube (quartz) is placed under an argon atmosphere using a T-connector. 100 µL of the oxanickelacycle **1b** solution is introduced into this tube at room temperature, and the tube is washed with a drop of toluene. At this point, the bottom of the tube (until half of the tube) is placed inside of a pentane/liquid nitrogen bath (–120 °C), which allow to freeze the solution. Then, 50 µL of the solution of NFTPT (**10f**) is introduced, which got frozen before touching the frozen deep blue solution. The tube is kept under positive argon pressure during the mixing times: first, the frozen solution of NFTPT is allowed to warm slowly out of the bath, thus allowing drops to form on the sidewall of the tube, then frozen again. This cycle is made several times and until the oxidant solution reached the nickel complex solution. A gradient of color appeared, from deep blue/purple at the top, brown/dark orange in the middle and colorless at the bottom of the sample (the oxidant went down during this phase). At this stage, the sample

was allowed one more time to warm up (–95 °C), then shaken gently, and finally frozen definitively at –120 °C. At this point, the EPR tube was disconnected under positive pressure of argon, capped and transferred in liquid nitrogen for storage before EPR analysis.

The intermediate ***int-I*** resulting from the reaction of **1a/b** with **10f** was very short lived but a sufficient amount could be trapped after rapid (see *vide supra*) mixing at –95 °C and subsequent freezing in liquid nitrogen. The overall intensity of the EPR spectrum at 20 K (Fig. 55) was quite smaller than that of **9a/b**. However, the EPR spectrum did show similarities to that of **9a/b** (Fig. 30), i.e. additional splittings with an intensity ratio consistent with a Ni^{III} dimer species. The width of the spectrum, however, is reduced with respect to that of **9a/b** suggesting a reduction in the dipolar interaction between the two Ni^{III} centers. Spectral fits (Fig. 55) indeed resulted in a smaller dipolar interaction (299 MHz vs 517 MHz) whereas the g-tensor only changed slightly (Table S6). It should be noted that the fitting parameters of **9a/b** and ***int-I*** are probably not unique, given the small number of spectral features and the large number of free parameters. The fitting of multi-frequency EPR experiments on the same compounds should certainly enhance the reliability of the obtained parameters. Nevertheless, the current fits do confirm that the observed EPR spectra are consistent with a Ni^{III} dimer with the (twofold axis) symmetry properties of **9a**.

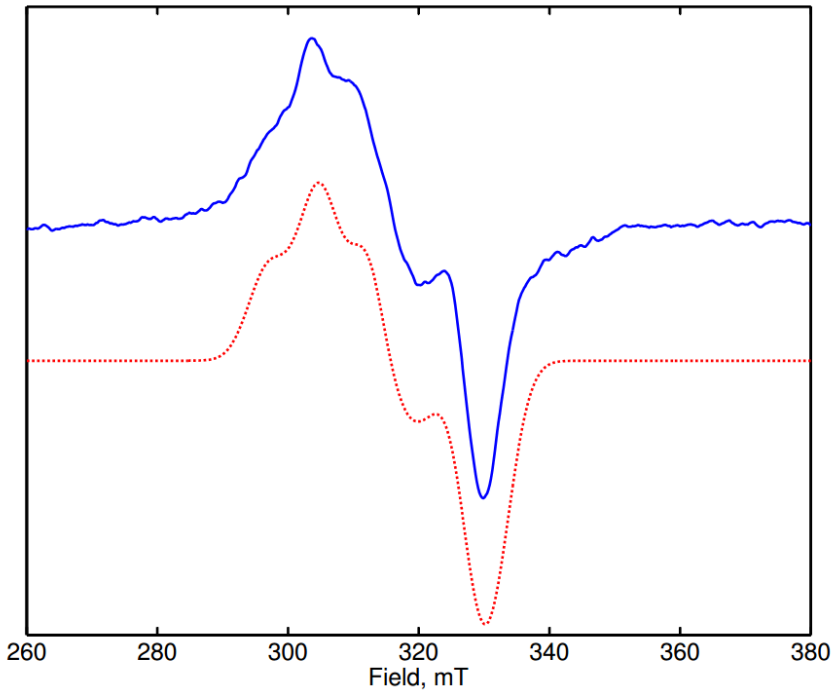

Fig. 55. EPR of ***int-I*** at 20K. Experimental conditions: Power=2 mW, Modulation (100kHz) amplitude 7.5 Gauss. The dotted red trace represents the Easyspin (esfit) simulation with

parameters g=(2.103 2.200 2.227). Dipolar interaction *D*=299 MHz, *J*=100 MHz. All fitted parameters are listed in table S6.

Table S6. Overview of Experimental and Theoretical Spectral Parameters for **9a/b** and ***int-I***. DFT g-values were obtained from the corresponding NiGa Model.

Compound	g1	g2	g3	α	β	γ	J (MHz)	D (MHz)	d
9a	2.081	2.155	2.279	12	-167	99	50	550	-0.11
9b	2.084	2.144	2.287	-36	163	52	50	517	-0.12
9a-DFT	2.094	2.135	2.200						
Int-I	2.103	2.200	2.227	-35	-154	17	100	299	+0.30
***Int-I*-DFT**	2.080	2.136	2.190						

6.4.7. DFT Calculation for Ni^{III}–Ni^{III} dimer *Int-I*

To verify if a fluoride bridged Ni^{III} dimer of the same type as the iodide bridged complex **9a** is feasible, a DFT geometry optimization was run on the coordinates of **9a** replacing iodide by fluoride. The complex geometry changed slightly by shortening the Ni-F bonds from 2.9 Å (iodide) to 2.0 Å (fluoride). For the iodide bridged complex the Ni-O-Ni angles were 90 degrees whereas the Ni-I-Ni angle was 60 degrees. For the fluoride bridged complex this changed to 80 degrees for all angles. The almost undistorted octahedral coordination of the Ni^{III} centers, however, did not change significantly. As can be seen in figure 56 and 57 the bipyridine ligands rotate significantly when the iodide bridge is replaced by fluoride. It remains to be investigated if and how these structural changes are related to the reactivity of the halide bridged Ni^{III} dimer complex.

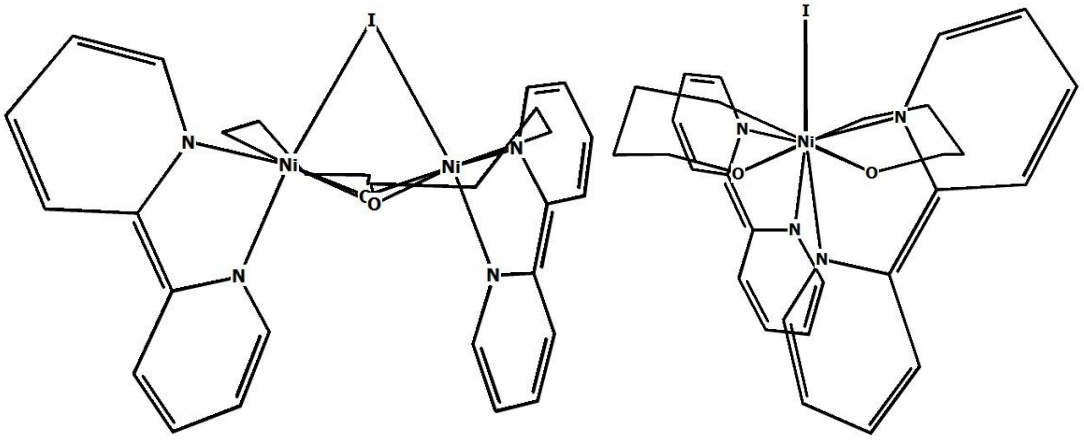

Fig. 56. Structural view of **9a** perpendicular to Ni-I-Ni plane (left) and along Ni-Ni axis (right). (Bond orders not represented)

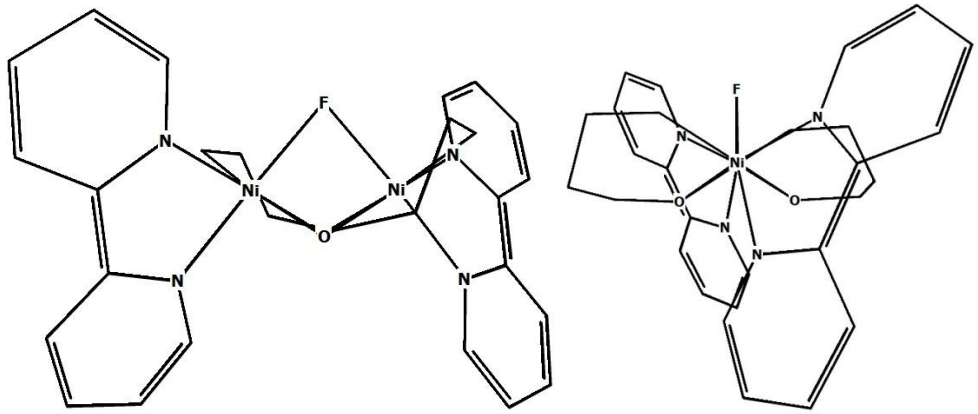

Fig. 57. Structural view of ***Int-I*** perpendicular to Ni-F-Ni plane (left) and along Ni-Ni axis (right). (Bond orders not represented)

6.4.8. Attempts of ^{19}F NMR measurement for the detection of *int-I*

We performed ^{19}F NMR experiments at –110 °C in PrCN that would indicate the presence of F in such paramagnetic intermediate. However, the low concentration and the high paramagnetic nature of this complex prevented the detection of any F signal. Therefore, the actual structure and connectivity is still unknown at this moment and more studies are needed to fully characterize such species.

6.4.9. Reaction using 0.5 equiv. of 10f

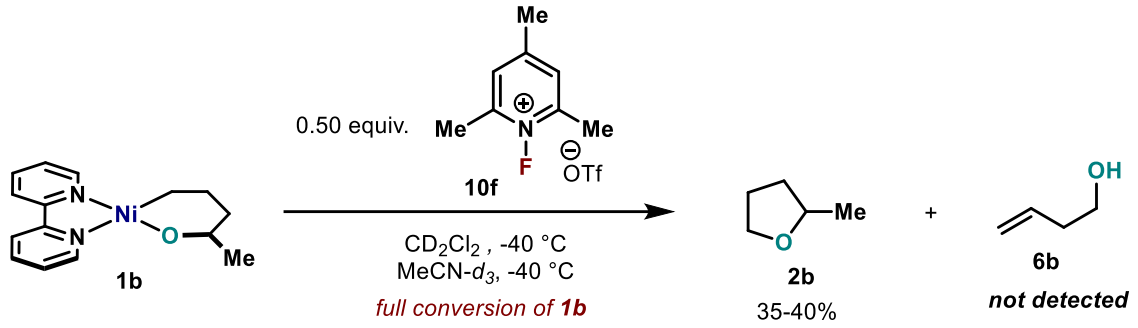

Upon several trials (CD_2Cl_2 or MeCN-d_3), we observed full conversion of **10f**, with yield of **2b** in the range of 35-40%, and the formation of **6b** was not detected. The absence of **6b** would suggest that cationic Ni^{III} species are not operative and would strongly speak against *path a*. The fact that when using 0.5 instead of 1.05 equiv of **10f**, the yield is reduced in half, would be in agreement with a scenario where both *path b* and *path c* could be operative. As for the fate of the Ni, no other aromatic protons than the 2,4,6-trimethylpyridine were observed, suggesting the formation of NMR silent Ni species.

A putative mechanism for when 0.5 equiv **10f** are used as oxidant is depicted in figure 58.

First, oxidation of 1b occurs very fast with only 0.5 equiv. of **10f** upon sequential SET and dimerization, generating the short lived ***int-1*** (trapped by EPR and HRMS). Compared to the corresponding iodine-bridged complexes **9a-b**, ***int-1*** seems to be unstable and evolves quickly to only half of the yield observed for 1 equiv of oxidant **10f**. Three mechanistic scenarios are possible, paths a-c.

According to the product distribution, *path a* appears unlikely (*vide supra*). It is also not sure that ***int-III*** is sufficiently reactive to promote the C-O bond formation at such cryogenic temperature.

If *path c* is operative, the dissociation of ***int-I*** would lead to ***int-IV*** and **1b**. Such cationic Ni^{IV} intermediate would be very reactive and lead to a fast C–O bond formation upon reductive elimination. We did not detect the formation of **1b**. However, it is possible that **1b** was released followed by association with *bipyNiFOTf*, formed after reductive elimination. This process would stabilize the ionic complex and lead to a dinuclear structure bearing two high spin tetrahedral Ni. Such complexes are expected to be EPR and NMR silent. This mechanistic scenario in which Ni^{IV} complexes are responsible for C–O bond formation is consistent with our current observations.

If *path b* is operative, a mono- or bimetallic process could lead to **2b** along with a dinuclear Ni^{I}-Ni^{III} complex. It could be envisioned that this complex undergo redox isomerization to furnish the same dinuclear structure with Ni^{II}-Ni^{II}. This pathway cannot be excluded currently.

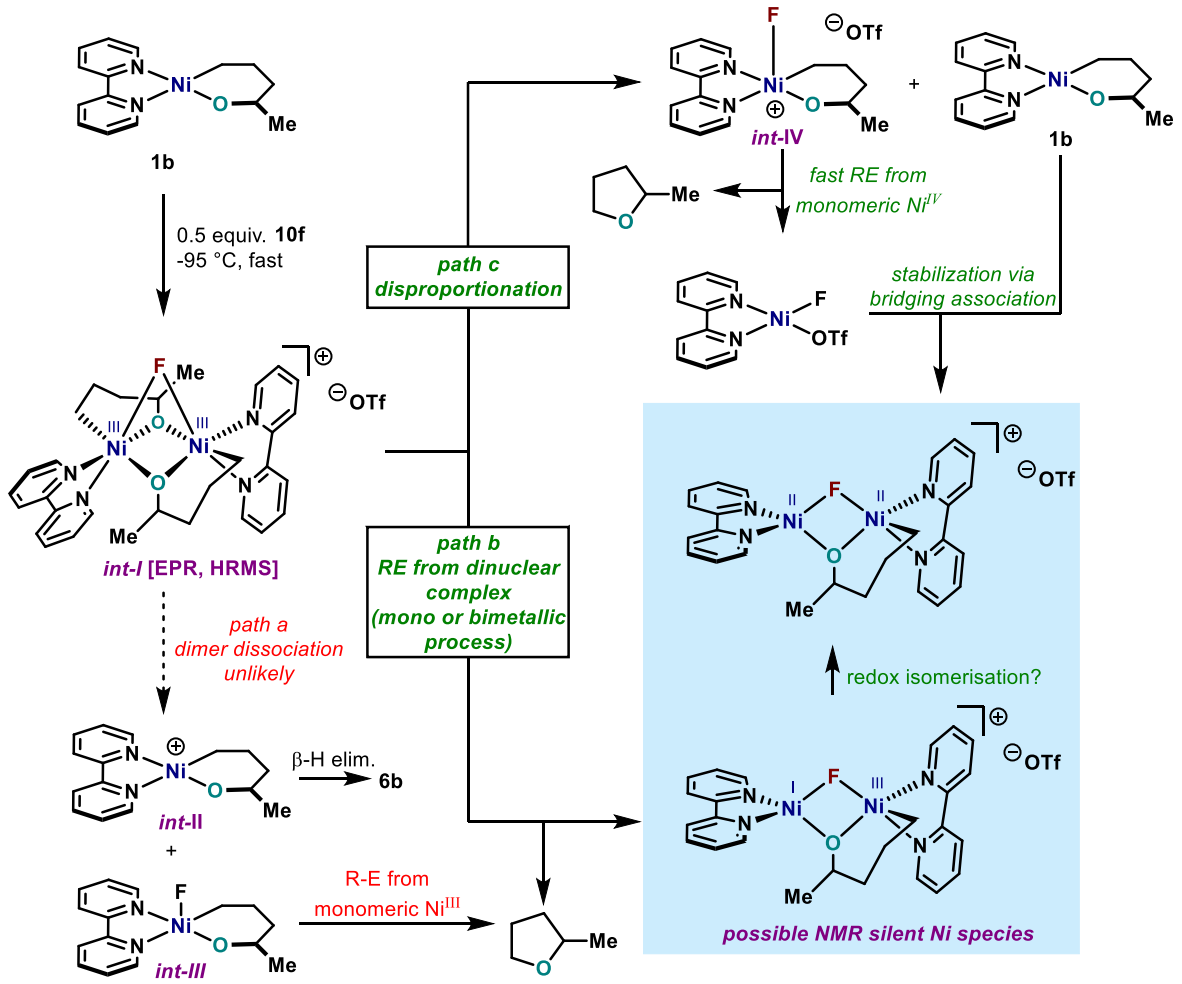

Fig. 58. Overview of the possible scenario for the mechanistic description of the C-O bond formation using **1b** and 0.5 equiv. of **10f** in CD_2Cl_2 at –95 °C.

6.4.10. X-Ray structure of one Ni product after the reaction

It was possible to recover some crystals directly from the J-Young tube after the reaction at low-temperature for NMR studies using **10f**. These crystals were suitable for X-ray analysis and their structure revealed a formula of $(bipy)_2Ni(OTf)_2$ (**S1**). The formation of such complexes is consistent with the intermediacy of $(bipy)Ni^{II}(OTf)(F)$ complex after reductive elimination.

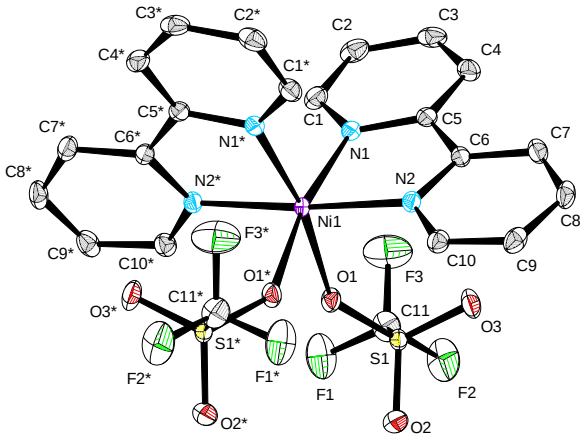

Fig. 59. X-ray structure of $(bipy)_2Ni(OTf)_2$ (**S1**)

7. X-ray characterization

X-ray details of polymeric Ni^{II} 8

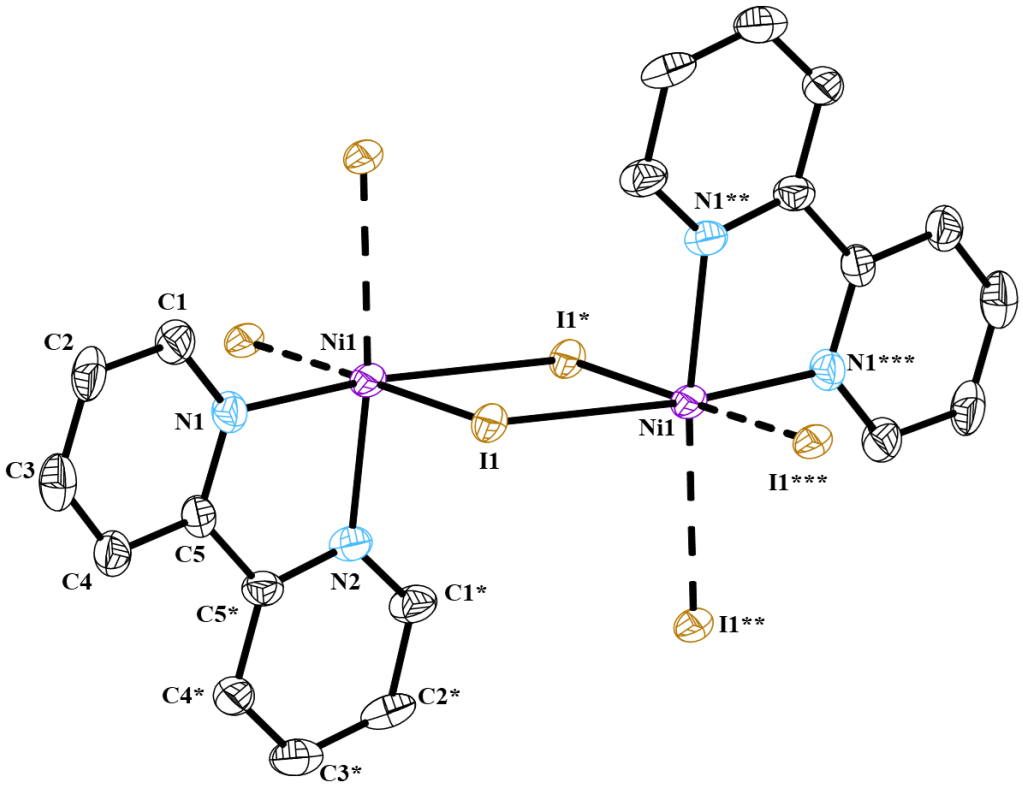

(Disordered iodine atoms are omitted for clarity).

Table 1. Crystal data and structure refinement.

Identification code	13009sadabs	
Empirical formula	$C_{10}H_8I_2N_2Ni$	
Color	red	
Formula weight	468.69 g · mol^{-1}	
Temperature	100(2) K	
Wavelength	0.71073 Å	
Crystal system	MONOCLINIC	
Space group	**I2/c, (no. 15)**	
Unit cell dimensions	a = 7.2343(6) Å	α= 90°.
	b = 9.8155(8) Å	β= 98.063(9)°.
	c = 16.4624(19) Å	γ = 90°.
Volume	1157.41(19) $Å^3$	
Z	4	

Density (calculated)	2.690 $Mg \cdot m^{-3}$	
Absorption coefficient	6.977 mm^{-1}	
F(000)	864 e	
Crystal size	0.1 x 0.06 x 0.06 mm^3	
θ range for data collection	3.521 to 33.202°.	
Index ranges	$-11 \le h \le 11$, $-15 \le k \le 15$, $-25 \le l \le 25$	
Reflections collected	17044	
Independent reflections	2202 [R_{int} = 0.0780]	
Reflections with I>2σ(I)	1764	
Completeness to θ = 25.242°	99.8 %	
Absorption correction	Gaussian	
Max. and min. transmission	0.753 and 0.48	
Refinement method	Full-matrix least-squares on F^2	
Data / restraints / parameters	2202 / 0 / 77	
Goodness-of-fit on F^2	1.050	
Final R indices [I>2σ(I)]	R_1 = 0.0336	wR^2 = 0.0814
R indices (all data)	R_1 = 0.0466	wR^2 = 0.0878
Largest diff. peak and hole	1.4 and -1.3 e $\cdot$ $Å^{-3}$	

Table 2. Bond lengths [Å] and angles [°].

I(1A)-Ni(1)	2.7859(5)	I(1A)-Ni(1)*	
2.8275(4)	Ni(1)-N(1)	2.065(3)	Ni(1)-
N(1)**	2.065(3)	Ni(1)-I(1B)**	
2.824(11)	Ni(1)-I(1B)	2.824(11)	Ni(1)-
I(1C)**	2.89(2)	Ni(1)-I(1C)*	2.11(3)
Ni(1)-I(1C)	2.89(2)	Ni(1)-I(1C)***	2.11(3)
N(1)-C(1)	1.341(4)	N(1)-C(5)	
1.344(5)	C(1)-C(2)	1.395(6)	C(2)-
C(3)	1.391(7)	C(3)-C(4)	
1.379(6)	C(4)-C(5)	1.397(5)	C(5)-
C(5)**	1.478(7)	I(1C)-I(1C)*	2.95(4)
Ni(1)-I(1A)-Ni(1)*	94.241(12)	I(1A)-Ni(1)-I(1A)*	
85.758(12)	I(1A)**-Ni(1)-I(1A)*	94.954(14)	I(1A)**-

Ni(1)-I(1A)	89.21(2)	I(1A)***-Ni(1)-I(1A)*	
179.00(3)	I(1A)**-Ni(1)-I(1A)***	85.758(12)	I(1A)-
Ni(1)-I(1A)***	94.953(13)	I(1A)**-Ni(1)-I(1B)**	15.0(3)
I(1A)-Ni(1)-I(1B)**	86.6(2)	I(1A)-Ni(1)-I(1C)**	90.3(4)
I(1A)**-Ni(1)-I(1C)**	14.4(5)	I(1A)***-Ni(1)-I(1C)**	71.4(5)
I(1A)*-Ni(1)-I(1C)**	109.3(5)	N(1)-Ni(1)-I(1A)	
172.38(9)	N(1)-Ni(1)-I(1A)**	95.84(8)	N(1)**-
Ni(1)-I(1A)***	88.12(8)	N(1)**-Ni(1)-I(1A)*	
91.12(8)	N(1)**-Ni(1)-I(1A)	95.84(8)	N(1)-
Ni(1)-I(1A)*	88.12(8)	N(1)**-Ni(1)-I(1A)**	
172.38(9)	N(1)-Ni(1)-I(1A)***	91.12(8)	N(1)**-
Ni(1)-N(1)	79.74(17)	N(1)-Ni(1)-I(1B)	
170.7(3)	N(1)**-Ni(1)-I(1B)**	170.7(3)	N(1)**-
Ni(1)-I(1B)	96.8(2)	N(1)-Ni(1)-I(1B)**	96.8(2)
N(1)-Ni(1)-I(1C)**	96.0(4)	N(1)-Ni(1)-I(1C)*	89.1(6)
N(1)**-Ni(1)-I(1C)	96.0(4)	N(1)-Ni(1)-I(1C)***	90.9(6)
N(1)**-Ni(1)-I(1C)**	159.1(6)	N(1)-Ni(1)-I(1C)	
159.1(6)	N(1)**-Ni(1)-I(1C)***	89.1(6)	N(1)**-
Ni(1)-I(1C)*	90.9(6)	I(1C)***-Ni(1)-I(1C)	
109.6(8)	I(1C)**-Ni(1)-I(1C)	94.8(9)	I(1C)*-
Ni(1)-I(1C)	70.3(9)	C(1)-N(1)-Ni(1)	
126.7(3)	C(1)-N(1)-C(5)	118.9(3)	C(5)-
N(1)-Ni(1)	114.3(2)	N(1)-C(1)-C(2)	
122.4(4)	C(3)-C(2)-C(1)	118.4(4)	C(4)-
C(3)-C(2)	119.3(4)	C(3)-C(4)-C(5)	
119.1(4)	N(1)-C(5)-C(4)	121.9(3)	N(1)-
C(5)-C(5)**	115.69(19)	C(4)-C(5)-C(5)**	
122.4(2)	Ni(1)*-I(1C)-Ni(1)	109.7(9)	Ni(1)*-
I(1C)-I(1C)*	67.3(10)	Ni(1)-I(1C)-I(1C)*	42.4(7)

–

Symmetry transformations used to generate equivalent atoms:

* -x-1/2,-y+1/2,-z+1/2 ** -x,y,-z+1/2 *** x+1/2,-y+1/2,z

X-Ray details of Ni^{III}-Ni^{III} complex 9a

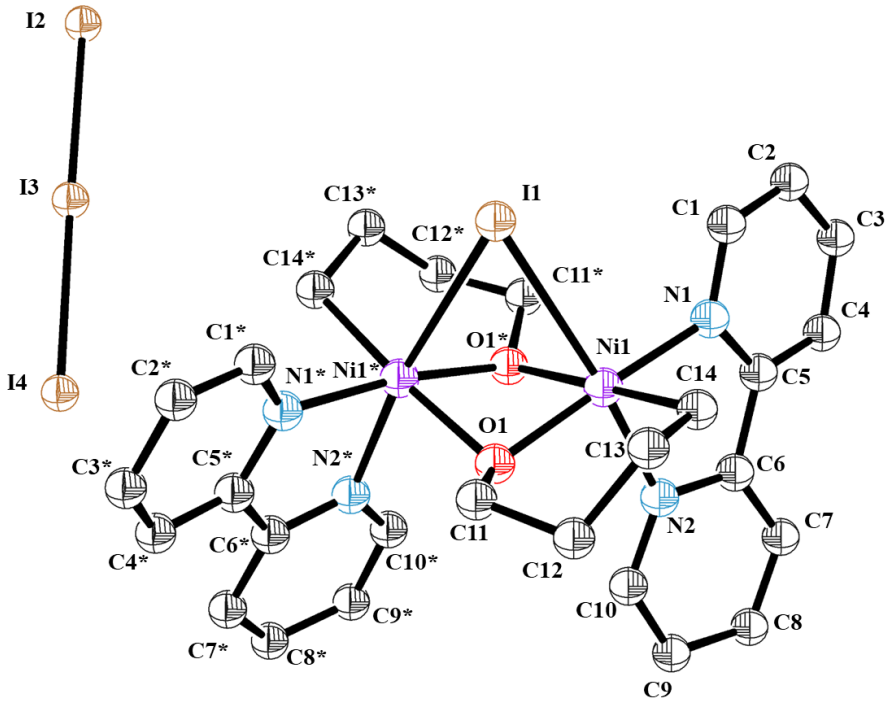

(Disordered iodine atoms in the triiodide couterion are omitted for clarity)

Table 1. Crystal data and structure refinement.

Identification code	13042	
Empirical formula	$C_{28}H_{32}I_4N_4Ni_2O_2$	
Color	orange	
Formula weight	1081.59 g · mol^{-1}	
Temperature	100(2) K	
Wavelength	0.71073 Å	
Crystal system	ORTHORHOMBIC	
Space group	**Pbcm, (no. 57)**	
Unit cell dimensions	a = 10.0648(10) Å	α= 90°.
	b = 12.5024(10) Å	β= 90°.
	c = 26.0452(15) Å	γ = 90°.
Volume	3277.4(5) $Å^3$	
Z	4	
Density (calculated)	2.192 Mg · m^{-3}	
Absorption coefficient	4.949 mm^{-1}	
F(000)	2048 e	
Crystal size	0.11 x 0.08 x 0.03 mm^3	

θ range for data collection	2.713 to 27.497°.	
Index ranges	$-13 \le h \le 13$, $-14 \le k \le 16$, $-33 \le l \le 33$	
Reflections collected	38897	
Independent reflections	3844 [$R_{int} = 0.0801$]	
Reflections with $I>2\sigma(I)$	3107	
Completeness to $\theta = 25.242°$	99.9 %	
Absorption correction	Gaussian	
Max. and min. transmission	0.81 and 0.50	
Refinement method	Full-matrix least-squares on F^2	
Data / restraints / parameters	3844 / 0 / 195	
Goodness-of-fit on F^2	1.066	
Final R indices [$I>2\sigma(I)$]	$R_1 = 0.0377$	$wR^2 = 0.0906$
R indices (all data)	$R_1 = 0.0517$	$wR^2 = 0.1021$
Largest diff. peak and hole	1.3 and -2.1 e · Å^{-3}	

Table 2. Bond lengths [Å] and angles [°].

I(1)-Ni(1)*	2.9260(7)	I(1)-Ni(1)	
2.9260(7)	Ni(1)-Ni(1)*	2.8402(11)	Ni(1)-
O(1)	1.916(3)	Ni(1)-O(1)*	
2.007(3)	Ni(1)-N(1)	1.996(4)	Ni(1)-
N(2)	2.049(4)	Ni(1)-C(14)	
2.013(5)	O(1)-C(11)	1.407(5)	N(1)-
C(1)	1.339(6)	N(1)-C(5)	
1.354(6)	N(2)-C(6)	1.352(6)	N(2)-
C(10)	1.326(6)	C(1)-C(2)	
1.375(7)	C(2)-C(3)	1.375(8)	C(3)-
C(4)	1.386(8)	C(4)-C(5)	
1.387(7)	C(5)-C(6)	1.471(7)	C(6)-
C(7)	1.391(7)	C(7)-C(8)	
1.384(8)	C(8)-C(9)	1.389(7)	C(9)-
C(10)	1.383(7)	C(11)-C(12)	
1.518(6)	C(12)-C(13)	1.526(7)	C(13)-
C(14)	1.491(7)	I(2A)-I(3A)	
2.9116(11)	I(2B)-I(3B)	2.95(3)	I(3A)-
I(4A)	2.9694(11)	I(3B)-I(4B)	2.94(3)

Ni(1)*-I(1)-Ni(1)	58.07(2)	Ni(1)*-Ni(1)-I(1)	
60.966(12)	O(1)*-Ni(1)-I(1)	82.07(9)	O(1)-
Ni(1)-I(1)	83.53(10)	O(1)*-Ni(1)-Ni(1)*	
42.36(9)	O(1)-Ni(1)-Ni(1)*	44.90(9)	O(1)-
Ni(1)-O(1)*	79.55(15)	O(1)-Ni(1)-N(1)	
172.61(15)	O(1)-Ni(1)-N(2)	93.83(15)	O(1)*-
Ni(1)-N(2)	89.67(14)	O(1)*-Ni(1)-C(14)	
175.95(17)	O(1)-Ni(1)-C(14)	97.39(17)	N(1)-
Ni(1)-I(1)	101.32(12)	N(1)-Ni(1)-Ni(1)*	
132.97(11)	N(1)-Ni(1)-O(1)*	95.49(14)	N(1)-
Ni(1)-N(2)	80.58(16)	N(1)-Ni(1)-C(14)	
87.80(18)	N(2)-Ni(1)-I(1)	171.65(11)	N(2)-
Ni(1)-Ni(1)*	111.78(11)	C(14)-Ni(1)-I(1)	
94.98(15)	C(14)-Ni(1)-Ni(1)*	133.67(15)	C(14)-
Ni(1)-N(2)	93.21(18)	Ni(1)-O(1)-Ni(1)*	
92.74(13)	C(11)-O(1)-Ni(1)*	121.0(3)	C(11)-
O(1)-Ni(1)	127.0(3)	C(1)-N(1)-Ni(1)	
125.4(3)	C(1)-N(1)-C(5)	119.0(4)	C(5)-
N(1)-Ni(1)	115.1(3)	C(6)-N(2)-Ni(1)	
114.0(3)	C(10)-N(2)-Ni(1)	126.5(3)	C(10)-
N(2)-C(6)	119.5(4)	N(1)-C(1)-C(2)	
122.9(5)	C(1)-C(2)-C(3)	118.1(5)	C(2)-
C(3)-C(4)	120.1(5)	C(3)-C(4)-C(5)	
118.7(5)	N(1)-C(5)-C(4)	121.0(5)	N(1)-
C(5)-C(6)	115.4(4)	C(4)-C(5)-C(6)	
123.5(5)	N(2)-C(6)-C(5)	114.5(4)	N(2)-
C(6)-C(7)	121.1(5)	C(7)-C(6)-C(5)	
124.4(4)	C(8)-C(7)-C(6)	118.7(5)	C(7)-
C(8)-C(9)	119.7(5)	C(10)-C(9)-C(8)	
118.0(5)	N(2)-C(10)-C(9)	122.8(5)	O(1)-
C(11)-C(12)	112.2(4)	C(11)-C(12)-C(13)	
110.0(4)	C(14)-C(13)-C(12)	116.0(4)	C(13)-
C(14)-Ni(1)	114.7(3)	I(2A)-I(3A)-I(4A)	
175.46(2)	I(4B)-I(3B)-I(2B)	174.4(11)	

_

Symmetry transformations used to generate equivalent atoms: * x,-y+1/2,-z+1

X-Ray details of byproduct Ni^{II} complex S1

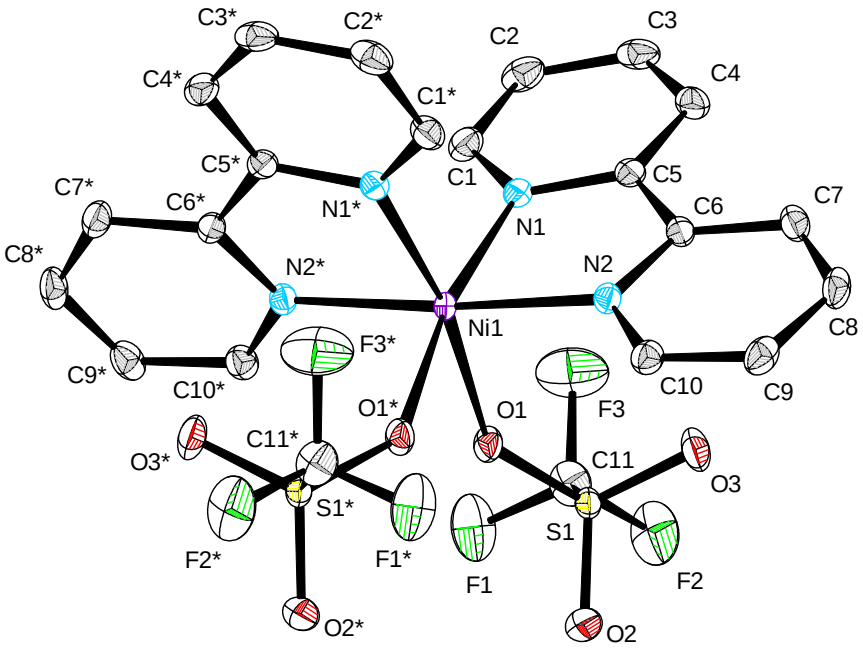

Table 1. Crystal data and structure refinement.

Identification code	13189	
Empirical formula	$C_{22}H_{16}F_6N_4NiO_6S_2$	
Color	light violet	
Formula weight	669.22 g·mol^{-1}	
Temperature	100(2) K	
Wavelength	0.71073 Å	
Crystal system	MONOCLINIC	
Space group	**C2/c, (no. 15)**	
Unit cell dimensions	a = 9.8858(3) Å	α= 90°.
	b = 14.1256(5) Å	β= 102.0660(10)°.
	c = 18.5755(7) Å	γ = 90°.
Volume	2536.63(15) Å^3	
Z	4	
Density (calculated)	1.752 Mg · m^{-3}	
Absorption coefficient	1.022 mm^{-1}	
F(000)	1352 e	
Crystal size	0.040 x 0.032 x 0.022 mm^3	
θ range for data collection	2.242 to 29.566°.	
Index ranges	$-13 \le h \le 13$, $-19 \le k \le 19$, $-25 \le l \le 25$	
Reflections collected	39008	

Independent reflections	3550 [R_{int} = 0.0368]	
Reflections with I>2σ(I)	3073	
Completeness to θ = 25.242°	100.0 %	
Absorption correction	Gaussian	
Max. and min. transmission	0.99 and 0.98	
Refinement method	Full-matrix least-squares on F^2	
Data / restraints / parameters	3550 / 0 / 186	
Goodness-of-fit on F^2	1.046	
Final R indices [I>2σ(I)]	R_1 = 0.0268	wR^2 = 0.0626
R indices (all data)	R_1 = 0.0351	wR^2 = 0.0660
Largest diff. peak and hole	0.5 and -0.4 e · Å^{-3}	

Table 2. Bond lengths [Å] and angles [°].

Ni(1)-O(1)	2.1290(10)	Ni(1)-O(1)*	2.1290(10)
Ni(1)-N(1)*	2.0505(12)	Ni(1)-N(1)	2.0505(12)
Ni(1)-N(2)	2.0522(12)	Ni(1)-N(2)*	2.0523(12)
S(1)-O(1)	1.4586(10)	S(1)-O(2)	1.4342(12)
S(1)-O(3)	1.4371(11)	S(1)-C(11)	1.8249(17)
F(1)-C(11)	1.321(2)	F(2)-C(11)	1.335(2)
F(3)-C(11)	1.3301(19)	N(1)-C(1)	1.3394(19)
N(1)-C(5)	1.3510(18)	N(2)-C(6)	1.3519(18)
N(2)-C(10)	1.3387(19)	C(1)-C(2)	1.384(2)
C(2)-C(3)	1.388(2)	C(3)-C(4)	1.386(2)
C(4)-C(5)	1.389(2)	C(5)-C(6)	1.481(2)
C(6)-C(7)	1.3902(19)	C(7)-C(8)	1.383(2)
C(8)-C(9)	1.386(2)	C(9)-C(10)	1.388(2)

O(1)*-Ni(1)-O(1)	84.46(6)	N(1)-Ni(1)-O(1)	90.41(4)
N(1)*-Ni(1)-O(1)*	169.58(4)	N(1)-Ni(1)-O(1)*	90.41(4)

169.58(4)	N(1)*-Ni(1)-N(1)	96.03(7)	N(1)-Ni(1)-N(2)*
79.85(5)	N(1)*-Ni(1)-N(2)	96.80(5)	N(1)-Ni(1)-N(2)
92.39(4)	N(2)*-Ni(1)-O(1)*	91.28(4)	N(2)*-Ni(1)-O(1)
91.28(4)	N(2)-Ni(1)-N(2)*	101.82(7)	O(2)-S(1)-O(3)
103.65(8)	O(3)-S(1)-C(11)	140.27(6)	C(1)-N(1)-C(5)
114.91(9)	C(10)-N(2)-Ni(1)	118.88(12)	C(3)-C(2)-C(1)
119.47(14)	N(1)-C(5)-C(4)	115.11(12)	N(2)-C(6)-C(5)
121.29(14)	C(8)-C(7)-C(6)	118.97(14)	N(2)-C(10)-C(9)
111.87(11)	F(1)-C(11)-F(3)	110.84(12)	F(3)-C(11)-S(1)
175.04(7)	O(1)-S(1)-O(2)	116.22(7)	O(2)-S(1)-O(3)
103.93(7)	S(1)-C(1)-N(1)-Ni(1)	119.15(12)	C(5)-C(6)-N(2)-Ni(1)
126.25(10)	C(10)-N(1)-C(1)-C(2)	118.42(15)	C(2)-C(3)-C(4)-C(5)
121.35(14)	N(1)-C(4)-C(5)-C(6)	115.32(12)	N(2)-C(7)-C(6)-C(5)
119.54(14)	C(7)-C(8)-C(9)-C(10)	122.62(14)	F(1)-C(11)-F(2)
108.53(15)	F(2)-C(11)-F(3)	110.71(12)	

_ Symmetry transformations used to generate equivalent atoms: * -x+1,y,-z+3/2

8. References

1. Bogdanovic´, B.; Kröner, M.; Wilke; G. Olefin-komplexe des Nickel(0). *Liebigs Ann. Chem.* **1966**, *699*, 1.

2. Le Vaillant, F.; Garreau, M.; Nicolai, S.; Gryn'ova, G.; Corminboeuf, C.; Waser, J. Fine-tuned Organic Photoredox Catalysts for Fragmentation-alkynylation Cascades of Cyclic Oxime Ethers. *Chem. Sci.* **2018**, *9*, 5883.

3. Binger, P.; Doyle, M. J.; Krüger, C.; Tsay, Y.-H. Z. Metallacycloalkane, III [1] Darstellung und Charakterisierung von α.α'-Dipyridyl-Nickelacyclopentan. *Naturforsch.* **1979**, *34B*, 1289. For a direct link, see: http://zfn.mpdl.mpg.de/data/Reihe_B/34/ZNB-1979-34b-1289.pdf

4. Matsunaga, P. T.; Mavropoulos, J. C.; Hillhouse, G. L. Oxygen-atom Transfer from Nitrous Oxide (N=N=O) to Nickel Alkyls. Syntheses and Reactions of Nickel(II) Alkoxides. *Polyhedron*. **1995**, *14*, 175.

5. Saito, T.; Uchida, Y.; Misono, A.; Yamamoto, A.; Morifuji, K.; Ikeda, S. Diethyldipyridylnickel. Preparation, Characterization, and Reactions. *J. Am. Chem. Soc.* **1966**, *88*, 5198.

6. For similar experiment, see: Terrett, J. A.; Cuthbertson, J. D.; Shurtleff, V. W.; MacMillan, D. W. C. Switching on Elusive Organometallic Mechanisms with Photoredox Catalysis. *Nature*, **2015**, *524*, 330.

7. For a NMR reference of iodobutan-1-ol (**7a**) in $CDCl_3$, see: Zeng, C.; Shen, G.; Yang, F.; Chen, J.; Zhang, X.; Gu, C.; Zhou, Y.; Fan, B. Rhodium-Catalyzed Generation of Anhydrous Hydrogen Iodide: An Effective Method for the Preparation of Iodoalkanes. *Org. Lett*. **2018**, *20*, 6859. ^{1}H NMR (400 MHz, $CDCl_3$) δ 4.23 (s, 1H), 3.59 (t, *J* = 6.4 Hz, 2H), 3.15 (t, *J* = 6.8 Hz, 2H), 1.85 - 1.81 (m, 2H), 1.63 - 1.58 (m, 2H).

8. For a NMR reference of 3-butene-1-ol (**6a**) in $CDCl_3$, see: Wozniak, B.; Li, Y.; Tin, S.; de Vries, J. G. Rhenium-catalyzed Deoxydehydration of Renewable Triols Derived from Sugars. *Green Chem.* **2018**, *20*, 4433. ^{1}H NMR (400 MHz, $CDCl_3$) δ = 5.70 (ddt, *J* = 17.1 Hz, 10.3 Hz, 6.9 Hz, 1H), 5.14-5.05 (m, 2H), 3.63 (q, *J* = 6.1 Hz, 2H), 2.23 (q, *J* = 6.6 Hz, 2H), 2.12 (brs, 1H). ^{13}C NMR (100 MHz, $CDCl_3$) δ = 135.0, 117.5, 61.6, 37.1.

9. For a NMR reference of 5-iodopentan-2-ol (**7b**) in $CDCl_3$, see: Cossette, C.; Chourey, S.; Ye, Q.; Reddy, C. N.; Gore, V.; Gravel, S.; Slobodchikova, I.; Vuckovic, D.; Rokach, J. and Powell, W. S. Pharmacokinetics and Metabolism of Selective Oxoeicosanoid (OXE) Receptor Antagonists and Their Effects on 5-Oxo-6,8,11,14-eicosatetraenoic Acid (5-Oxo-ETE)-Induced Granulocyte Activation in Monkeys. *J. Med. Chem.* **2016**, *59*, 10127. ^{1}H NMR (400 MHz, $CDCl_3$): δ 3.89−3.83 (m, 1H), 3.23 (t, *J* = 6.9 Hz, 2H), 2.10 (br s, 1H), 2.04−1.83 (m, 2H), 1.63−1.50 (m, 2H), 1.23 (d, *J* = 6.2 Hz, 3H). ^{13}C NMR ($CDCl_3$): δ 67.4, 39.8, 29.8, 23.7, 6.9.

10. For a NMR reference of pent-4-en-2-ol (**6b**) in $CDCl_3$, see: (a) Show, K.; Gupta, P.; Kumar, P. Stereoselective Synthesis of Ophiocerins A and C. *Tetrahedron Asymmetry*. **2011**, 22, 1212. ^{1}H NMR (200 MHz, $CDCl_3$): δ 5.78–5.85 (m, 1H), 5.14 (d, *J* = 6.6 Hz,1H), 5.10 (d, *J* = 2.4 Hz, 1H), 3.80–3.86 (m, 1H), 2.22–2.38 (m, 2H), 1.82 (s, 1H), 1.18 (d, *J* = 6.1 Hz, 3H); ^{13}C NMR (50 MHz, $CDCl_3$): δ 134.6, 116.6, 66.5, 43.2, 22.1. (b) 1H NMR (400 MHz, $CDCl_3$) δ 5.87−5.65 (m, 1H), 5.19−4.93 (m, 2H), 3.86−3.72 (m, 1H), 2.25−2.07 (m, 2H), 1.13 (d, *J* = 6.1 Hz, 3H).

11. For the original publication, see: Evans, D. F. The Determination of the Pararnagnetic Susceptibility of Substances in Solution by Nuclear Magnetic Resonance. *J. Chem. Soc.* **1959**, 2003-2005.

12. Calculated according to the following publications: (a) Naklicki, M. L.; White, C. A.; Plante, L. L.; Evans, C. E. B.; Crutchley, R. J. Metal−Ligand Coupling Elements and Antiferromagnetic Superexchange in Ruthenium Dimers. *Inorg. Chem.* **1998**, *37*, 1880; (b) Bryliakov, K. P.; Duban, E. A.; Talsi, E. P. The Nature of the Spin-State Variation of $[Fe^{II}(BPMEN)(CH_3CN)_2](ClO_4)_2$ in Solution. *Eur. J. Inorg. Chem.* **2005**, 72.

13. Pantazis, D. A.; Chen, X. Y.; Landis, C. R.; Neese, F. All-electron Scalar Relativistic Basis Sets for Third-row Transition Metal Atoms. *J. Chem. Theory Comput.* **2008**, *4*, 908.

14. Pantazis, D. A.; Neese, F., All-Electron Scalar Relativistic Basis Sets for the Lanthanides. Journal of Chemical Theory and Computation 2009, 5, 2229.

15. Pantazis, D. A.; Neese, F., All-Electron Scalar Relativistic Basis Sets for the Actinides. *J. Chem. Theory Comput.* **2011**, *7*, 677.

16. Pantazis, D. A.; Neese, F., All-electron Scalar Relativistic Basis Sets for the 6p Elements. *Theor. Chem. Acc.* **2012**, 131.

17. Stephens, P. J.; Devlin, F. J.; Chabalowski, C. F.; Frisch, M. J., Ab-initio Calculation of Vibrational Absorption and Circular-dichroism Spectra using Density-functional Force-fields. *J. Phys. Chem.* **1994**, *98*, 11623.

18. Becke, A. D., Density-functional thermochemistry .3. The Role of Exact Exchange. *J. Chem. Phys.* **1993**, *98*, 5648.

19. Lee, C. T.; Yang, W. T.; Parr, R. G., Development of the Colle-Salvetti Correlation-Energy Formula into a Functional of the Electron-density. *Phys. Rev. B* **1988**, *37*, 785.

20. Vosko, S. H.; Wilk, L.; Nusair, M., Accurate Spin-dependent Electron Liquid Correlation Energies for Local Spin-density Calculations - a Critical Analysis. *Can. J. Phys.* **1980**, *58*, 1200.

21. Weigend, F.; Ahlrichs, R., Balanced Basis Sets of Split Valence, Triple Zeta Valence and Quadruple Zeta Valence Quality for H to Rn: Design and Assessment of Accuracy. *Phys. Chem. Chem. Phys.* **2005**, *7*, 3297.

22. Grimme, S.; Antony, J.; Ehrlich, S.; Krieg, H., A Consistent and Accurate Ab Initio Parametrization of Density Functional Dispersion Correction (DFT-D) for the 94 Elements H-Pu. *J. Chem. Phys.* **2010**, 132.

23. Grimme, S.; Ehrlich, S.; Goerigk, L., Effect of the Damping Function in Dispersion Corrected Density Functional Theory. *J. Comp. Chem.* **2011**, *32*, 1456.

24. Xu, H.; Diccianni, J. B.; Katigbak, J.; Hu, C.; Zhang, Y.; Diao, T. Bimetallic C–C Bond Forming Reductive Elimination from Nickel. *J. Am. Chem. Soc.* **2016**, *138*, 4779.

25. For a reference of 2-Me-THF in CD_2Cl_2, see: Leger, P. R.; Murphy, R. A.; Pushkarskaya, E.; Sarpong, R. Synthetic Efforts toward the Lycopodium Alkaloids Inspires a Hydrogen Iodide Mediated Method for the Hydroamination and Hydroetherification of Olefins. *Chem. Eur. J.* **2015**, *21*, 4377. ^{1}H NMR (500 MHz, CD_2Cl_2) δ 3.91 (dt, *J* =7.8, 6.1 Hz, 1H), 3.84 (dt, *J* = 7.9, 6.0 Hz, 1H), 3.66 (dt, *J* = 8.0, 6.6 Hz, 1H), 2.03-1.80 (m, 3H), 1.39 (dq, *J* = 11.8, 7.9 Hz, 1H), 1.19 (d, *J* = 6.1 Hz, 3H).

26. Butschke, B.; Schwarz, H. Mechanistic Study on the Gas-Phase Generation of "Rollover"-Cyclometalated [M(bipy - H)]þ (M = Ni, Pd, Pt). *Organometallics*, **2010**, *29*, 6002.

9. Spectra of nickelacycles

^{1}H-NMR (400 MHz, C_6D_6) of compound **4a**

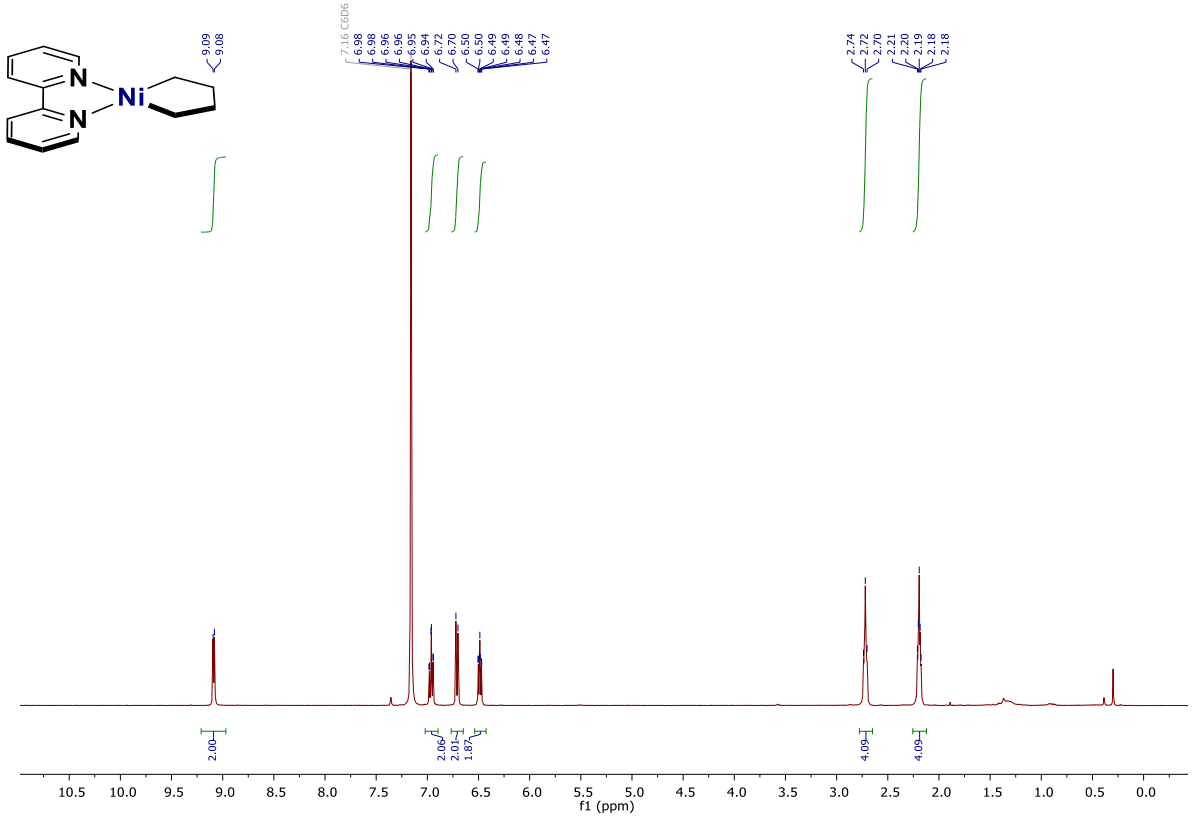

^{13}C-NMR (100 MHz, C_6D_6) of compound **4a**

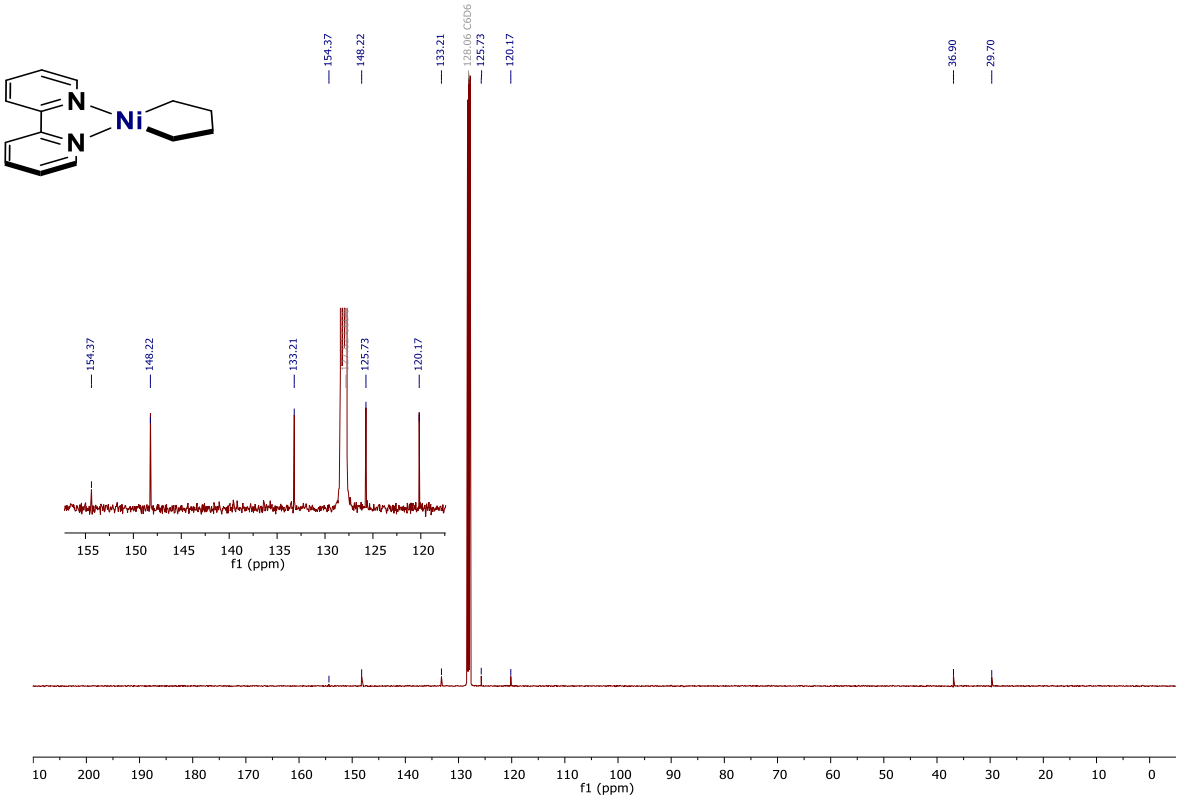

^{1}H-NMR (400 MHz, C_6D_6) of compound **4b**

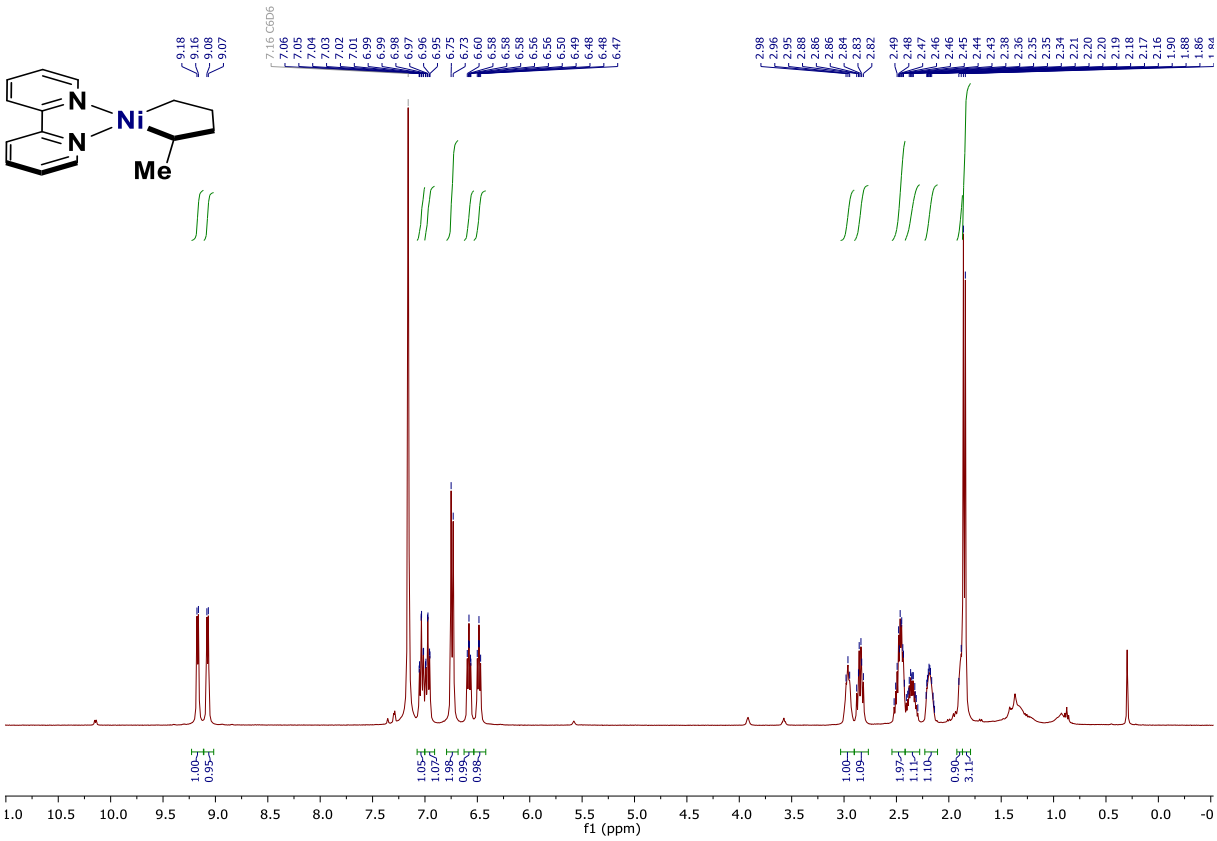

^{13}C-NMR (100 MHz, C_6D_6) of compound **4b**

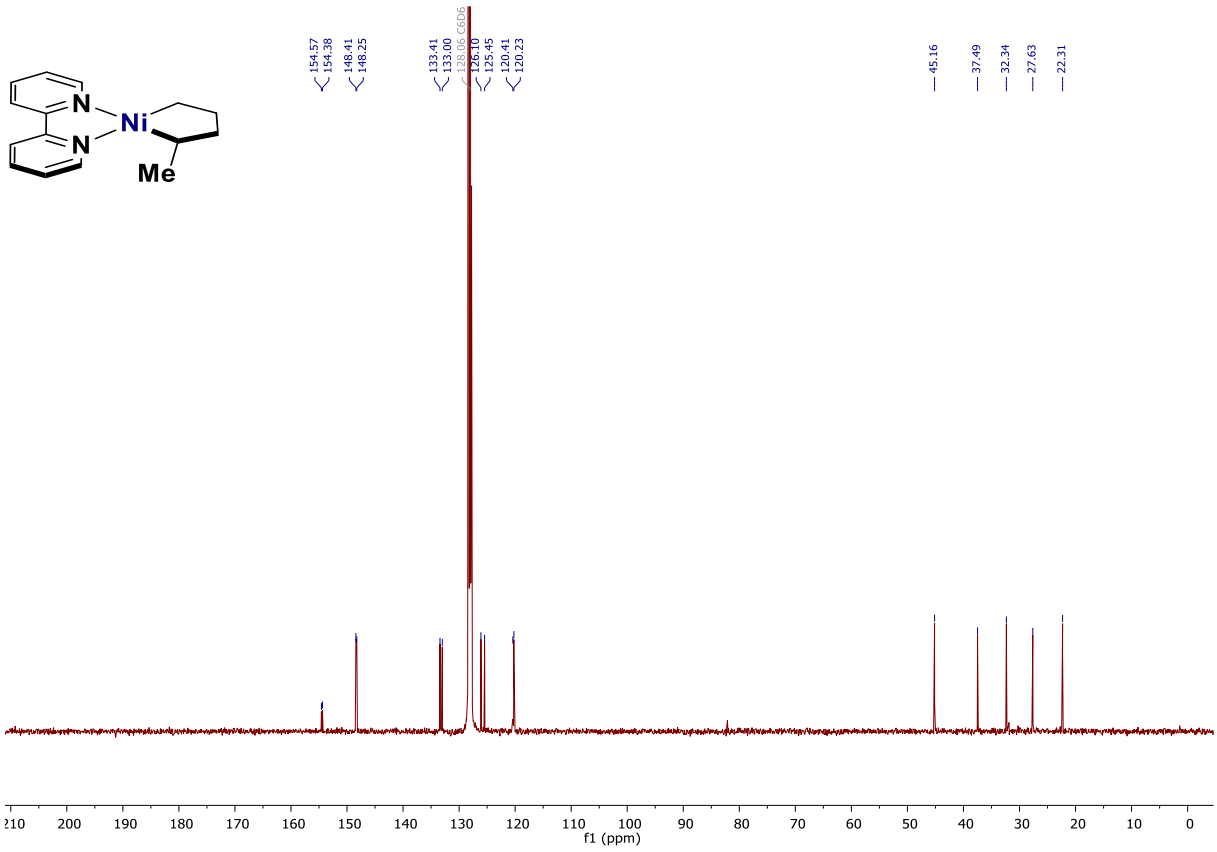

^{1}H-NMR (400 MHz, C_6D_6) of compound **11**

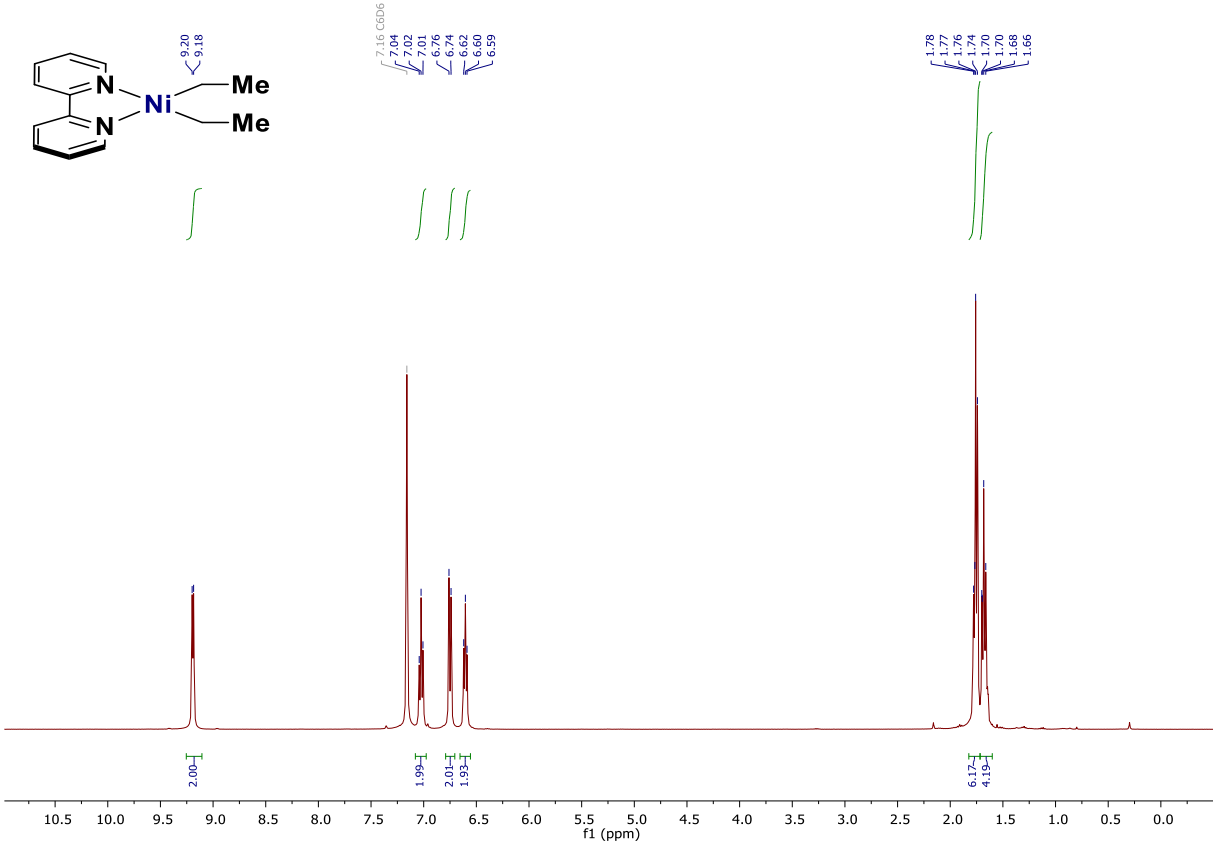

^{13}C-NMR (100 MHz, C_6D_6) of compound **11**

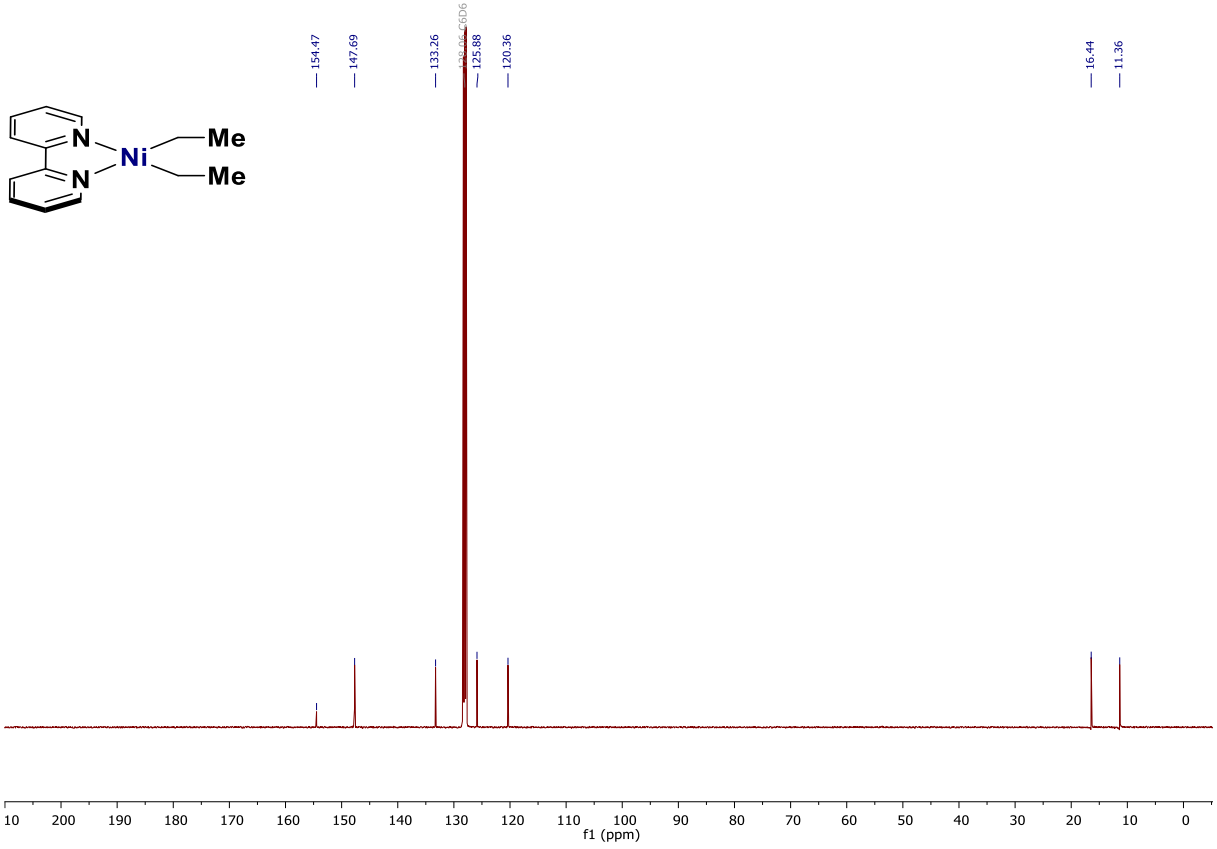

^{1}H-NMR (600 MHz, C_6D_6) of compound **1a**

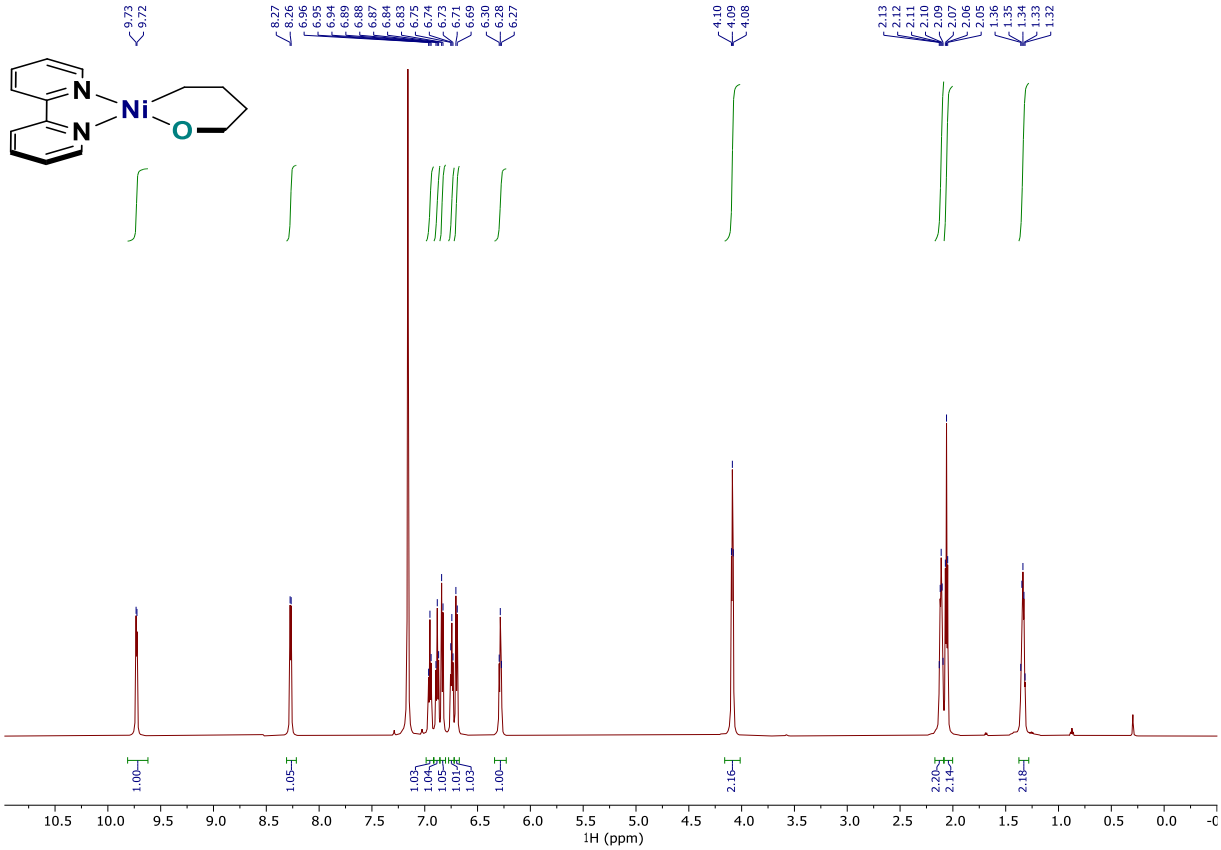

^{13}C-NMR (150 MHz, C_6D_6) of compound **1a**

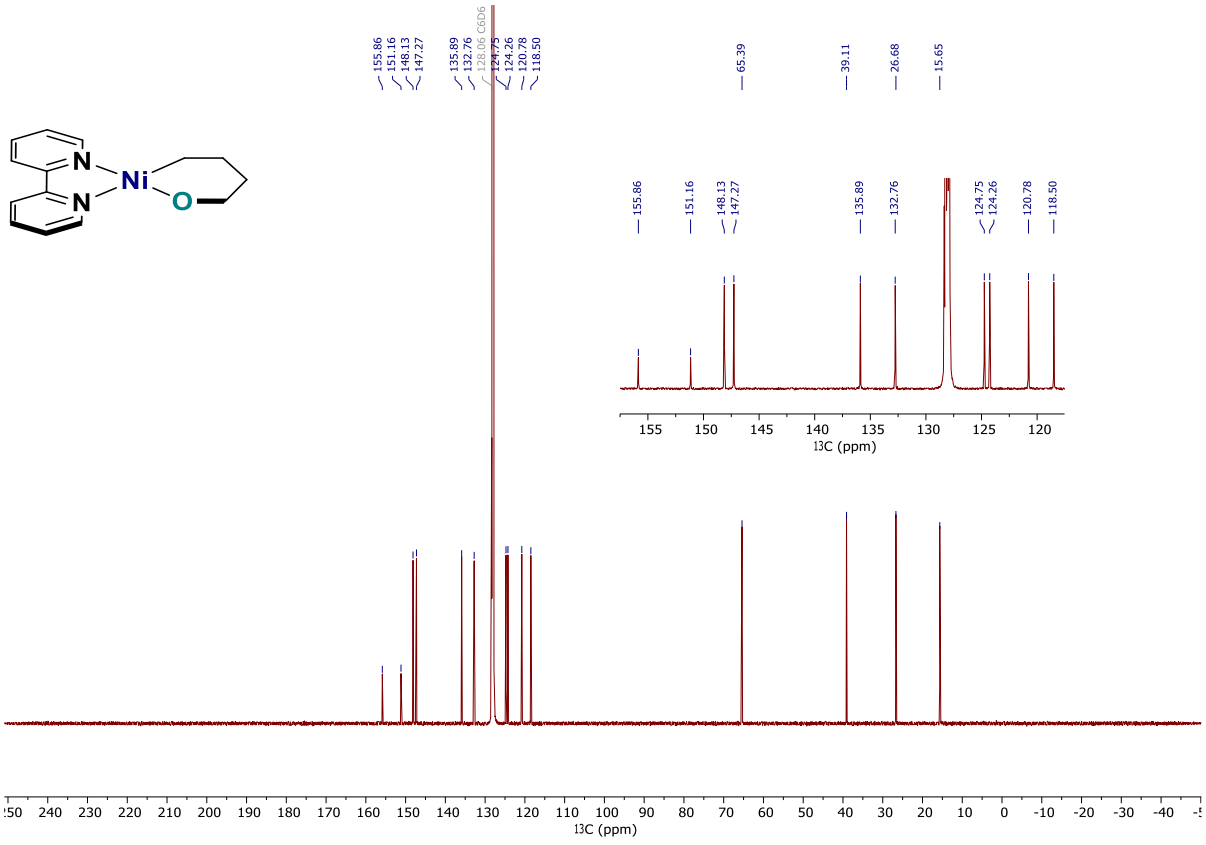

HSQC of compound **1a**

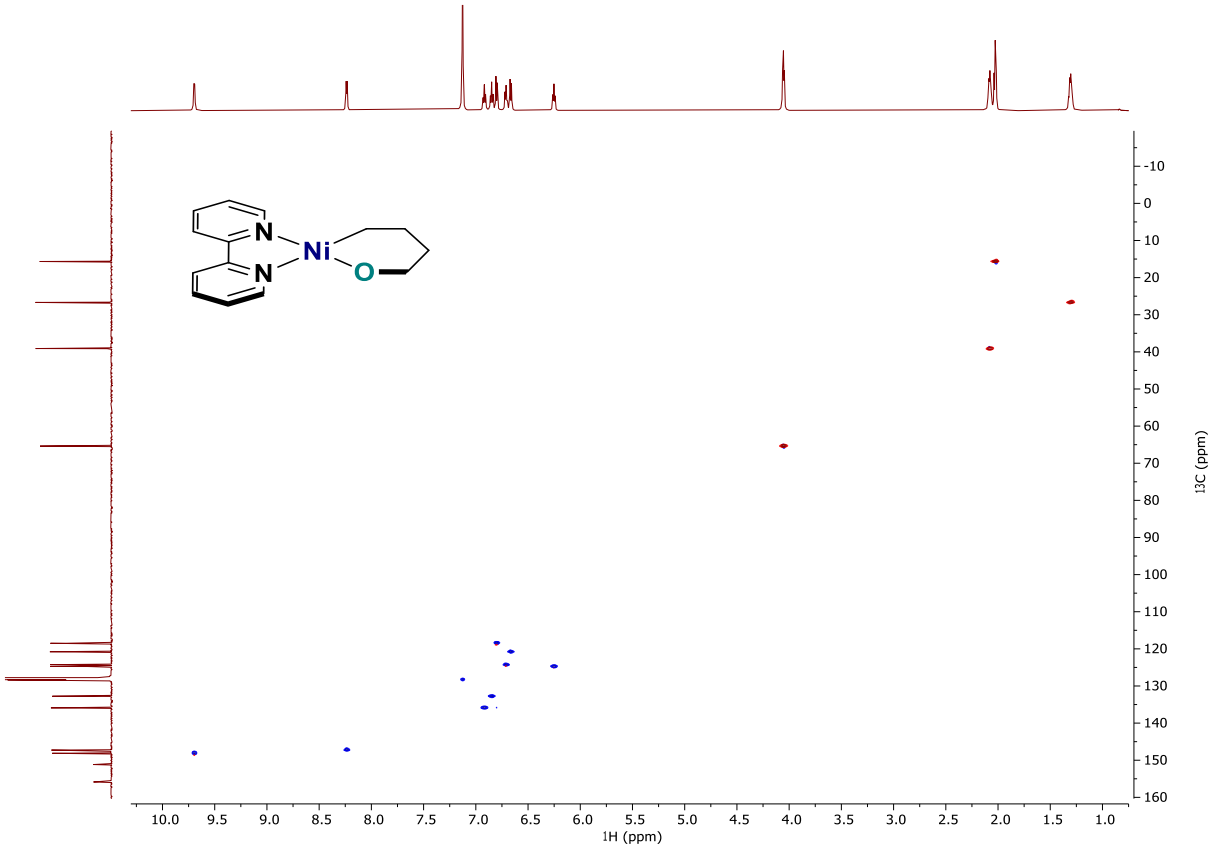

HMBC of compound **1a**

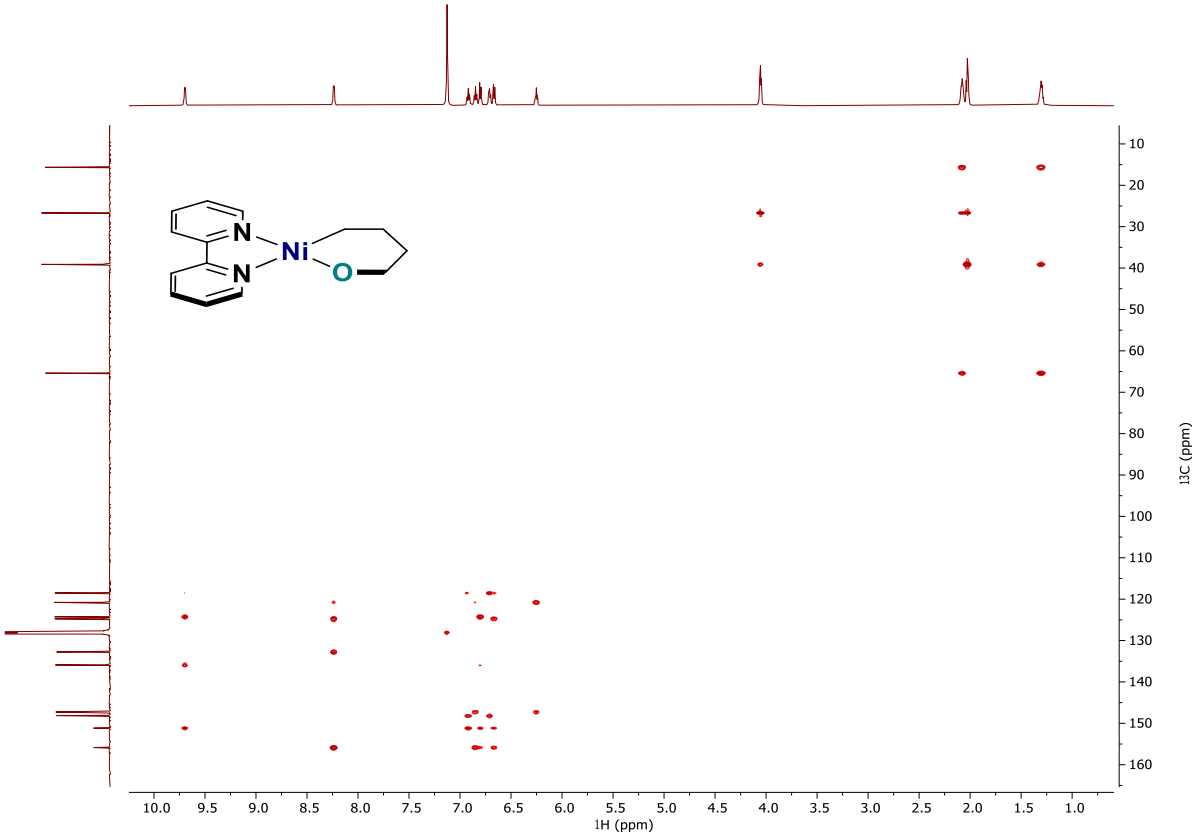

COSY of compound **1a**

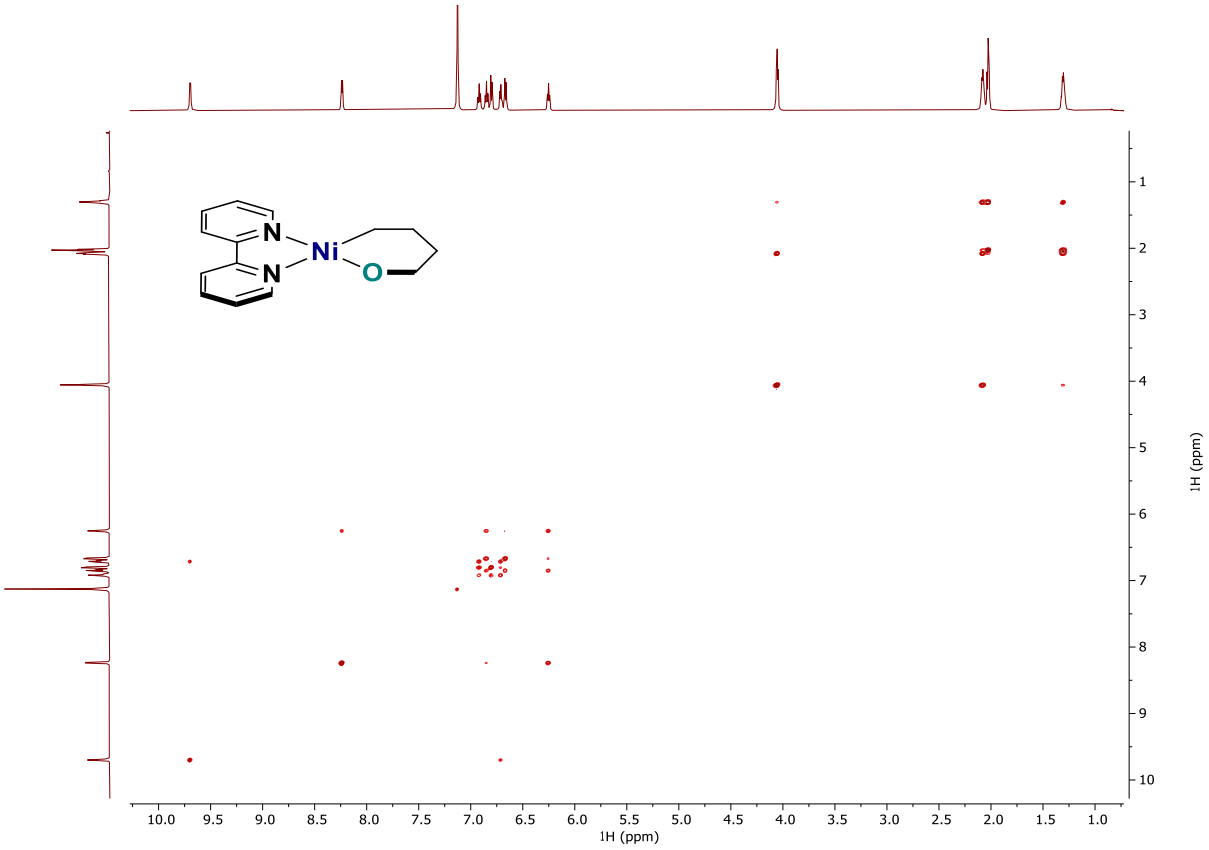

ROESY of compound **1a**

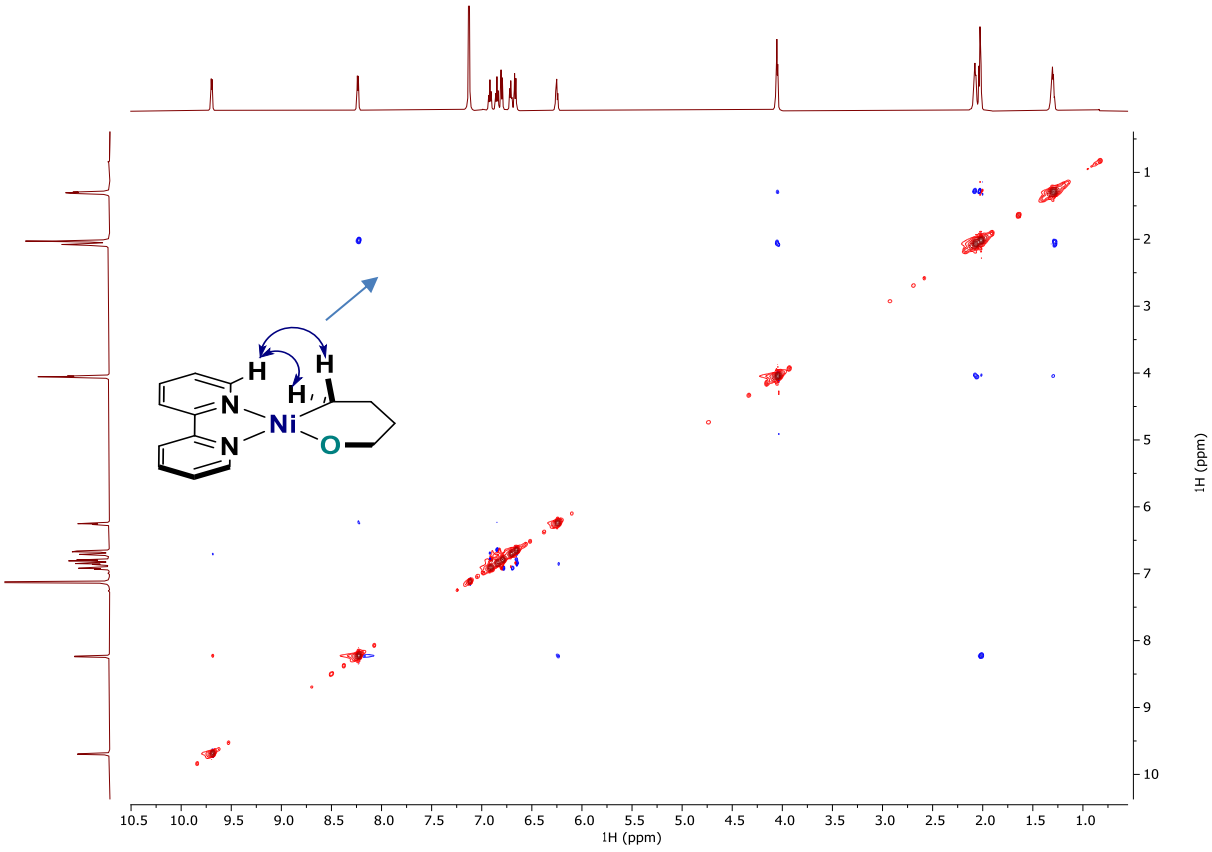

^{1}H-NMR (600 MHz, C_6D_6) of compounds **1b** and **1b-isomer**

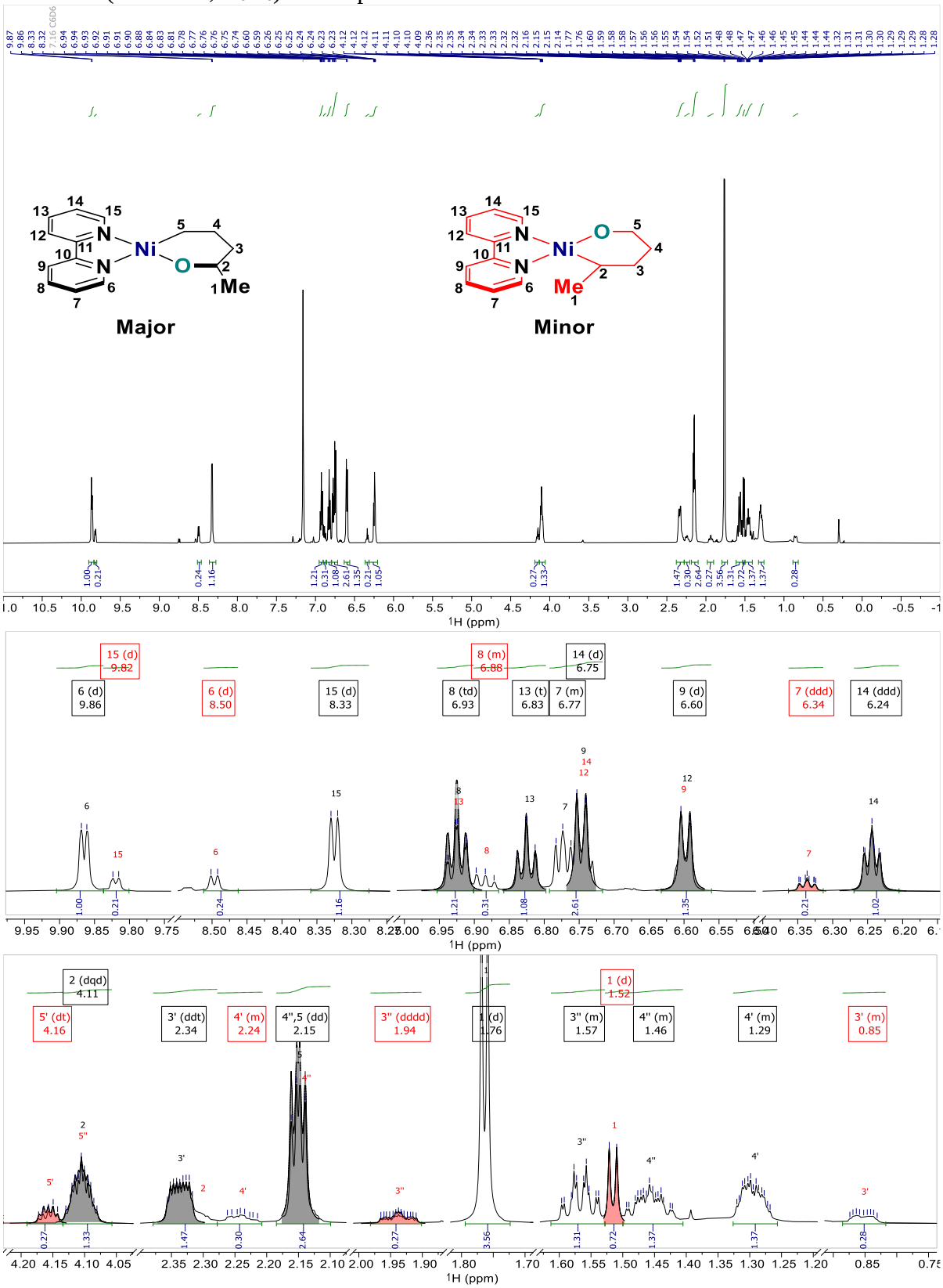

^{13}C-NMR (125 MHz, C_6D_6) of compounds **1b** and **1b-isomer**

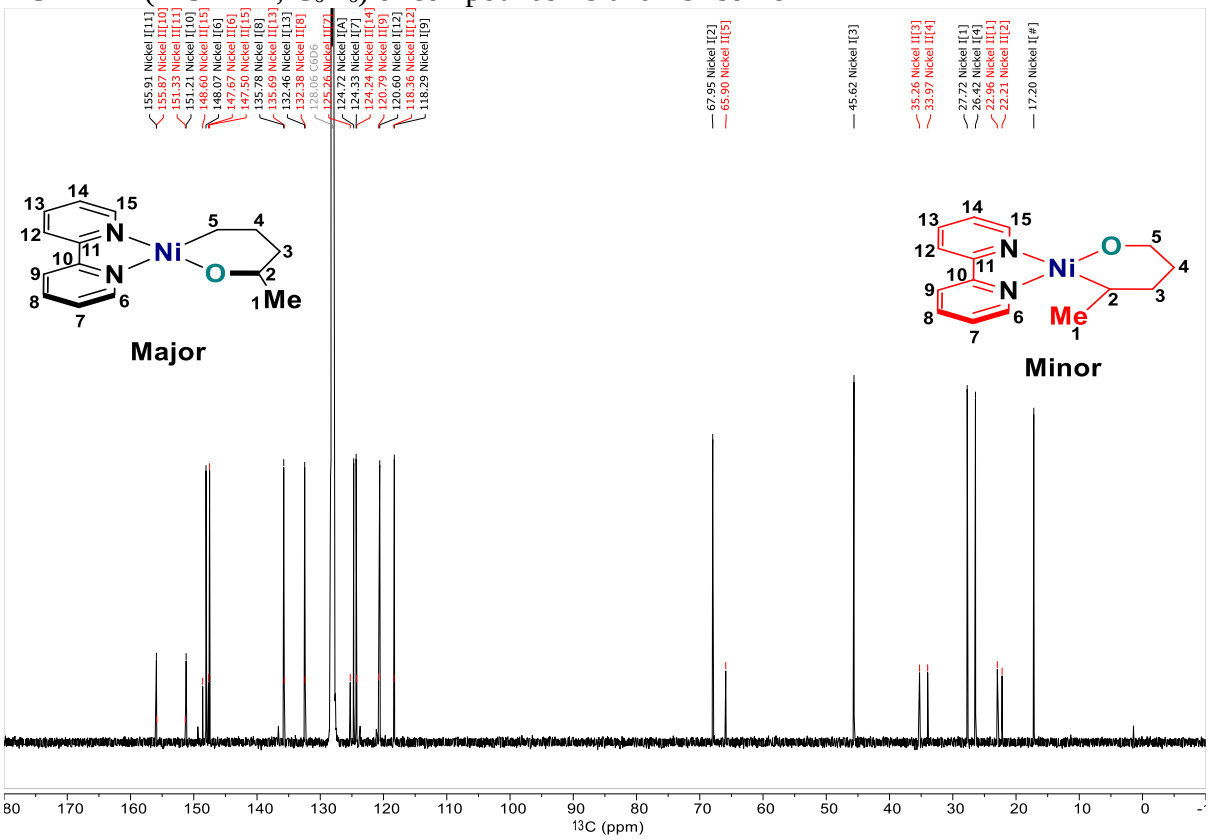

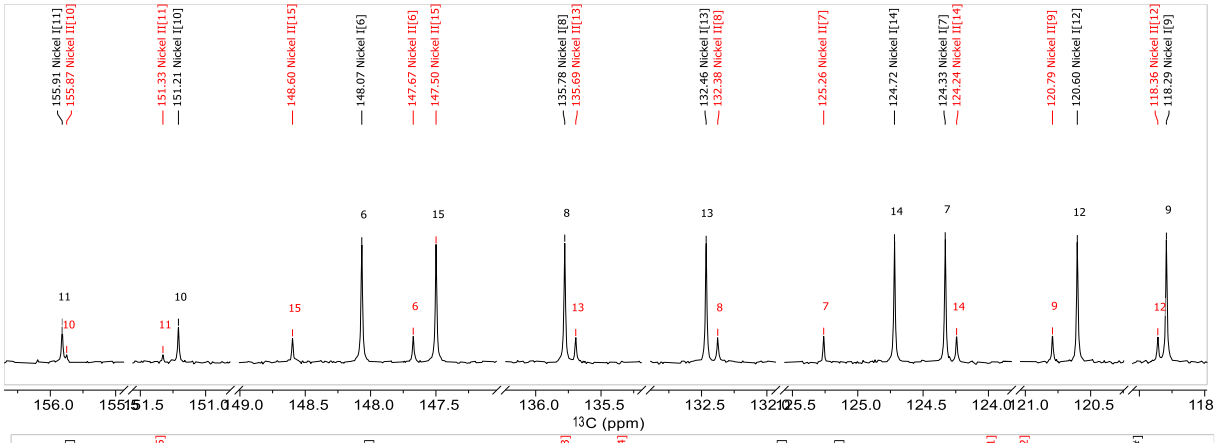

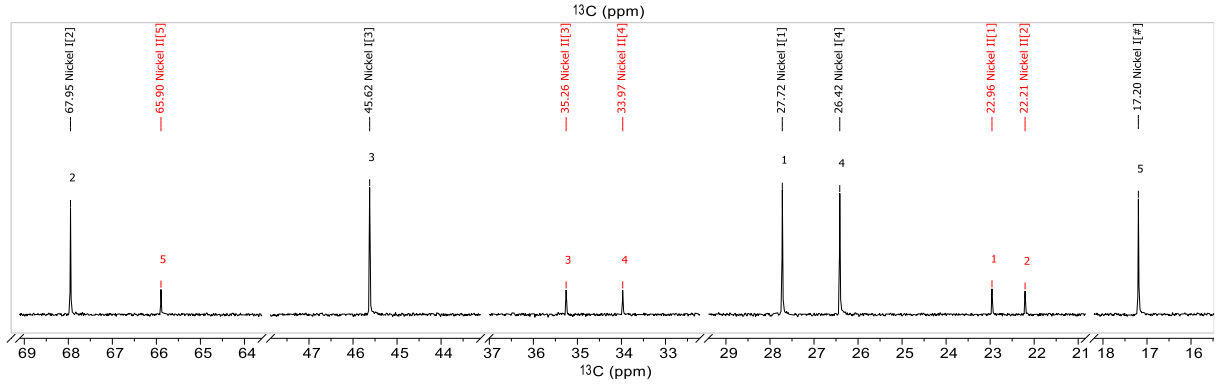

^{1}H-^{13}C-edited-HSQC of compounds **1b** and **1b-isomer**

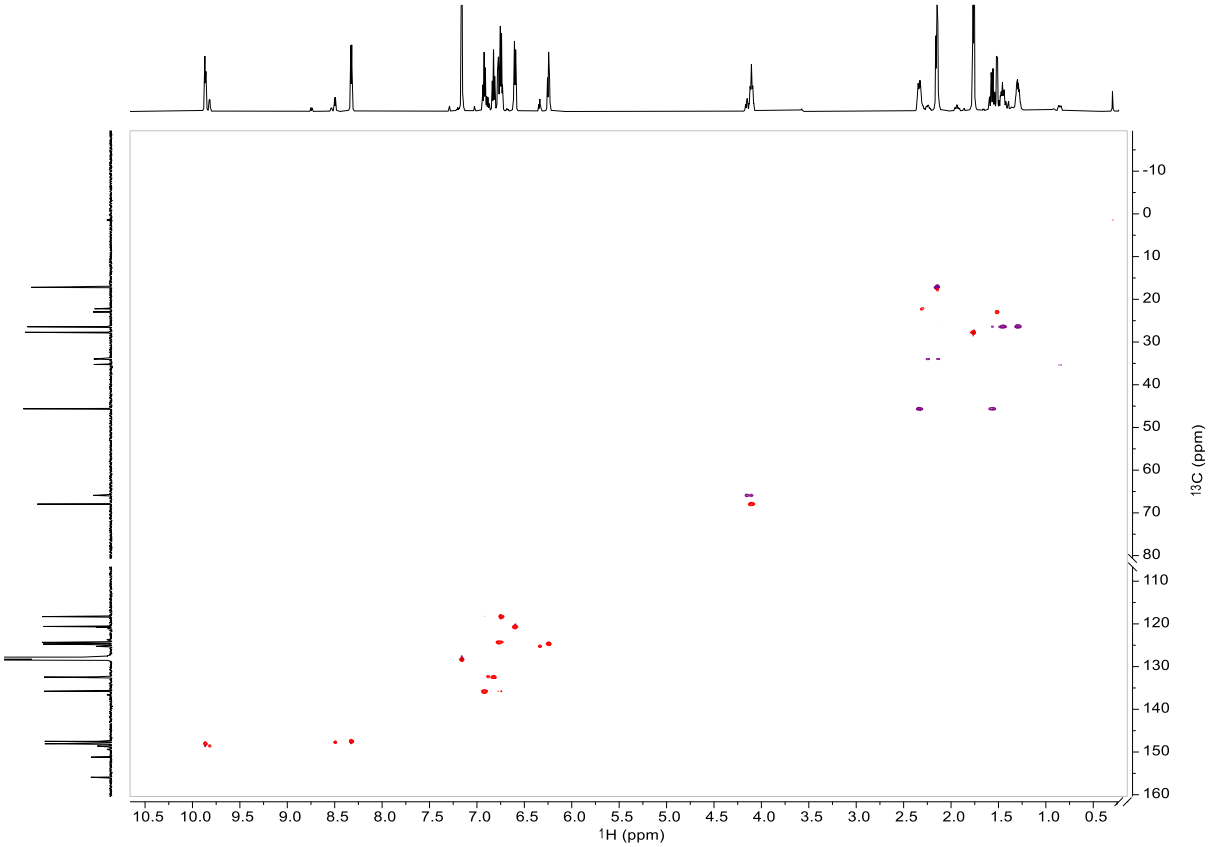

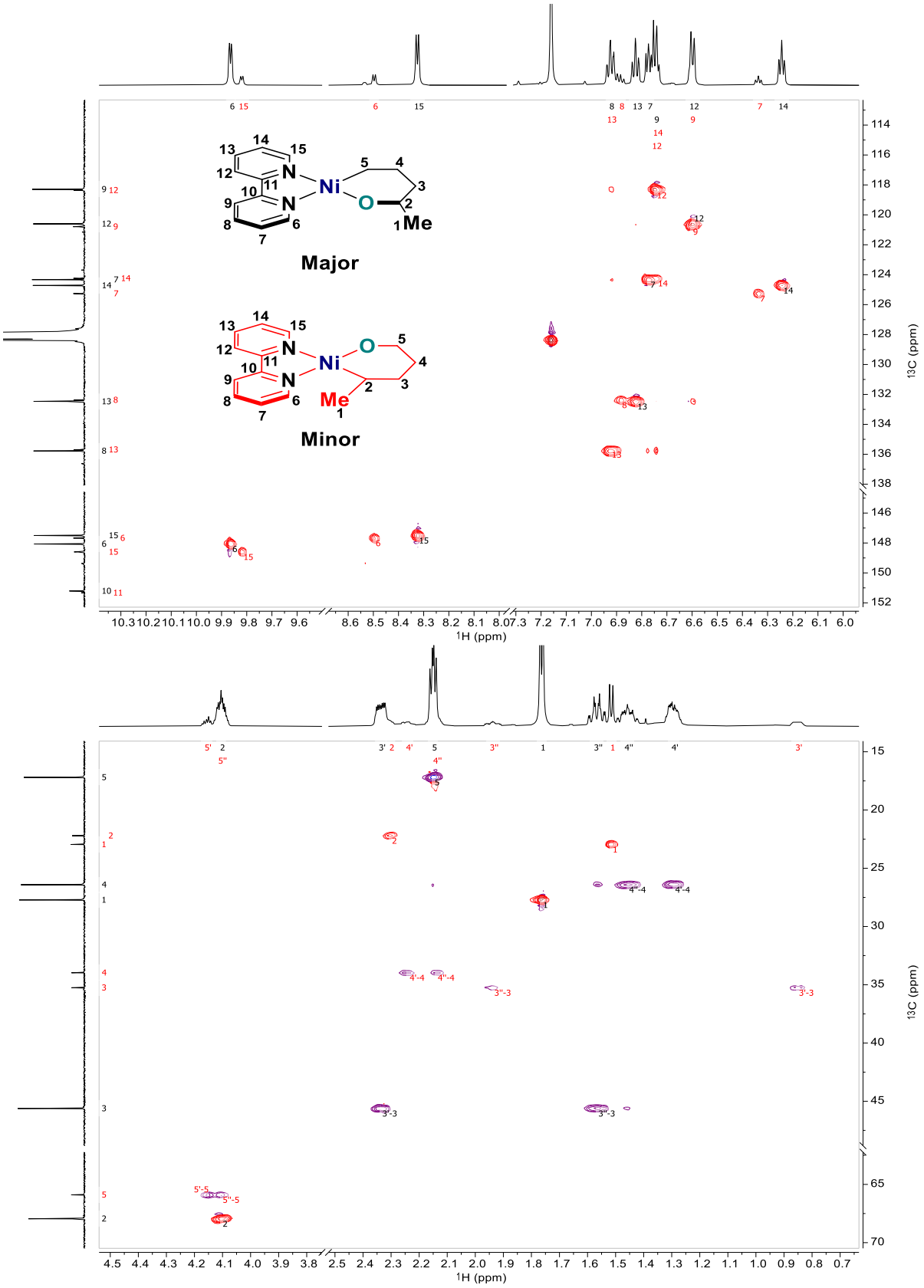
Major
Minor
1H (ppm)
13C (ppm)
1H (ppm)
13C (ppm)

^{1}H-^{13}C-HMBC of compounds **1b** and **1b-isomer**

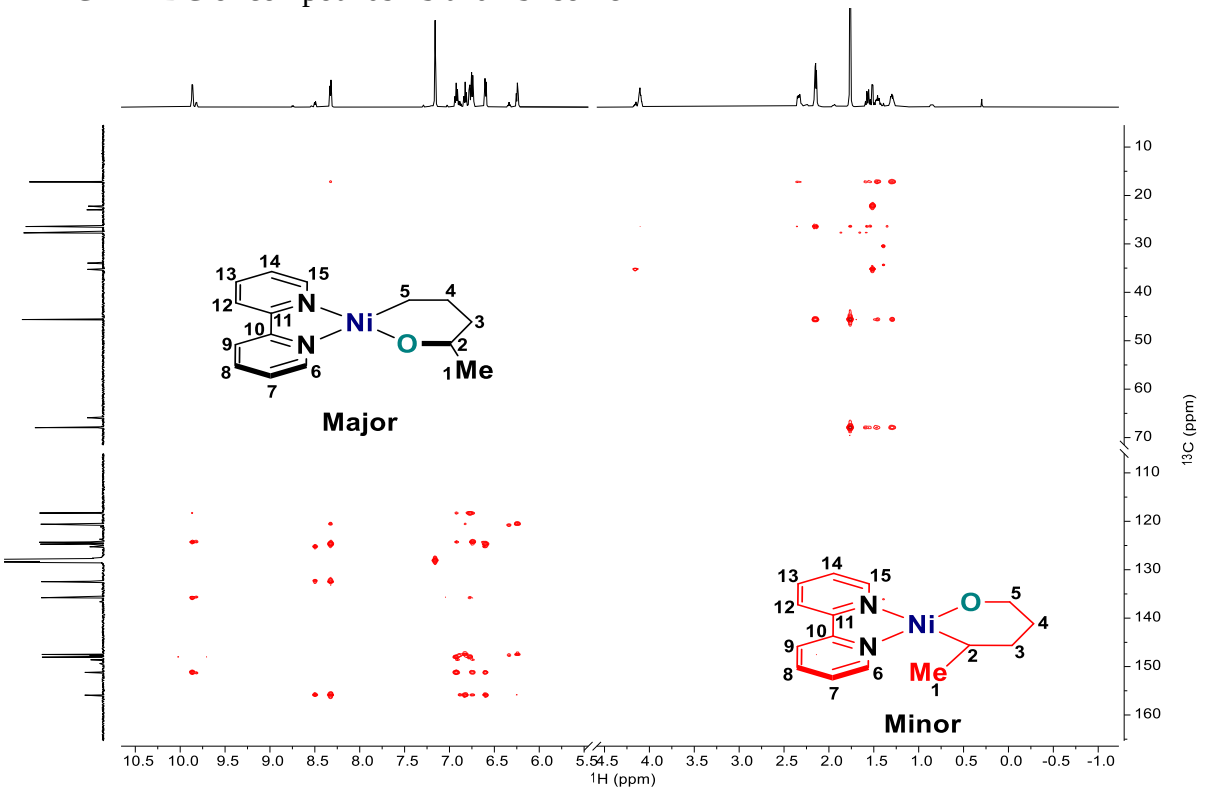

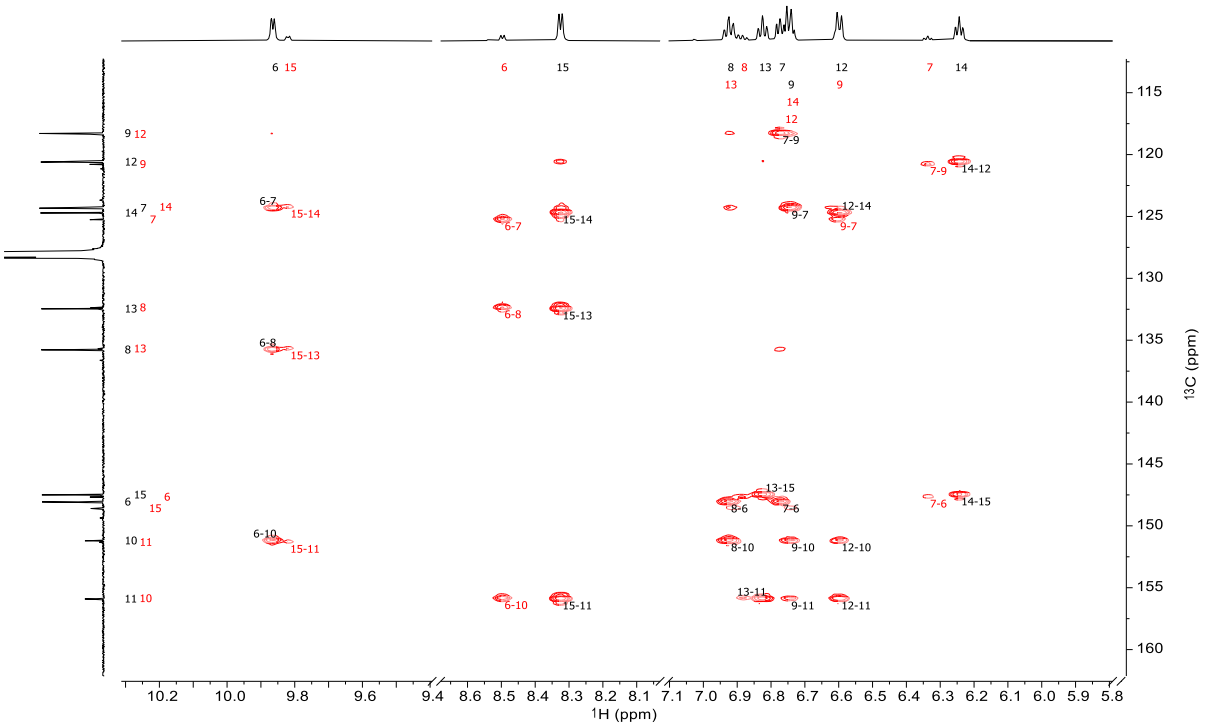

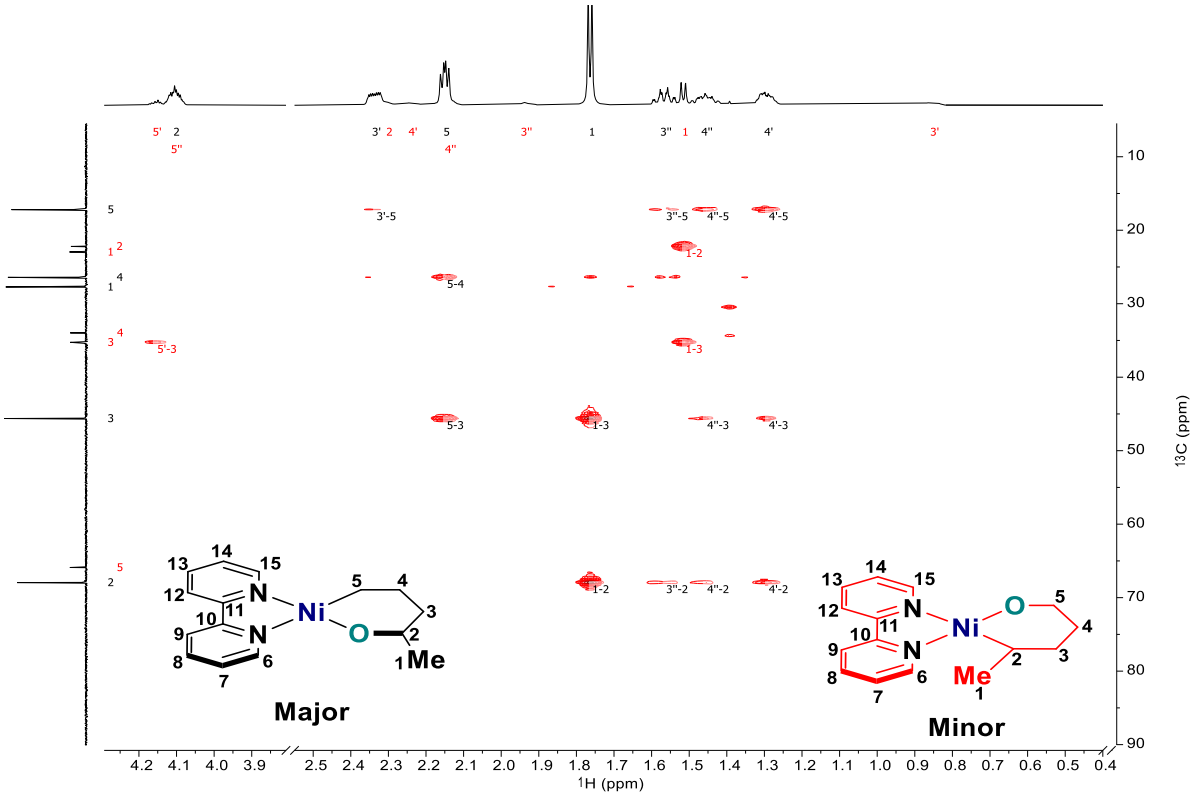
Major
Minor
Me
1Me
1H (ppm)
13C (ppm)

^{1}H-^{1}H-COSY of compounds **1b** and **1b-isomer**

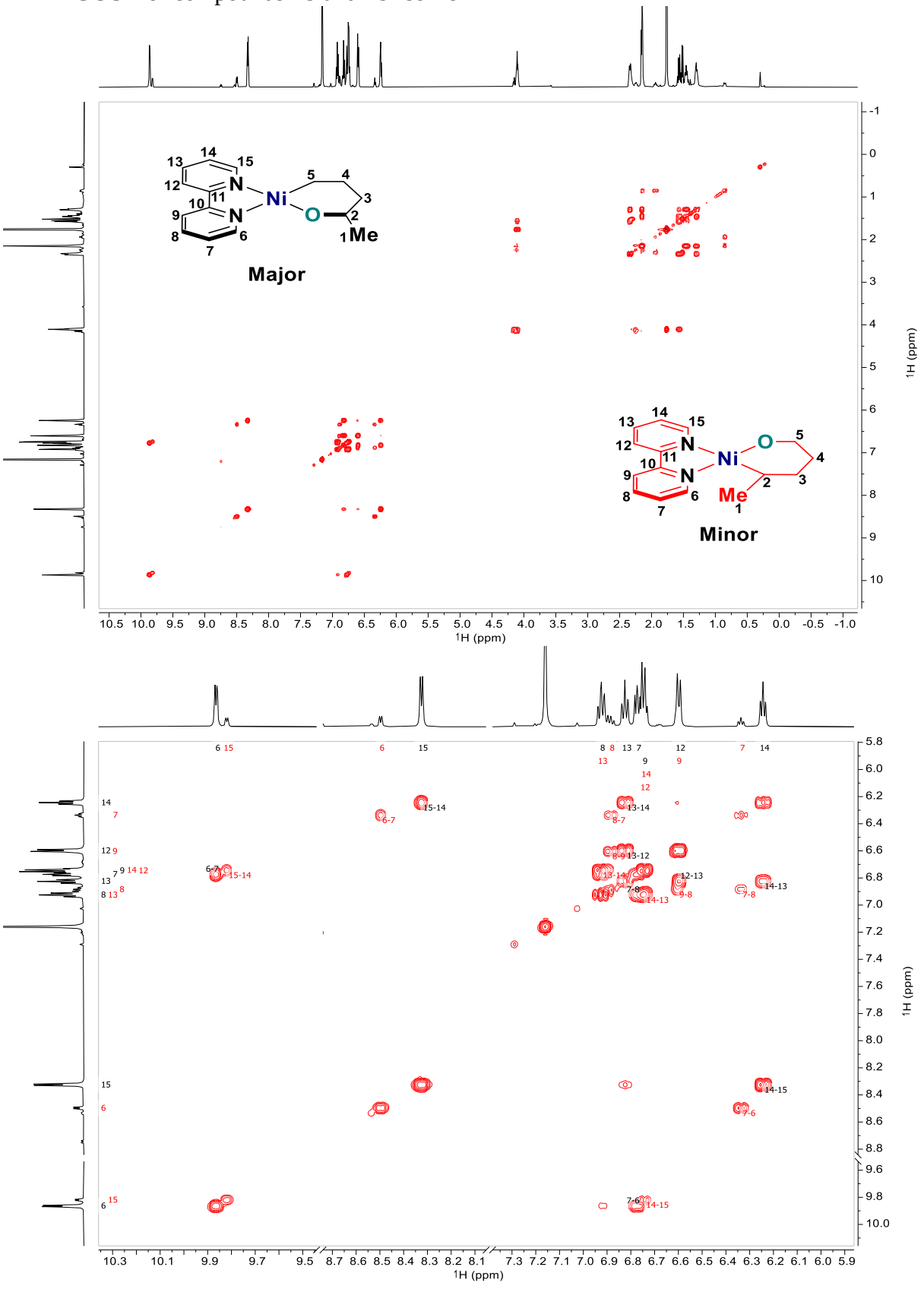

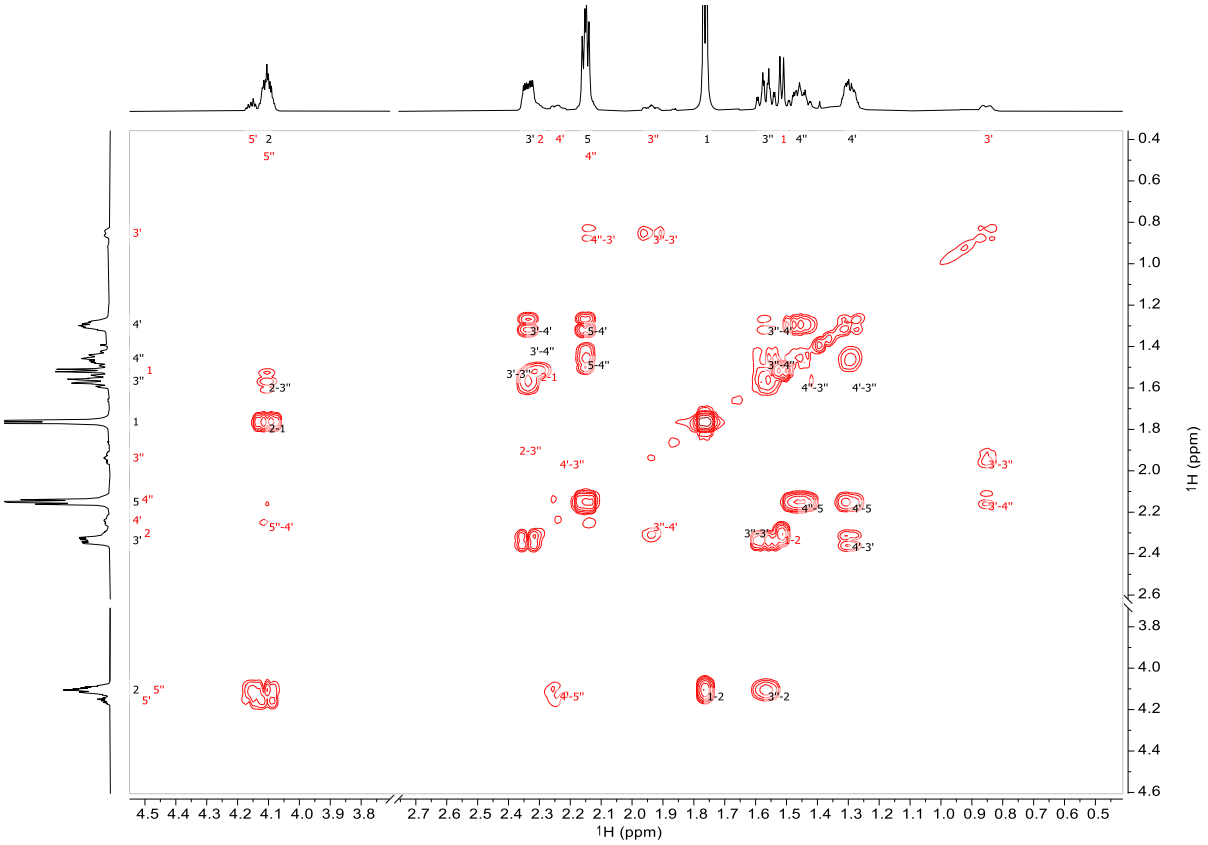
1H (ppm)
1H (ppm)

^{1}H-^{1}H-ROESY of compounds **1b** and **1b-isomer**

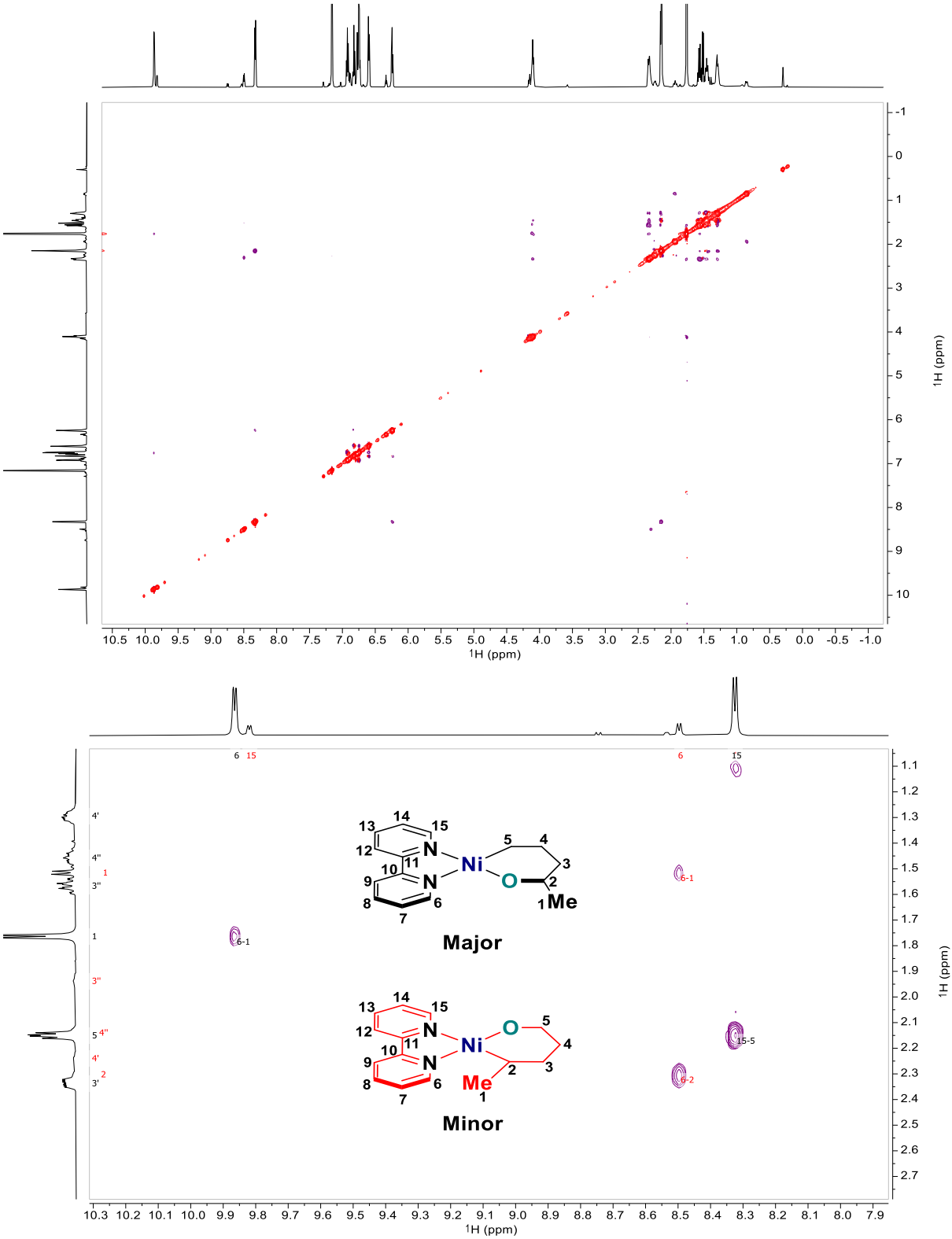

^{1}H-NMR (600 MHz, C_6D_6) of compound **1f**

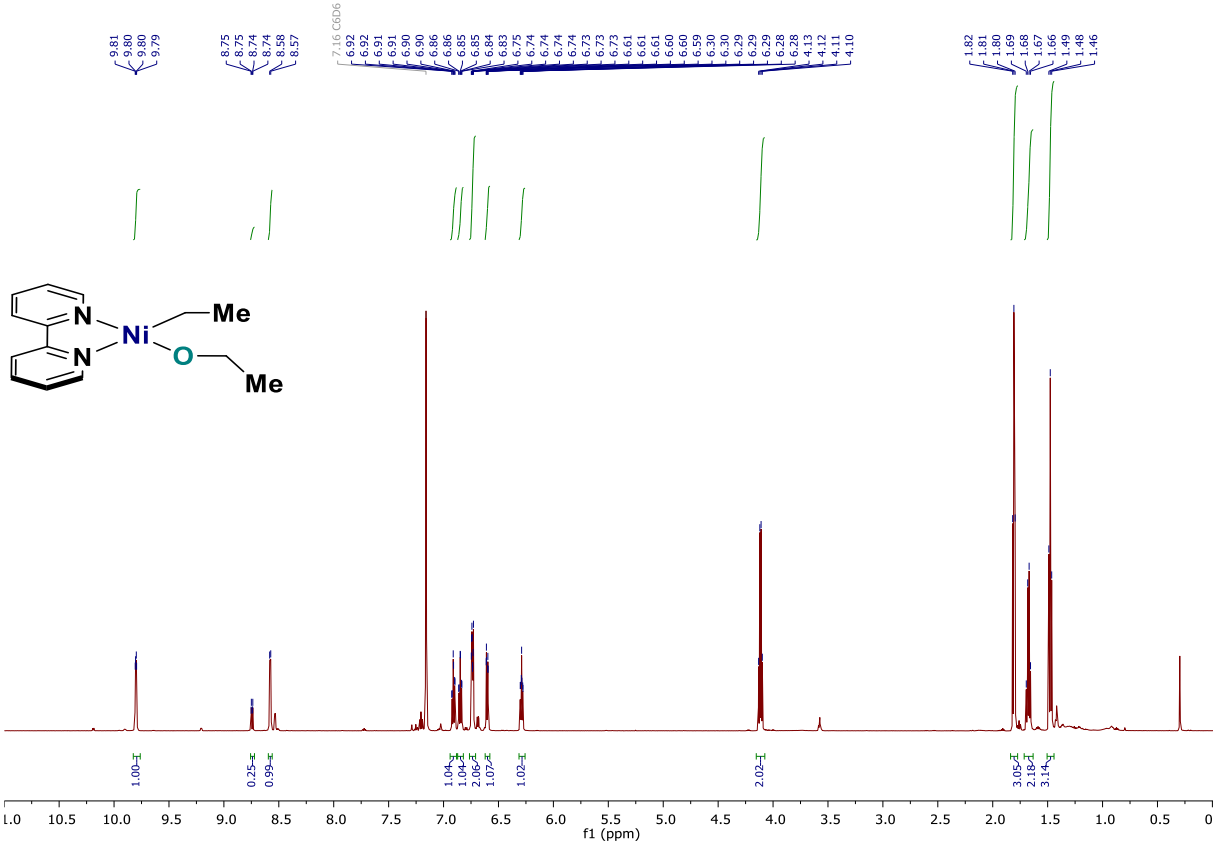

^{13}C-NMR (150 MHz, C_6D_6) of compound **1f**

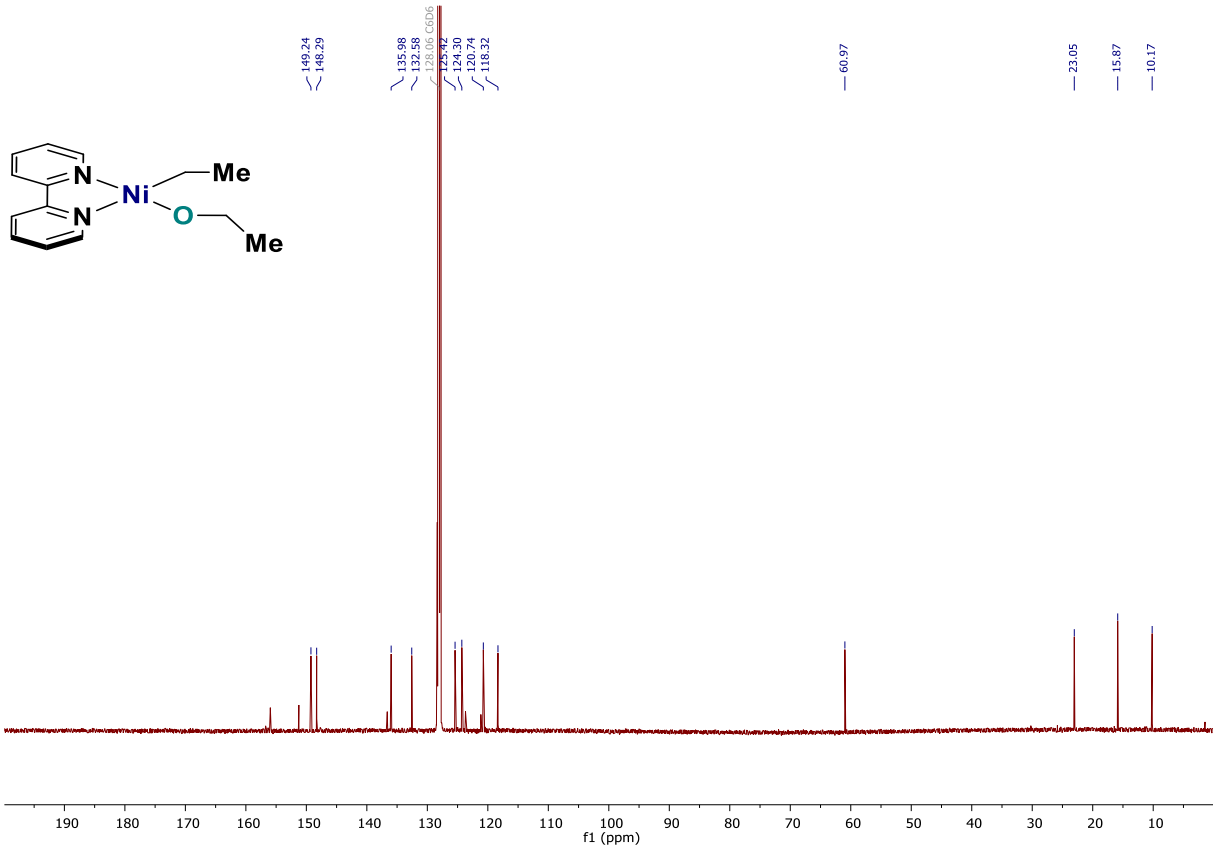

10. Coordinates for the DFT calculations

Coordinates of ***9a***

C	2.918970000	-0.274516000	14.122506000
H	3.907435000	-0.213554000	14.589598000
H	2.735957000	-1.328069000	13.894830000
H	1.731503000	-0.469364000	15.903328000
H	-0.033566000	0.150589000	8.586945000
C	2.056489000	0.143127000	8.045844000
H	1.948175000	-0.553249000	7.225036000
I	0.177059000	3.125905000	13.022462000
Ni	2.691732000	3.008976000	14.429264000
O	3.261015000	1.852963000	12.991771000
N	2.343628000	4.321489000	15.914234000
N	4.609462000	3.184909000	15.230028000
C	1.143778000	4.819265000	16.213468000
H	0.326074000	4.481821000	15.590164000
C	0.956139000	5.719955000	17.250021000
H	-0.033672000	6.100101000	17.459113000
C	2.056423000	6.107443000	18.000066000
H	1.948146000	6.803479000	18.821166000
C	3.303029000	5.587230000	17.687059000
H	4.169695000	5.872024000	18.264139000
C	3.422747000	4.690615000	16.630856000
C	4.706661000	4.087259000	16.213799000
C	5.944435000	4.418508000	16.759220000
H	6.026788000	5.151301000	17.547924000
C	7.081723000	3.796137000	16.265718000
H	8.052723000	4.038413000	16.677014000
C	6.960087000	2.866824000	15.240564000
H	7.825394000	2.364007000	14.831735000
C	5.694071000	2.590584000	14.745701000
H	5.515275000	1.893488000	13.937924000
C	2.906448000	0.505136000	12.819149000
H	3.616267000	0.055720000	12.111458000
H	1.904589000	0.416024000	12.379825000
C	1.842705000	0.241623000	15.073145000
H	0.884109000	0.263368000	14.550482000
C	2.122876000	1.583799000	15.687563000
H	2.958344000	1.558002000	16.387180000
H	1.241945000	2.008559000	16.162325000
Ni	2.691893000	3.242419000	11.615807000
O	3.261125000	4.398390000	13.053343000
N	2.343781000	1.929856000	10.130972000
N	4.609648000	3.066295000	10.815077000
C	1.143919000	1.431968000	9.831995000
H	0.326255000	1.769598000	10.455248000
C	0.956240000	0.530877000	8.795804000

C	3.303107000	0.663481000	8.358567000
H	4.169752000	0.378448000	7.781577000
C	3.422874000	1.560471000	9.414444000
C	4.706803000	2.163907000	9.831328000
C	5.944536000	1.832716000	9.285789000
H	6.026845000	1.099922000	8.497082000
C	7.081834000	2.455188000	9.779147000
H	8.052804000	2.212978000	9.367742000
C	6.960251000	3.384515000	10.804292000
H	7.825570000	3.887400000	11.213012000
C	5.694267000	3.660700000	11.299274000
H	5.515509000	4.357837000	12.107026000
C	2.906522000	5.746209000	13.225947000
H	3.616286000	6.195631000	13.933688000
H	1.904638000	5.835291000	13.665221000
C	2.919106000	6.525879000	11.922604000
H	3.907608000	6.464952000	11.455586000
H	2.736043000	7.579423000	12.150287000
C	1.842938000	6.009725000	10.971863000
H	0.884300000	5.987924000	11.494447000
H	1.731775000	6.720734000	10.141695000
C	2.123215000	4.667575000	10.357432000
H	2.958755000	4.693394000	9.657903000
H	1.242337000	4.242807000	9.882575000

Coordinates of ***Int-I***

C	3.489801000	-0.252253000	14.184934000
H	4.314963000	-0.086021000	14.897923000
H	3.462003000	-1.333661000	13.975114000
H	1.850921000	-0.514504000	15.566810000
H	-0.514751000	0.190902000	9.699917000
C	1.285413000	0.195435000	8.482707000
H	0.901280000	-0.495508000	7.731854000
F	1.467032000	3.125595000	13.022604000
Ni	3.044273000	3.013269000	14.369480000
O	3.874318000	1.879251000	13.017670000
N	2.267540000	4.288845000	15.661421000
N	4.650760000	3.235024000	15.655997000
C	1.025057000	4.785862000	15.541905000
H	0.474266000	4.439211000	14.665194000
C	0.497022000	5.677338000	16.473894000
H	-0.514752000	6.060279000	16.345301000
C	1.285417000	6.055753000	17.562504000
H	0.901283000	6.746695000	18.313359000
C	2.574928000	5.540116000	17.680321000
H	3.204829000	5.826760000	18.521156000
C	3.050322000	4.652394000	16.708017000
C	4.404982000	4.057039000	16.703124000
C	5.389065000	4.314227000	17.665920000

H	5.184790000	4.974099000	18.508015000
C	6.641137000	3.716547000	17.531093000
H	7.419331000	3.902507000	18.271825000
C	6.885296000	2.884938000	16.436154000
H	7.853841000	2.406629000	16.293041000
C	5.857514000	2.671471000	15.517614000
H	5.978938000	2.041549000	14.634892000
C	3.760553000	0.479062000	12.872175000
H	4.706789000	0.107058000	12.431633000
H	2.946770000	0.211510000	12.169999000
C	2.159193000	0.208218000	14.785818000
H	1.379268000	0.170293000	14.008330000
C	2.184559000	1.566847000	15.436759000
H	2.754322000	1.569272000	16.376997000
H	1.175010000	1.963233000	15.600654000
Ni	3.044268000	3.237931000	11.675721000
O	3.874307000	4.371956000	13.027528000
N	2.267535000	1.962350000	10.383784000
N	4.650751000	3.016183000	10.389198000
C	1.025055000	1.465327000	10.503306000
H	0.474266000	1.811976000	11.380019000
C	0.497021000	0.573848000	9.571320000
C	2.574922000	0.711079000	8.364884000
H	3.204820000	0.424438000	7.524047000
C	3.050315000	1.598804000	9.337186000
C	4.404972000	2.194165000	9.342074000
C	5.389055000	1.936979000	8.379276000
H	5.184780000	1.277105000	7.537183000
C	6.641125000	2.534665000	8.514099000
H	7.419317000	2.348706000	7.773366000
C	6.885283000	3.366277000	9.609036000
H	7.853826000	3.844590000	9.752145000
C	5.857503000	3.579741000	10.527578000
H	5.978927000	4.209666000	11.410298000
C	3.760530000	5.772144000	13.173022000
H	4.706761000	6.144155000	13.613567000
H	2.946742000	6.039690000	13.875196000
C	3.489775000	6.503456000	11.860262000
H	4.314939000	6.337226000	11.147274000
H	3.461972000	7.584864000	12.070080000
C	2.159169000	6.042977000	11.259378000
H	1.379244000	6.080902000	12.036866000
H	1.850895000	6.765696000	10.478384000
C	2.184541000	4.684347000	10.608442000
H	2.754301000	4.681922000	9.668201000
H	1.174994000	4.287955000	10.444552000